Mississippi State University
Scholars Junction

Theses and Dissertations | Theses and Dissertations

12-13-2014

A Comparative Study of Diesel Ignited Methane and Propane Dual Fuel Low Temperature Combustion in a Single Cylinder Research Engine

Mostafa Shameem Raihan

Follow this and additional works at: https://scholarsjunction.msstate.edu/td

Recommended Citation
Raihan, Mostafa Shameem, "A Comparative Study of Diesel Ignited Methane and Propane Dual Fuel Low Temperature Combustion in a Single Cylinder Research Engine" (2014). *Theses and Dissertations*. 55.
https://scholarsjunction.msstate.edu/td/55

This Graduate Thesis - Open Access is brought to you for free and open access by the Theses and Dissertations at Scholars Junction. It has been accepted for inclusion in Theses and Dissertations by an authorized administrator of Scholars Junction. For more information, please contact scholcomm@msstate.libanswers.com.

www.manaraa.com

A comparative study of diesel ignited methane and propane dual fuel low temperature combustion in a single cylinder research engine

By

Mostafa Shameem Raihan

A Thesis
Submitted to the Faculty of
Mississippi State University
in Partial Fulfillment of the Requirements
for the Degree of Master of Science
in Mechanical Engineering
in the Department of Mechanical Engineering

Mississippi State, Mississippi

December 2014

www.manaraa.com

Copyright by

Mostafa Shameem Raihan

2014

www.manaraa.com

A comparative study of diesel ignited methane and propane dual fuel low temperature combustion in a single cylinder research engine

By

Mostafa Shameem Raihan

Approved:

_____

Sundar R. Krishnan
(Major Professor)

_____

Kalyan K. Srinivasan
(Co-Major Professor and Graduate Coordinator)

_____

Keith Hodge
(Committee Member)

_____

Jason Keith
Interim Dean
Bagley College of Engineering

www.manaraa.com

Name: Mostafa Shameem Raihan

Date of Degree: December 13, 2014

Institution: Mississippi State University

Major Field: Mechanical Engineering

Major Professor: Sundar Rajan Krishnan

Title of Study: A comparative study of diesel ignited methane and propane dual fuel low temperature combustion in a single cylinder research engine

Pages in Study: 140

Candidate for Degree of Master of Science

The objective of this thesis is to investigate and compare the performance and emissions characteristics of diesel-ignited methane and diesel-ignited propane dual fuel LTC in a single cylinder research engine (SCRE) at a constant engine load of 5.1 bar *net* indicated mean effective pressure (IMEP) and at a constant engine speed of 1500 RPM. Percentage of energy substitution of propane or methane (0 - 90 percent), diesel injection timing (SOI: 355 CAD – 280 CAD), rail pressure (200 bar – 1300 bar) and boost pressure (1.1 bar – 1.8 bar) were varied to quantify their impact on engine performance and engine-out $ISNO_x$, ISHC, ISCO, and smoke emissions. Advancing SOI to 310 CAD and beyond yielded simultaneous $ISNO_x$ and smoke emissions. A rail pressure of 500 bar was the optimal one for both fueling combinations while increasing boost pressure over 1.2 bar had a very little effect on $ISNO_x$ and smoke emissions.

www.manaraa.com

DEDICATION

This thesis is dedicated to my parents for their love and affection that shaped me who I am, and also to my lovely wife, Fahmida who has been a constant source of encouragement and support during the challenges of graduate life.

www.manaraa.com

ACKNOWLEDGEMENTS

I would like to thank my advisors Dr. Sundar Krishnan and Dr. Kalyan Srinivasan for their valuable guidance, support, intellectual stimulation and hours of engaging conversation. Without their support, I may not have found myself at Mississippi State University, nor had the opportunities to work with engines and combustion. They have helped me cultivate my passion, formulate my outlook, determination and motivation which would govern my entire life. Additional thank you goes to Dr. Keith Hodge for his valuable advice through-out my graduate study.

I would like to recognize my friends and colleagues Scott Guerry, Taylor Bohach, Aamir Sohail, Kyle Hodges, David Dickerson, Kendyl Partridge and Navid Zanganeh for their assistance in performing this study.

I also gratefully acknowledge financial support from the Sustainable Energy Research Center (US DOE Award # DE-FG36-06GO86025) and facilities support from the Center for Advanced Vehicular Systems at Mississippi State University.

www.manaraa.com

TABLE OF CONTENTS

www.manaraa.com

www.manaraa.com

www.manaraa.com

LIST OF TABLES

www.manaraa.com

LIST OF FIGURES

www.manaraa.com

www.manaraa.com

www.manaraa.com

www.manaraa.com

www.manaraa.com

NOMENCLATURE

η_{comb}	Combustion efficiency
AHRR	Apparent Heat Release Rate
BDC	Bottom Dead Center
CA10-90	Crank angle duration between 10 percent and 90 percent cumulative heat release
CA50	Crank angle corresponding to 50 percent of cumulative heat release
MPRR	Maximum Pressure Rise Rate
CA5	Crank angle corresponding to 5 percent of cumulative heat release
CAD	Crank Angle Degrees
EGR	Exhaust Gas Recirculation
EOI	End of Injection of diesel fuel
SCRE	Single Cylinder Research Engine
EVO	Exhaust Valve Opening
FCE	Fuel Conversion Efficiency
FSN	Filter Smoke Number
ID	Ignition Delay
IFCE	Net Indicated Fuel Conversion Efficiency
IMEP	Net Indicated Mean Effective Pressure
IVO	Intake Valve Opening

www.manaraa.com

IVC	Intake Valve Closing
LHV	Lower Heating Value
LTC	Low Temperature Combustion
LTHR	Low Temperature Heat Release
PES	Percent Energy Substitution of methane
SADI	Stand Alone Direct Injection
SOC	Start of Combustion
EVC	Exhaust Valve Closing
SOI	Start of Injection of diesel fuel
TDC	Top Dead Center
UHC	Unburned Hydro Carbon

www.manaraa.com

CHAPTER I

INTRODUCTION AND REVIEW OF EXISTING LITERATURE

The increasingly stringent exhaust emissions standards, the need for finding alternatives to liquid petroleum fuels, and the desire for higher fuel conversion efficiencies (FCEs) are key factors that have motivated research on advanced engine combustion strategies. Conventional diesel engines are constrained by tradeoffs between oxides of nitrogen (NO_x) and particulate matter (PM) emissions. Current regulations for brake-specific PM and NO_x emissions from heavy-duty diesel engines are 0.013 g/kWh and 0.268 g/kWh, respectively (DieselNet, 2014). Simultaneous reduction of NO_x and PM emissions without sacrificing fuel conversion efficiency (FCE) is an inherent challenge with conventional diesel combustion. On the other hand, several low temperature combustion (LTC) concepts that promise low NOx and PM emissions have been investigated over the past decade (Dec 2009, Musculus et al. 2013). Alternatives to fossil-based fuels, including natural gas (Beck et al. 1997, Wong et al. 2000), propane (Goldsworthy 2012, Polk et al. 2014a), and biofuels from various sources (Agarwal 2007, Contino et al. 2013, Giakoumis et al. 2013, Lee et al. 2013, Sayin 2010) have also been considered. Although various biodiesel blends can be used in existing diesel engines without any hardware modifications, the NO_x emissions are normally higher with biodiesel operation (Giakoumis et al. 2013).

www.manaraa.com

1.1 Fundamentals of Diesel Engine Combustion

The combustion process in a diesel engine is a very complex process whose detailed mechanism is still not completely understood. In typical diesel combustion, the diesel fuel is sprayed into the combustion chamber with the help of a high pressure injector near the end of the compression stroke (Heywood 1988). The fuel atomizes and mixes with the surrounding air to form a combustible mixture. After a short ignition delay period, diesel autoignition occurs volumetrically throughout the diesel jet. Diesel combustion heat release profiles are typically characterized by two stages, viz., first stage heat release due to "premixed combustion" and second stage heat release due to "mixing controlled combustion." Since engine performance and pollutant exhaust emissions directly depend on the combustion process, it is important to gain a detailed knowledge of diesel combustion.

The most commonly accepted conceptual model of diesel combustion was proposed by Dec (Dec 1997). Dec presents a clear view of how combustion occurs in a diesel engine from the start of injection to the end of injection. The application of laser-sheet visualization techniques performed in research engines with optical access into the combustion chamber allowed Dec and co-workers to obtain hitherto unavailable images of the diesel combustion process. Multiple imaging techniques were used to obtain images of different phenomena; e.g., liquid fuel droplets, fuel vaporization, soot concentration, PAH distribution, NO formation, and OH radicals at different combustion phases. Dec's schematic of his conceptual diesel combustion model is reproduced in Figure 1.1.

www.manaraa.com

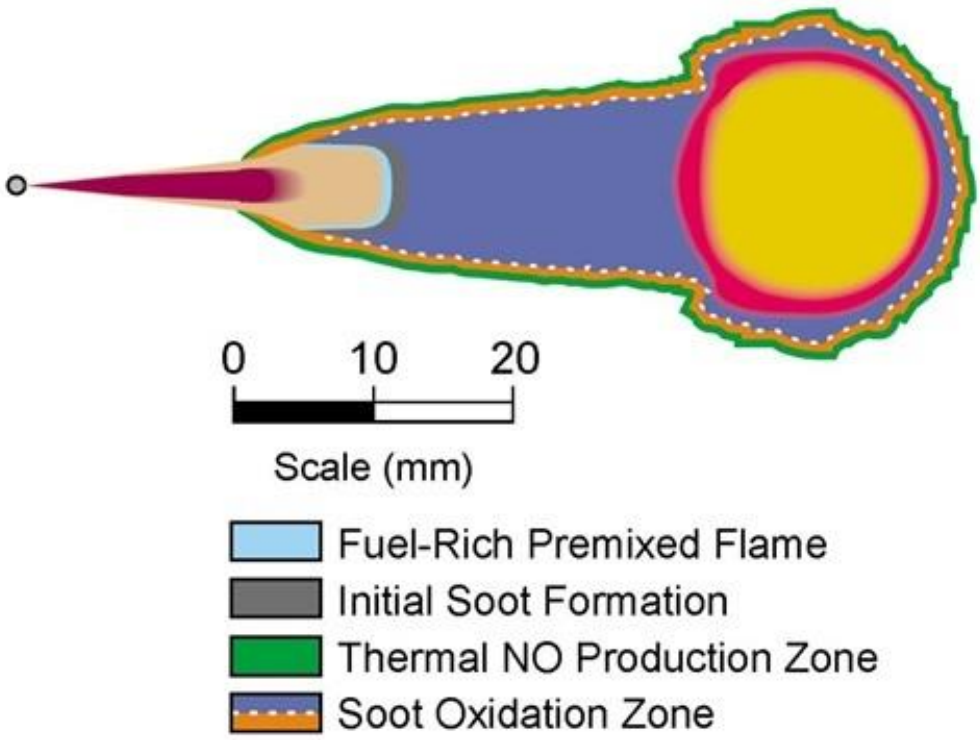

Figure 1.1 A schematic showing the conceptual model of DI diesel combustion

Note: Adapted from Dec, 1997.

A brief summary of Dec's model is presented here. After the start of diesel injection, the liquid jet emerges from the tip and mixes with the entrained air. The rate of entrainment varies spatially and thus forms mixtures with different composition of air and fuel throughout the combustion chamber. There is a definite ignition delay period, which is defined as the time difference between the start of injection and the start of detectable combustion. The start of combustion is characterized by about 5 percent of fuel burn, which is referred to as "premixed burn." The premixed portions of the diesel jet, where combustion is initiated, have a rich (equivalence ratio between 2 and 4) but combustible mixture throughout the cross section and near-stoichiometric mixture occurs only in the narrow peripheral regions. While the premixed burn is still occurring, the diffusion flame

www.manaraa.com

arises at the peripheral regions of the jet. Dec pointed out that the PM formation occurs in rich premixed combustion regions while NO_x forms in the hot, near-stoichiometric mixtures of the diffusion fame surrounding the jet. So, rich premixed regions are responsible for PM emissions and near-stoichiometric regions with high local temperatures are responsible for forming NO_x.

1.2 Low temperature combustion strategies

Historically, to reduce exhaust emissions from diesel engines, engine manufacturers mostly relied upon exhaust aftertreatment systems coupled with some in-cylinder emissions reduction strategies. A selective catalytic reduction (SCR) system is used to control NO_x and a diesel particulate filter (DPF) is used to trap and subsequently burn off soot particles in the exhaust (Dieselnet 2014). The SCR systems typically use a urea-based diesel exhaust fluid (DEF), which needs to be refilled at regular intervals. Further, DPFs need to be regenerated (i.e., trapped soot should be burned off) at regular intervals and this requires additional diesel fuel. Consequently, SCR and DPF systems lead to higher initial costs, present additional difficulties to the consumer, and also impact the overall fuel conversion efficiencies in diesel engines. In-cylinder emission control strategies such as injection timing variations, combustion chamber design optimizations, low or moderate exhaust gas recirculation (EGR) along with expensive aftertreatment devices were adopted to meet the emissions regulations in the past. However, these technologies come with a penalty of higher economic cost, lower fuel economy and higher maintenance. As a result, further improvements to in-cylinder strategies to control NO_x and PM are highly desirable.

www.manaraa.com

In a diesel engine, NO_x forms primarily by the so-called thermal mechanism for nitric oxide (NO), where formation rate increases exponentially with temperature (Plee et al. 1981, Plee et al. 1982). To reduce NO_x emissions by reducing the local in-cylinder combustion temperatures, several LTC strategies have been proposed in the open literature (Krishnan et al. 2004, Hanson et al. 2010, Northrop et al. 2009, Jacobs & Assanis 2007) In all LTC strategies, in-cylinder temperature reduction is achieved by dilution of combustible mixtures, either with excess air or with low-to-moderate EGR levels. While the formation of soot, which is the primary component of PM, also decreases with the decrease of in-cylinder temperature (Dobbins 2002), soot oxidation rate also decreases and resulted in a net increase in PM emissions (Park & Appleton 1973, Dec 2009). This problem can be overcome by utilizing high EGR levels, but unfortunately, excessive EGR used with some LTC strategies can lead to poor combustion efficiencies (Huestis et al. 2007) due to the presence of high unburned hydrocarbons (HC) and carbon monoxide (CO) in the exhaust.

Various LTC strategies have been proposed to control NO_x and PM emissions simultaneously. Homogeneous charge compression ignition (HCCI) combustion is one popular concept where vaporized fuel is mixed with the intake air prior to compression and thus creates a uniform fuel-air mixture in the combustion chamber at the end of the compression stroke. Fuel may be introduced either by direct injection into the combustion chamber during the intake stroke or early in the compression stroke (Dec 2009), or outside the combustion chamber during or prior to the intake stroke (Ryan & Callahan 1996), i.e., port fueling. In both cases, LTC is achieved by separating the fuel injection process and the combustion process, thus facilitating the formation of a uniform fuel-lean mixture

www.manaraa.com

throughout the chamber. In general, HCCI combustion is limited by high peak pressures, high pressure rise rates, and knocking that prevent engine operation beyond medium loads. In a spark-ignited gasoline engines, knocking occurs when the unburned fuel-air mixture ahead of the flame front (end-gas region) is compressed to sufficiently high temperatures, leading to spontaneous combustion of the unburned mixture. On the other hand, normal diesel combustion is characterized by spontaneous autoignition of the fuel. 'Diesel knock' refers to the high pressure rise rates associated with the autoignition of fuel during the premixed combustion phase. While this is a part of normal diesel engine operation, some operating conditions can lead to excessively high pressure rise rates that are extremely detrimental to engine life (Hsu 2002). Diesel knock is considered as a significant problem allowing utilization of alternative fuels in diesel engine (Saidi et al. 2005).

Another broad classification of LTC strategies is termed partially premixed compression ignition (PPCI), which utilizes more moderate mixing times and more heterogeneous charge distribution compared to HCCI. In PPCI strategies, fuel can be injected in the middle or late compression stroke ((Kook et al. 2005, Hardy & Reitz 2006) or near TDC or early expansion stroke (de Ojeda et al. 2008). Although PPCI strategies demonstrated excellent control of engine-out NO_x and PM emissions, CO and unburned hydrocarbon (UHC) emissions are substantially higher. Moreover, fuel consumption can be higher than conventional diesel combustion due to the increase of CO and UHC emissions.

1.3 Conventional Dual Fuel Combustion and Dual Fuel LTC

To address the challenge of simultaneous NOx and PM reduction in diesel engines, dual fuel combustion has been investigated with a variety of alternative fuels, including

www.manaraa.com

natural gas, propane, biogas, etc. (Gibson et al. 2011, Karim 2003, Krishnan et al. 2004, Kusaka et al. 2000, McTaggart-Cowan et al. 2006, Papagiannakis & Hountalas 2004, Polk et al. 2013, 2014a, 2014b, Tira et al. 2014). Dual fuel combustion utilizes an easily ignitable, high-cetane, pilot fuel to ignite an autoignition-resistant, low-cetane, primary fuel, which is typically premixed along with air in the intake manifold and introduced into the cylinder during the intake stroke. Several high-cetane pilot fuels such as diesel (Badr et al. 1999, Krishnan et al. 2002, Selim 2004, Srinivasan et al. 2006), biodiesel (Bedoya et al. 2009, Debnath et al. 2013, Northrop et al. 2010, Ryu 2013a, Shoemaker et al. 2011), and dimethyl ether (Chen et al. 2009, Yao et al. 2006) have been considered. Of the various primary fuels discussed above, natural gas, which has methane as the major constituent, is a popular choice for many dual fuel applications. The relative percentage of natural gas and diesel, the injection timing of diesel, and the availability of air within the cylinder play major roles in the dual-fuel combustion process (Liu & Karim 1995, Karim 2003, Papagiannakis & Hountalas 2003). Karim (2003) divided conventional diesel-ignited methane dual fuel combustion into three distinct stages. After an ignition delay period, the diesel fuel releases energy and initiates the combustion process, which in turn ignites the surrounding methane-air mixture. Lastly, combustion proceeds by flame propagation through the remainder of the lean methane-air mixture. Although dual fuel engines exhibit some advantages over conventional diesel engines such as higher fuel conversion efficiencies and lower emissions under certain engine operating conditions, they tend to knock at high loads (Liu & Karim 1995) and produce higher HC from crevices and bulk quenching and CO emissions from partial fuel oxidation at low loads (Srinivasan 2006b, Papagiannakis et al. 2010). The ignition delay period (ID) is one of the most important

www.manaraa.com

parameters in single fuel LTC strategies as well as in dual fuel combustion. The ID is defined as the time period between the start of injection (SOI) and the start of combustion (SOC) and depends on the type of fuel used, the percentage of energy substituted by the primary fuel, the pilot injection timing and the intake pressure. Another important parameter with relevance to any PPCI and dual fuel combustion strategies is ignition dwell, which is the time from end of injection (EOI) to SOC. In conventional diesel combustion, ignition dwell is usually negative as SOC occurs before EOI. In PPCI and dual fuel LTC strategies, longer ignition dwells are used to separate the injection and combustion events to reduce NO_x and PM emissions.

Several past studies have focused on the characterization of diesel-ignited natural gas (conventional) dual fuel combustion (Daisho et al. 1995, Kusaka et al. 2000, Selim 2004, Papagiannakis et al. 2010). In addition, the effects of critical engine parameters such as pilot fuel quantity (Abd Alla et al. 2000, Krishnan et al. 2004, Papagiannakis & Hountalas 2003, Papagiannakis et al. 2007), pilot injection timing (Abd Alla et al. 2002, Krishnan et al. 2004, Ryu 2013a, Sayin et al. 2008, Sayin & Canakci 2009), pilot injection pressure (Carlucci et al. 2008, Jindal et al. 2010, Ryu 2013b), and boost pressure (Krishnan et al. 2002, Singh et al. 2004) on dual fuel combustion have been investigated. For example, Carlucci et al. (2008) studied the effects of injection pressure (600-1000 bar) and found that NO_x emissions decreased with increasing injection pressure while CO emissions showed the opposite trend. These results are also supported by McTaggart-Cowan et al. (2004) for high load conditions. However, in both of these studies, the pilot injection timing was fixed close to top dead center (TDC) and the injection pressure variation was relatively narrow. Abd Alla et al. (2002) reported improvement in FCE and reduction in

www.manaraa.com

HC and CO emissions with the advancement of pilot injection timing as well as a slight increase in NO_x emissions. However, again, the scope of this study was also limited to injection timing variations between 325 CAD and 330 CAD. Polk et al. (2013) and Gibson et al. (2011) presented data for diesel-ignited methane dual fuel combustion on a turbocharged multi-cylinder light-duty engine but these data were limited by the use of the stock engine controller. Papagiannakis et al. (2007) suggested that a proper combination of injection timing and injection quantity might lead to lower CO emissions as well as higher FCEs.

Propane has also been explored as the primary fuel for dual fuel combustion in diesel engines. Polk et al. (2013) found that ID decreases with the increase of propane substitution at high loads while the opposite trend is observed when methane is used as the primary fuel. However, the author could not go beyond a propane percent energy substitution (PES) of 47 percent at high loads due to excessive pressure rise rates. Goldsworthy (2012) found that, at high loads, increasing propane substitution leads to slightly higher thermal efficiencies while CO, HC, and smoke increased. Goldsworthy also reported that at retarded injection timings, NO_x emissions decreased with increasing propane substitution. The combustion process was characterized by high peak pressures, excessive maximum pressure rise rates (MPRR), two distinct heat release rates, and audible knock at high loads. However, the range of injection timing and propane PES was very limited (355 to 335 CAD and up to 35 percent, respectively). On a similar study, using a four-stroke single cylinder engine, Poonia and coworkers (Poonia et al. 1999) reported an increase in CO emissions while HC emissions decreased with increasing propane PES at different load conditions. However, in all of the above reported cases, low to moderate

www.manaraa.com

level of EGR was used to control the combustion process and an optimum EGR level was reported to achieve the best possible brake thermal efficiency. Other studies (Abd Alla et al. 2002, Sudhir et al. 2003) described the effect of injection timing and PES on performance and emissions of dual fuel operation and found that the 330 CAD injection timing was optimal for achieving the highest brake thermal efficiency; however, the highest NO_x emissions were also obtained at this timing for all load conditions. Two separate studies (Polk et al. 2013a, Abd Alla et al. 2000) showed that the maximum achievable PES decreases with increasing load due to high MPRR and excessive combustion noise. It has also been reported that while keeping all other parameters constant, increasing PES typically increases the ID. A recent study by Polk et al. (2013b) suggested that with increasing PES, NO_x emissions decreased while smoke emissions increased maintaining all other parameters constant. In addition, diesel-propane dual fuel combustion yielded higher CO emissions, lower total hydrocarbon (THC) emissions, and marginally higher brake thermal efficiencies compared to diesel-methane dual fuel combustion under similar operating conditions.

To further reduce NO_x and PM emissions to meet current US EPA regulations, several dual fuel LTC strategies have been pursued. For example, the advanced low pilot ignited natural gas (ALPING) dual fuel LTC concept was demonstrated nearly a decade ago (Krishnan et al. 2004, Qi et al. 2007, and Srinivasan et al. 2006a, 2006b, 2007). In ALPING dual fuel LTC, about 97-98 percent of the total fuel energy is supplied by natural gas while diesel is used only as an ignition source using a dedicated micro-pilot injection system. The ALPING LTC concept yielded good FCEs and extremely low engine-out NO_x emissions (< 0.2 g/kWh); however, these benefits were accompanied by excessive HC and

www.manaraa.com

CO emissions (Krishnan et al. 2004). Subsequent experiments on ALPING dual fuel LTC employed hot EGR and intake charge heating to achieve up to 70 percent HC reductions along with low NO_x and high FCE benefits at low loads (Qi et al. 2007). Similarly, diesel-ignited propane dual fuel LTC was recently demonstrated with very similar NO_x emissions benefits on a multi-cylinder heavy-duty diesel engine (Polk et al. 2014a). Another dual fuel LTC strategy that involves diesel ignition of gasoline-air mixtures is reactivity controlled compression ignition (RCCI) combustion (Hanson et al. 2010, Kokjohn et al. 2011, and Splitter et al. 2011). Diesel-propane LTC, ALPING dual fuel LTC, and RCCI are all based on the idea that in-cylinder stratification of fuel reactivity between the low-cetane primary fuel and the high-cetane diesel pilot can be exploited to control the partially premixed combustion process.

1.4 Objectives of the present work

The objective of the present work is to investigate and compare the performance and emissions characteristics of diesel-ignited methane and diesel-ignited propane dual fuel LTC in a single cylinder research engine (SCRE) at a constant engine load of 5.1 bar *net* indicated mean effective pressure (IMEP) and at a constant engine speed of 1500 RPM. To accomplish this objective, one engine control parameter (e.g., PES, pilot SOI, injection pressure, or intake boost pressure) is systematically varied while keeping all others constant to quantify the effect of each parameter on performance and emissions.

www.manaraa.com

CHAPTER II

EXPERIMENTAL SETUP AND DEFINITIONS

2.1 Experimental Setup

Figure 2.1 shows a schematic of the experimental setup used in the present study. A four-stroke, compression ignition SCRE was used to conduct all of the experiments presented in this thesis. Relevant engine specifications are given in Table 2.1.

Table 2.1 Engine Specifications

Engine Type	Single-cylinder, compression-ignition research engine
Bore × Stroke (mm × mm)	128 × 142
Connecting rod length (mm)	228
Displaced volume (cc)	1827
Compression ratio	17.1 : 1
4Combustion chamber geometry	Mexican hat
Valve timings	IVO – 32 CAD, IVC – 198 CAD EVO – 532 CAD, EVC – 14 CAD
Diesel fuel injection system	Bosch CP3 common-rail
Injector nozzle hole diameter	0.197 mm
Number of nozzle holes	8
Gaseous fueling	Fumigation into intake manifold
Maximum speed (RPM)	1900

www.manaraa.com

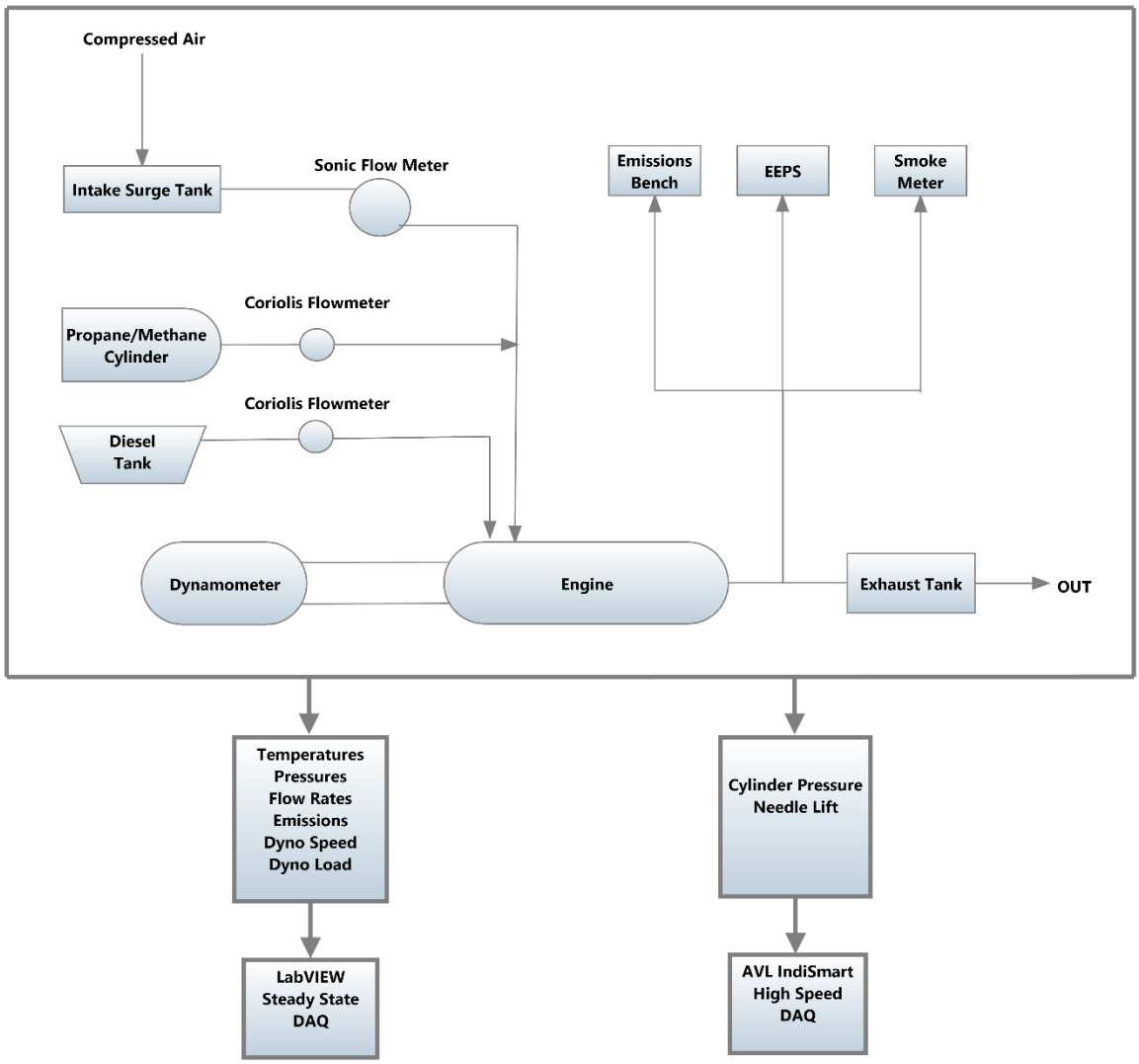

Figure 2.1 Schematic of the experimental setup

The engine was coupled to a 250 HP Dyne Systems AC regenerative dynamometer, which was controlled by an Inter-Lock V controller that also provided torque and speed measurements. Intake, exhaust, coolant, and oil temperatures were measured using Omega Type-K thermocouples. Gaseous and exhaust emissions were measured downstream of the exhaust manifold using an emissions sampling trolley and an integrated emissions bench (EGAS 2M) manufactured by Altech Environment S.A. The EGAS 2M bench

www.manaraa.com

measured THC) with a heated flame ionization detector, NO_x emissions with a chemiluminescence detector, carbon dioxide (CO_2) and CO emissions with a non-dispersive infrared analyzer, and oxygen (O_2) with a paramagnetic detector. Smoke was measured in filter smoke number (FSN) units using an AVL 415S variable sampling smoke meter. The exhaust was also sampled through a rotating disk thermo-dilutor with a dilution factor of 1870:1 to a TSI Model 3090 Engine Exhaust Particle Sizer (EEPS) spectrometer to measure particle size distributions.

Pilot diesel mass flow rate and methane or propane mass flow rate were measured with Emerson Micro Motion coriolis mass flow meters. A Bosch CP3 common-rail fuel injection pump and injector (capable of supplying a maximum injection pressure of 1500 bar) were used to inject pilot diesel fuel. Diesel injection parameters were controlled by a Drivven (National Instruments) stand-alone diesel injection (SADI) driver coupled with CALVIEW software. A HANBAY needle valve (Model MCM-050AB) was used to control the flow rate of methane or propane, which was fumigated in the intake manifold.

In-cylinder pressure was measured using a Kistler model 6052C pressure sensor and a Kistler Type 5010B charge amplifier. The diesel injector was instrumented with a Wolff Hall effect sensor to obtain the needle lift data. Both sensors were phased with respect to crank angle using a BEI incremental shaft encoder (Model no. XH25D-SS-3600-ABZC-28V/V-SM18) with a resolution of 0.1 crank angle degree (CAD), which was coupled to the engine crankshaft. Cylinder pressure and needle lift data were recorded and averaged over 1000 consecutive cycles, and an intake manifold pressure sensor was used to peg the cylinder pressure data at bottom dead center (BDC). It is well known from the literature that dual fuel combustion, utilizing diesel as the ignition source and any low

www.manaraa.com

cetane fuel as the primary fuel, tends to exhibit significant cyclic combustion variations depending on the concentration of primary fuel and engine operating parameters (cf. Rakopoulos et al. 2013, Selim 2005). In the present study, cyclic combustion variations over 1000 consecutive cycles were quantified as the coefficient of variation (COV) of indicated *net* mean effective pressure (IMEP), which is the ratio of the standard deviation in net IMEP to the arithmetic mean of the net IMEP expressed as a percentage. To provide compressed air in the intake manifold, an Atlas Copco air compressor (Model GA75) coupled with a heatless desiccant dryer (Model CD 250) were used Air flow rate was measured using a FlowMaxx sonic orifice (Model SN16–SA–235). To ensure choked flow across the sonic orifice flow meter, the pressure ratio across the orifice (inlet to outlet) was always maintained above a critical value of 1.2 at all engine operating conditions. This was accomplished with the help of a manual pressure regulator placed upstream of the flow meter. Subsequently, air mass flow rate was directly determined from the sonic orifice calibration curve by measuring the pressure and temperature upstream of the sonic orifice. Temperature of the intake air was maintained at around 37°C for all of the experiments in this thesis with the help of a Chromalox intake air heater. All of the steady state data were recorded and averaged over 60 seconds. Steady state condition at a particular operating condition was ensured by allowing the engine to run for a few minutes maintaining the same level of load and PES. The measured experimental parameters and their accuracies are summarized in Table 2.2.

www.manaraa.com

Table 2.2 Accuracies of Various Experimental Measurements

Measured parameters	Unit	Accuracy
Engine speed	RPM	± 1 RPM
Engine torque	Nm	± 0.06 percent of reading
Cylinder pressure	bar	±0.005 bar
Diesel flow rate	kg/h	±0.05 percent of reading
Methane flow rate	kg/h	±0.35 percent of reading
Air flow rate	kg/h	±0.1 percent of reading
Temperatures	°C	±0.75 percent of reading
Pressures (intake, exhaust, coolant and lubrication oil)	psig	±0.25 percent of reading
Smoke number	FSN	±0.001 FSN
THC emissions	ppm	<0.5 percent of full scale
NO_x emissions	ppm	<1 percent of full scale
CO	percent	<1 percent of full scale
CO_2	percent	<1 percent of full scale
O_2	percent	<1 percent of full scale

2.2 Definitions

To clarify the various terms used in this thesis, relevant parameters such as equivalence ratio (Φ), percent energy substitution (PES), ignition delay (ID), combustion efficiency (η_c), indicated fuel conversion efficiency (IFCE), brake fuel conversion efficiency (BFCE), apparent heat release rate (AHRR), and the ratio of specific heats (γ) are defined below.

$$PES = \frac{\dot{m}_g LHV_g}{\dot{m}_d LHV_d + \dot{m}_g LHV_g} \tag{2.1}$$

www.manaraa.com

$$\Phi = \frac{\left(A/F\right)_{st-tot}}{\left(\frac{\dot{m}_a}{\dot{m}_d + \dot{m}_g}\right)} \tag{2.2}$$

In Equations 2.1 and 2.2, $\dot{m}$ refers to the mass flow rates of diesel (subscript d), methane/propane (subscript g), and air (subscript a), respectively, and LHV refers to the corresponding lower heating values of the fuels. The PES is the percentage of the total fuel energy that is substituted by the gaseous fuel (propane or methane). Stoichiometric air-fuel ratio $(A/F)_{st\text{-}tot}$ is defined as the stoichiometric air required for complete oxidation of both diesel and gaseous fuels into CO_2 and H_2O. Therefore, $(A/F)_{st\text{-}tot}$ depends on the PES of propane or methane (Equation 2.2).

$$ID = CA5 - SOI \tag{2.3}$$

The start of combustion (SOC) is defined as CA5, or the crank angle at which 5 percent of the cumulative heat release occurs. Ignition delay is referred as the difference between SOC (CA5) and start of injection (SOI). Combustion phasing is defined as the crank angle at which 50 percent of the cumulative heat release occurs and denoted as CA50. Also, CA10-90, which is defined as the difference between the crank angle at which 10 percent of cumulative heat release occurs and the crank angle at which 90 percent of cumulative heat release occurs, gives an estimation of overall combustion duration.

$$\eta_c = 1 - \frac{\sum x_f LHV_f}{\frac{\dot{m}_f}{\dot{m}_a + \dot{m}_f}} \tag{2.4}$$

In Equation 2.4, combustion efficiency (η_c) is calculated using the mass fractions (x_f) of CO, H_2, HC, and PM using their respective LHVs (Heywood 1988). Since the

www.manaraa.com

composition of HC in the exhaust, and thus its LHV, are not known, Heywood recommends using the LHV of the fuel as they are expected to be of comparable magnitude (Heywood 1988). However, for this study, since two fuels were used, the combined mass-fraction-weighted LHV of diesel and methane (or propane) is used to represent the LHV of HC. The lower heating values for methane, propane, CO and H_2 are assumed to be 50.0 MJ/kg, 46.4 MJ/kg, MJ/kg, 10.1 MJ/kg and 120 MJ/kg, respectively. Also, since gravimetric PM was not measured in the present experiments, it was not considered in the combustion efficiency calculations.

$$IFCE = \frac{IP}{\dot{m}_d LHV_d + \dot{m}_g LHV_g} \tag{2.5}$$

The net IFCE was calculated as shown in Equation 2.5 using the net indicated power estimated from the measured cylinder pressure data and the measured fuel flow rates and their respective LHVs.

$$AHRR(\theta) = \frac{\gamma}{\gamma - 1} P \frac{dV}{d\theta} + \frac{1}{\gamma - 1} V \frac{dP}{d\theta} \tag{2.6}$$

$$\gamma = 1.338 - 6 \times 10^{-5} T + 1 \times 10^{-8} T^2 \tag{2.7}$$

The net apparent heat release rate (AHRR) presented in this study was derived from measured in-cylinder pressure data using Equation 2.6. The instantaneous volume (V) was calculated from the engine geometry and derivatives of pressure and volume ($dP/d\theta$ and $dV/d\theta$) were calculated numerically using a four point central difference formula. The specific heat ratio (γ) required in Equation 2.6 was evaluated as a function of mass averaged temperature (T) using Equation 2.7 (Brunt et al. 1998). In this regard, it may be noted that

www.manaraa.com

there are more sophisticated models for deriving gross and net heat release rates from experimental cylinder pressure data that may account for heat transfer to cylinder walls, different compositions for burned and unburned gases, etc. (cf., Rakopoulos et al. 2010; Krishnan et al. 2002). However, since the objective of the present work was to compare heat release trends in dual fuel LTC rather than the precise determination of gross heat release rates, the simpler net AHRR approach described above was adopted.

$$\phi_{emissions} = \frac{2n_{O_2}}{n_p \tilde{X}_{H_2O} + n_p(1-\tilde{X}_{H_2O})(\hat{\tilde{X}}_{CO} + 2\hat{\tilde{X}}_{CO_2} + 2\hat{\tilde{X}}_{O_2} + \hat{\tilde{X}}_{NO} + 2\hat{\tilde{X}}_{NO_2})} \tag{2.8}$$

$$\tilde{X}_i = (1-\tilde{X}_{H_2O})\hat{\tilde{X}}_i \tag{2.9}$$

$$n_P = \frac{n}{\tilde{X}_{CH_{b/a}} + (1-\tilde{X}_{H_2O})(\hat{\tilde{X}}_{CO} + \hat{\tilde{X}}_{CO_2})} \tag{2.10}$$

$$\tilde{X}_{H_2O} = \frac{m}{2n} \frac{\hat{\tilde{X}}_{CO} + \hat{\tilde{X}}_{CO_2}}{[(1+\hat{\tilde{X}}_{CO}/K\hat{\tilde{X}}_{CO_2}) + (\frac{m}{2n})(\hat{\tilde{X}}_{CO} + \hat{\tilde{X}}_{CO_2})]} \tag{2.11}$$

$$\tilde{X}_{H_2} = \frac{m}{2n} \frac{\tilde{X}_{H_2O}\hat{\tilde{X}}_{CO}}{K\hat{\tilde{X}}_{CO_2}} \tag{2.12}$$

$$\tilde{X}_{N_2} = \frac{3.773 n_{O_2}}{\phi n_P} - (1-\tilde{X}_{H_2O}) \frac{\hat{\tilde{X}}_{NO} + \hat{\tilde{X}}_{NO_2}}{2} \tag{2.13}$$

Following Heywood, equivalence ratio was also calculated from measured emissions ($\phi_{emissions}$) using Equations 2.8 through 2.13. These equations are applicable for a fuel of composition $C_mH_nO_r$, considering b/a = m/n. $\tilde{X}_i$ and $\hat{\tilde{X}}_i$ stand for the wet and dry mole fractions of species *i*, respectively. For lean mixtures, the value of water gas shift

www.manaraa.com

reaction co-efficient denoted by K varies between 1.5 and 5.5 and has negligible effects on $\phi_{emissions}$. K was assumed to be 3.5 (average of 1.5 and 5.5) and as all other concentrations can be computed from measured emissions, $\phi_{emissions}$ was calculated using Equation 2.8. The emissions-based calculated equivalence ratio is an independent way to assess the accuracy of the equivalence ratio calculated using the measured fuel and air flow rates, since they are calculated using two completely different methods using different sets of instruments. It may be noted that, at some operating points, the measured values of the HC emissions exceeded the operational limit of the HC analyzer (i.e., above 10000 ppm for the FID) yielding a significant variation in $\phi_{emissions}$. In that case, HC emissions were *recalculated* maintaining $\phi_{emissions}$ within ±5 percent of the equivalence ratio (ϕ) measured from the flow rates of air and fuels. For example, if at any operating condition reported values of ϕ and $\phi_{emissions}$ are 0.27 and 0.35, respectively and HC emissions exceed the limit of 10000 ppm, then HC emissions are recalculated assuming the value of $\phi_{emissions}$ within +5 percent of measured ϕ. It may be noted that get a better *estimation* of ISHC and combustion efficiencies.

2.3 Experimental Matrix

The engine was operated at a fixed speed of 1500 RPM for all experimental results presented in this thesis. A PES sweep was performed at a "conventional" diesel injection timing of 355 CAD for diesel-ignited dual fuel combustion with both of the gaseous fuels while maintaining constant net IMEP, constant rail pressure and constant boost pressure of 5.1 bar, 500 bar, 1.5 bar, respectively. The PES sweep showed that 80 percent is the highest

www.manaraa.com

limit of substitution that would allow SOI and rail pressure sweeps while sustaining relatively stable combustion for both diesel-propane and diesel-methane dual fueling.

Pilot SOI is a very important parameter to achieve LTC conditions to get simultaneous reductions in NO_x and soot emissions, as described earlier. So, the next set of experiments were designed to isolate the effects of SOI keeping all other parameters constant. The PES, rail pressure and boost pressure were maintained at 80 percent, 500 bar and 1.5 bar, respectively, while varying SOI from 355 CAD to 310 CAD. At the SOI of 310 CAD, $ISNO_x$ and soot emissions decreased tremendously from straight diesel operation and reported $ISNO_x$ emissions were well below the US EPA 2010 regulation (0.268 g/kWh). Moreover, better values of IFCE and the possibility of more stable combustion at 310 CAD indicated the suitability of this particular SOI for subsequent sweeps of rail pressure and boost pressure.

Rail pressure (diesel injection pressure) is another important engine control parameter than can be optimized to achieve good performance-emissions tradeoffs. To investigate the effects of rail pressure on dual fuel LTC combustion, a rail pressure sweep was performed by varying the rail pressure from 200 bar to 1300 bar. The SOI was fixed at 310 CAD maintaining the same net IMEP of 5.1 bar, 80 PES and 1.5 bar boost pressure as was done during the SOI sweep. It was that a rail pressure of 500 bar or higher is required to achieve low NO_x emissions.

Finally, a boost pressure sweep was performed from 1.1 to 1.8 bar (in steps of 0.1 bar) maintaining net IMEP and PES. An SOI of 310 CAD and a rail pressure of 500 bar were selected due to very low NO_x emissions at those operating conditions. An experimental test matrix is presented in Table 2.3.

www.manaraa.com

Table 2.3 Experimental Test Matrix for Diesel-Ignited Methane and Propane Combustion

Engine Load (BMEP)	Constant Parameters	Varied Parameter
5.1 bar	SOI = 355 CAD Rail pressure = 500 bar Boost pressure = 1.5 bar	PES = 0 percent to 90 percent
	PES = 80 percent Rail pressure = 500 bar Boost pressure = 1.5 bar	SOI = 355 CAD to 280 CAD
	PES = 80 percent SOI = 310 CAD Boost pressure = 1.5 bar	Rail pressure = 200 bar 1300 bar
	PES = 80 percent SOI = 355 CAD Rail pressure = 500 bar	Boost pressure = 1.1 bar to 1.8 bar

www.manaraa.com

CHAPTER III

DIESEL-PROPANE DUAL FUEL LOW TEMPERATURE COMBUSTION

Diesel-ignited propane dual fuel combustion experiments were performed in a single-cylinder research engine (SCRE), equipped with a common-rail diesel injection system and a stand-alone diesel injection driver to maintain and control the rail pressure and also the timing and duration of diesel injection. Propane was fumigated into the intake manifold and a homogeneous mixture of air and propane entered into the combustion chamber during the intake stroke. First, a PES sweep was performed ranging from 0 to 90 percent at an SOI of 355 CAD which is typical of conventional diesel combustion to determine the baseline standard of performance and emissions. Then, SOI was varied to determine to achieve LTC condition which was determined by simultaneous reduction in NO_x and smoke emissions and SOI of 310 CAD was determined to be the optimal one. The next two set of sweeps of rail pressure and intake boost pressure were performed at 310 CAD SOI to determine the effects of these two important engine control parameters on performance and emissions for diesel-propane dual fuel combustion. All of the sweeps were performed at a constant load of 5.1 bar IMEP and an engine speed of 1500 RPM.

3.1 PES Sweep: Performance and Emissions

The SCRE was operated at a speed of 1500 RPM, a net IMEP of 5.1 bar, and rail pressure, intake boost pressure and injection timing were set to 500 bar, 1.5 bar and 355

www.manaraa.com

CAD respectively without any EGR. The PES was varied from 0 PES (straight diesel operation) to 90 PES for diesel-propane dual fuel operation.

3.1.1 Cylinder Pressure and Net Apparent Heat Release Rate

Figures 3.1 and 3.2 illustrate the effects of PES on cylinder pressure profiles and net AHRR profiles for diesel ignited propane dual fuel combustion. In Figures 3.1(a) and 3.1(b), the increase in pressure due to combustion (compared to the motoring traces) always occurs after TDC. As PES is increased, pressure profiles showed increasingly delayed combustion, ostensibly due to the fact that combustion of the propane-air mixture is slower than diesel combustion.

Two-stage AHRR profiles are observed for all PES while peak heat release rate in first and second stage varied in magnitude and phasing with respect to TDC. Needle lift curves show the SOI as 355 CAD and the AHRR values become negative just after the SOI as fuel vaporization cools the in-cylinder mixture. After SOC, the AHRR rises rapidly due to the energy release from the combustion process, attaining the first peak. Subsequently, the AHRR shows a decreasing trend for some CAD, only to rise again attaining a second peak later in the combustion process. The duration of the second AHRR peak is always longer than the first peak. The AHRR profiles show no significant variation in the CAD where AHRR becomes positive and this observation is also supported by CA5 which is plotted shown in Figure 3.3.

For straight diesel operation (PES = 0 percent), two-stage AHRR is observed with two distinct peaks which is very similar to conventional diesel combustion (Dec 1997). As described by Dec and his co-workers, the first stage of AHRR arises from the premixed burn which is determined by the amount of fuel mixture prepared during the ignition delay

www.manaraa.com

period. The second spike occurs from the mixing controlled burn resulted from the standing premixed flame and is affected by the size of the diffusion flame and the mixing rate of air and fuel inside the combustion chamber.

As PES is increased from 0 percent to 70 percent, the magnitude of the first AHRR peak increases while the opposite trend is observed for the second AHRR peak. Also, the location of the first and second AHRR peaks are always phased after TDC and shift away from TDC as PES of propane is increased. The reason behind the increase of first stage AHRR can be attributed to the entrainment of more premixed propane-air mixture into the diesel jet that burns simultaneously with diesel during the premixed burn. With the increase of PES, the equivalence ratio of the premixed propane-air mixture increases, and in turn also increases the amount of fuel availability (diesel and propane) in the diesel jet. On the other hand, for the second stage peak AHRR, the magnitude is decreased while the duration becomes longer due to the decrease of the surface area of the standing diffusion flame and the availability of more propane fuel for second stage combustion. The diffusion flame arises from the burning of diesel fuel and the reduction in size and surface area of the diffusion flame associated with decreasing PES (i.e., smaller diesel sprays) resulted a slower burn rate in the second stage. Moreover, as propane combustion is slower compared to diesel, an increasing percentage of propane is likely burned during the second stage of the combustion, leading to a longer burn duration.

On the contrary, if PES is increased beyond 70 percent, magnitude of the first stage peak starts decreasing along with the second AHRR peak. The magnitudes are still higher than pure diesel operation and demonstrate the reduction in availability of fuel for the premixed burn. Again, the first AHRR peak decreases with increasing PES beyond 70

www.manaraa.com

percent due to the reduced size of the diesel jets and relatively lower entrainment of the surrounding propane-air mixture into the jets at higher PES. In addition, at higher PES, bulk of the heat release (especially in the second AHRR stage) occurs due to propane combustion, which is considerably slower and leads to lower second AHRR peaks.

www.manaraa.com

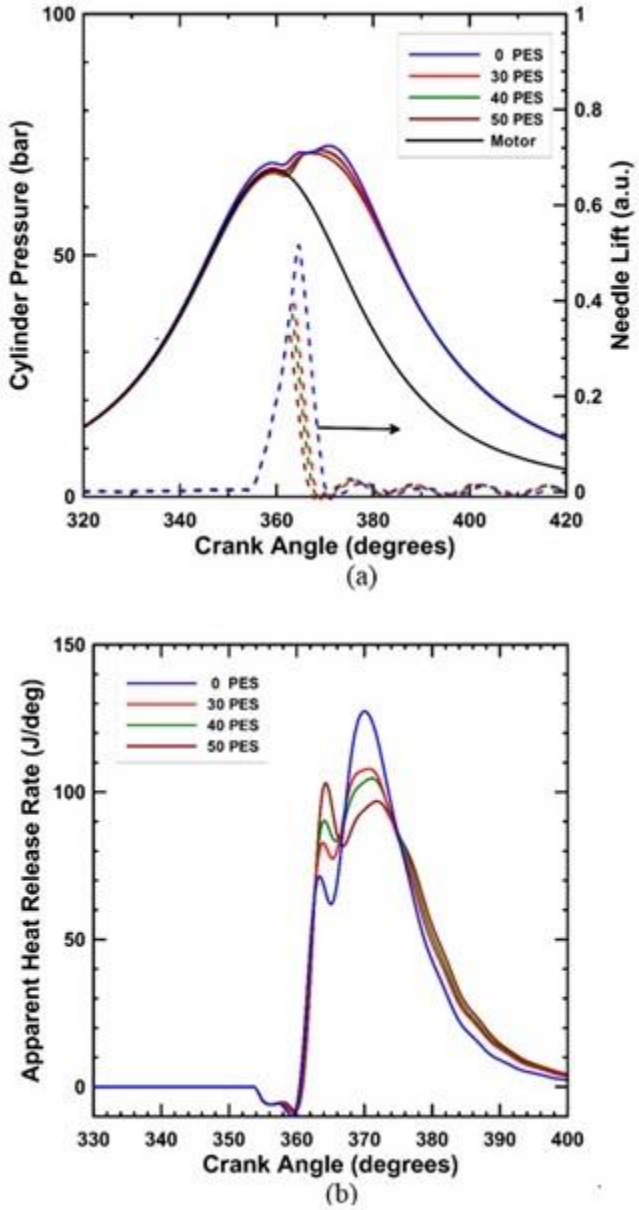

Figure 3.1 Transient data of diesel-propane dual-fueling for 0 to 40 PES

Note: (a) Cylinder pressure and needle lift profiles and (b) net AHRR profiles for 0 to 50 PES at 5.1 bar net IMEP, 1500 RPM, SOI = 355 CAD, P_{rail} = 500 bar.

www.manaraa.com

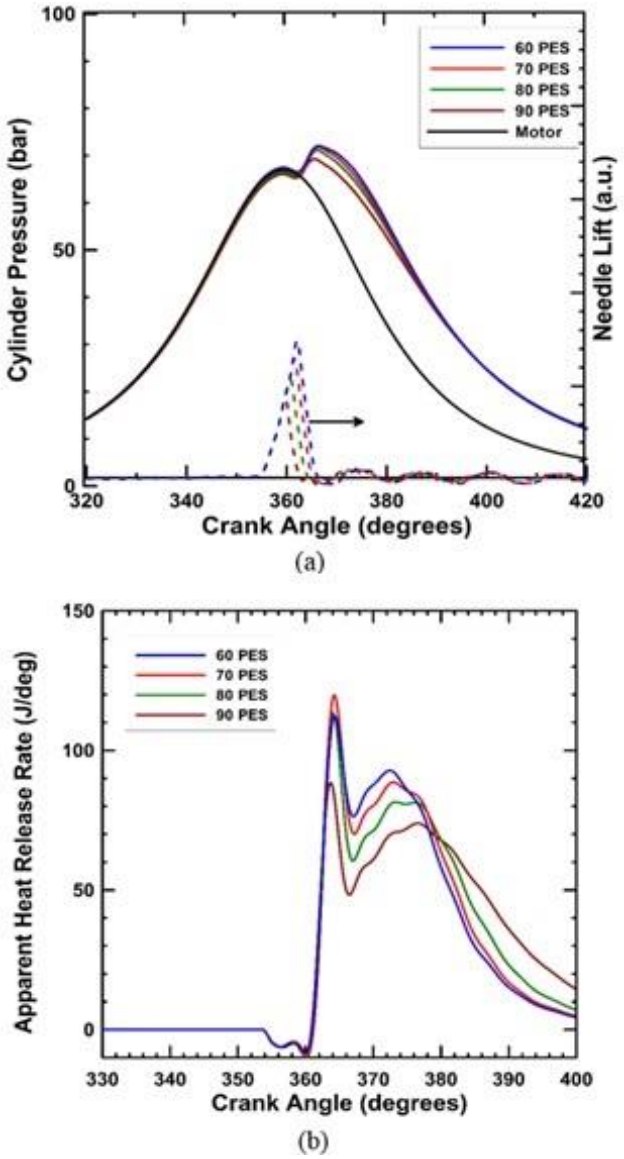

Figure 3.2 Transient data of diesel-propane dual fueling for 60 to 90 PES

Note: (a) Cylinder pressure and needle lift profiles and (b) net AHRR profiles for 60 to 90 PES at 5.1 bar net IMEP, 1500 RPM, SOI = 355 CAD, P_{rail} = 500 bar.

3.1.2 Maximum Pressure Rise Rate, Ignition Delay, Combustion Stability and Combustion Phasing

Figure 3.3 shows the variation of ignition delay, MPRR, and COV of IMEP with increasing propane PES. High MPRR often limits the operation of dual fuel combustion at high loads. However, since the entire PES sweep was performed at a relatively low load

www.manaraa.com

(5.1 bar net IMEP) and SOI was 355 CAD, combustion always started after TDC and peak pressures were relatively low, resulting in very low MPRRs for the entire PES sweep. Ignition delay was nearly invariant (between 8.6 and 8.8 CAD), which is also supported by the CA5 trends (Figure 3.4) and AHRR profiles (Figures 3.1 and 3.2). This suggests that the PES has virtually no effect on the onset of combustion. On the contrary, the COV of IMEP shows an increasing trend and rises steeply beyond 70 PES. While PES was varied from 0 to 70 PES, the COV of IMEP rises steadily from 1.3 percent to 3.1 percent, while beyond 70 PES, it rises very rapidly reaching 6.6 percent at 90 PES. For stable engine operation and vehicle drivability, the COV of IMEP should be less than 5 percent, and the trend shows more instability as PES goes up. Increasing combustion instability at higher PES may be attributed to the slower combustion of propane, which may lead higher cycle-to-cycle variability in combustion phasing, duration, etc.

Figure 3.4 shows the start of combustion (CA5), combustion phasing (CA50), and combustion duration (CA10-90) for different PES. The CA5 remains invariant at 363.5 CAD for all PES while CA50 and CA10-90 display increasing trend. The CA50 shifts away from TDC from 372 CAD at 0 PES to nearly 378 CAD at 90 PES This trend also supports the hypothesis that increasingly more fuel is burned during the second stage of combustion, which occurs later, while maintaining the same SOC. Also, an increase in CA10-90 indicates that combustion occurs for a longer duration at increased PES. The sharp increase of CA10-90 at 80 and 90 PES indicates that the mixture burned slower and the COV of IMEP reflects the same trend depicting the onset of partial misfire.

www.manaraa.com

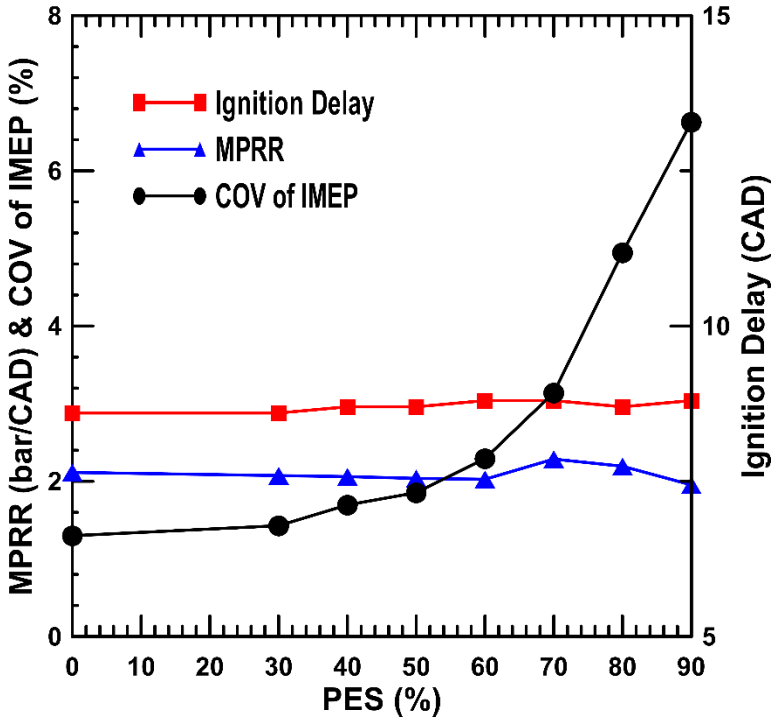

Figure 3.3 Ignition delay, MPRR and COV IMEP versus PES for diesel-propane

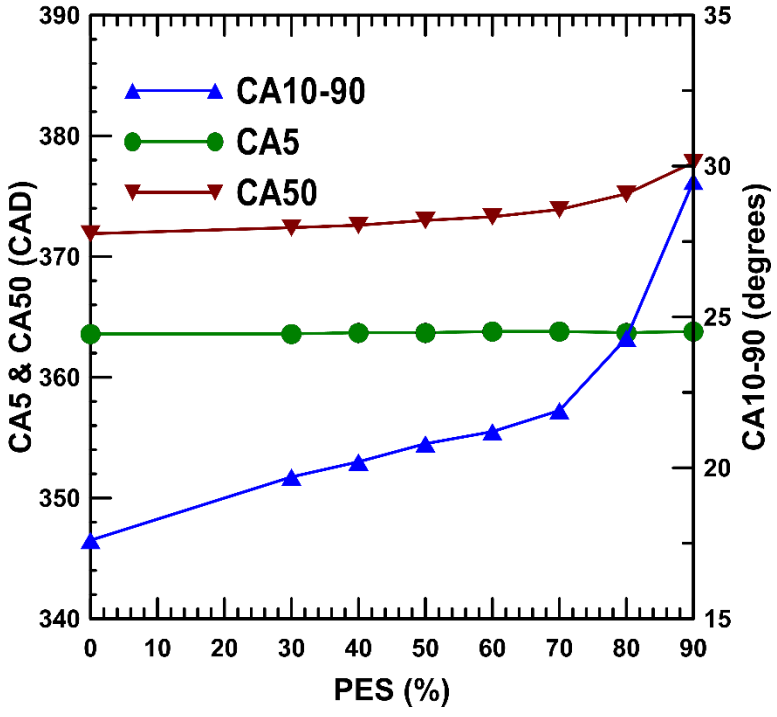

Figure 3.4 CA5, CA50, CA10-90 versus PES for diesel-propane

www.manaraa.com

3.1.3 Fuel Conversion Efficiency and Combustion Efficiency

The BFCE, IFCE, and combustion efficiency trends are shown in Figure 3.5. It is evident from the figure that all of the presented parameters attain maximum values for straight diesel operation and typically decrease with the increase of PES. For straight diesel operation, the combustion efficiency was almost 100 percent and decreased to 60 percent at 90 PES. It must be noted that, only for 80 and 90 PES, the THC emissions reported by the emission bench exceeded the upper limit of measurability of the FID analyzer (10000 ppm). So, for 80 and 90 PES, the THC emissions were recalculated by maintaining the equivalence ratio of emissions within ±5 percent of the equivalence ratio measured using the flow rates of air and fuel (Figure 3.7 and Figure 3.9). With these recalculated THC values, the combustion efficiency was re-estimated only for 80 and 90 PES (shown by the dotted curve in the Figure 3.5). As PES is increased, the diesel jets become smaller and more fuel is present in the surrounding propane-air mixture. Moreover, as the size of the jet is decreased with increasing PES, the diffusion flame present in the periphery of the diesel jet is not capable of burning all of the propane-air mixture remaining in the combustion chamber. This is also supported by the global bulk temperature profiles (Figure 3.8) showing that the temperatures schedules during combustion and expansion become lower for higher PES. All of these factors lead to partial or incomplete oxidation of fuel (HC) and CO, and therefore, poor combustion efficiencies at high PES. In addition, increased combustion instability (misfire) at 80 and 90 PES may also lead to higher HC and CO emissions and low combustion efficiencies.

www.manaraa.com

IFCE and BFCE decrease with increasing PES. The behavior of IFCE and BFCE is affected by both the combustion phasing and the combustion duration. For example, phasing of combustion closer to TDC accompanied by lower combustion duration work favorably in increasing efficiency. CA50 moves gradually toward TDC with decreasing PES, consequently, IFCE increases and attain a maximum value of 45.3 percent at 0 PES. Moreover, CA10-90 increases as PES is increased and bulk of the combustion happens later in the expansion stroke. As a result, bulk of the energy generated during combustion is lost in the expansion process, leading to lower IFCE at higher PES (e.g., about 30 percent at 90 PES).

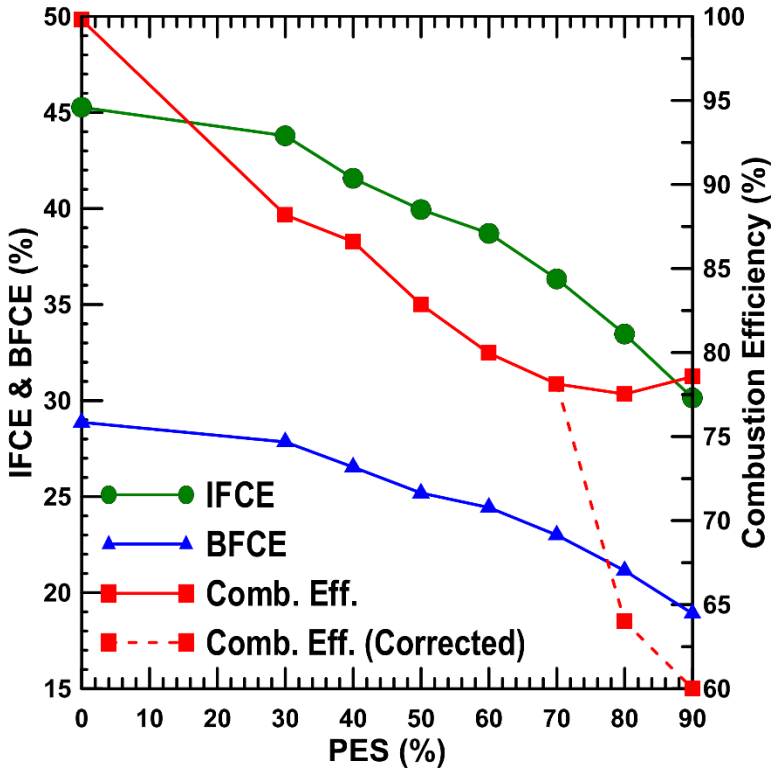

Figure 3.5 IFCE, BFCE and combustion efficiency versus PES for diesel-propane

www.manaraa.com

3.1.4 Emissions, Particle Concentrations and Size Distributions

Figure 3.6 shows indicated specific oxides of nitrogen ($ISNO_x$) and smoke emissions versus PES at 355 CAD injection timing. As PES is increased, $ISNO_x$ emission decreases. The value of $ISNO_x$ reduces from 6.8 g/kWh at 0 PES to 2.35 g/kWh at 90 PES This reduction in NO_x emissions can be attributed to the smaller diesel jets with increasing PES. NO_x primarily forms in the hot, near-stoichiometric mixtures of the diffusion fame surrounding the jet (Dec 1997) and this high temperature region around the jet reduces as the jets become smaller with increasing PES and less diesel fuel is injected into the combustion chamber.

Smoke emissions decrease with the increase of PES except for the two highest PES values. In conventional diesel combustion, soot forms in the rich premixed areas of the diesel jet where equivalence ratio is high (~2-4). Formation of soot can be avoided by keeping the local temperature of the rich premixed regions below 1800 K (Akihama et al. 2001). As PES is increased from 0 PES to 70 PES, only progressively smaller diesel jets can form a region conducive to form soot. As a result, smoke emission decreases from 0.85 FSN to 0.07 FSN at 70 PES. If PES is increased beyond 70, smoke emission increases very slightly but still remains very low compared to straight diesel operation.

www.manaraa.com

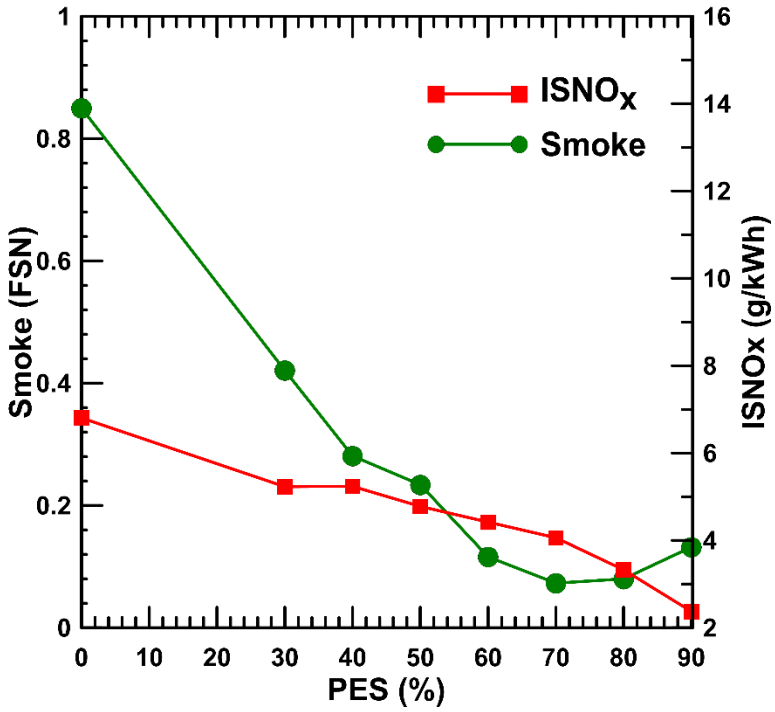

Figure 3.6 $ISNO_x$ and Smoke emissions versus PES for diesel-propane

The effect of increasing PES on HC and CO emissions are plotted in Figure 3.7. As PES is increased, both ISHC and ISCO emissions increase rapidly except for a slight decrease in ISCO emissions between 80 PES and 90 PES. It is evident that ISHC and ISCO emissions are extremely low for straight diesel operation. ISHC increases from 0.4 g/kWh at 0 PES to around 100 g/kWh at 90 PES while ISCO increases from 0.64 g/kWh at 0 PES to 47 g/kWh at 80 PES. However, the actual concentration of ISHC emissions cannot be quantified for 80 and 90 PES because the emissions levels were beyond the capability of the FID analyzer (as mentioned before) and were recalculated from equivalence ratio (Figure 3.9).

ISHC emissions for straight diesel operation are very low compared to dual fuel combustion, indicating that most of the intermediate hydrocarbon species formed during

www.manaraa.com

the combustion process are oxidized in the relatively hotter diffusion flame surrounding the diesel jet. For dual fuel operation, high HC emissions can be correlated to incomplete flame propagation (Karim 1991). As PES is increased, the flame initiated by the ignited diesel fuel becomes progressively smaller and cannot spread far enough or fast enough into the surrounding lean propane-air mixture leading to higher HC emissions. Also, since propane is premixed with intake air, the propane fuel trapped in the crevices can be a significant source of HC emissions in the exhaust, as PES is increased.

In addition, bulk in-cylinder temperature during combustion and post combustion and residence time play a significant role in the oxidation of HC and CO. As shown in Figure 3.8, the overall bulk gas temperatures as well as the peak bulk temperature gradually decrease with the increasing PES. Further, the bulk of the combustion happens later in the expansion stroke for higher PES (Figure 3.4). This reduction in bulk in-cylinder temperature may lead to lower oxidation rate of the original fuel molecules to intermediate HC species, as well as complete combustion of these intermediate species. Increased amount of unburned fuel molecules and partial oxidation of fuel molecules at higher PES, arising from the aforementioned affects, lead to an increase in engine-out HC emissions.

CO is in intermediate combustion species formed during the oxidation process of any hydrocarbon fuel. CO is converted to CO_2 by reacting with OH radicals available throughout the high temperature region in the periphery of the diffusion flame (Dec 1997). CO oxidation rate is slower than the HC oxidation rate (Glassman 1996) and occurs later in the combustion process. This CO oxidation reaction ($CO + OH \rightarrow CO_2 + H$) is strongly dependent on bulk in-cylinder temperature and relatively slow at temperatures below 1100 K (Glassman 1996). As PES is increased, the spatial size of the diffusion flame decreases

www.manaraa.com

and this may result in reduced availability of OH radicals during combustion. Moreover, overall bulk in-cylinder temperatures decrease for dual fuel conditions as PES is increased compared to straight diesel operation. It is more likely that, CO formed in the diesel jet is mostly oxidized in the relatively hotter zones in the periphery of the jet, while only a certain percentage of CO is oxidized which is formed in the lean premixed propane-air mixture. As with the increase of PES, more fuel is burned in the second stage of combustion, leading to higher CO emissions. At 90 PES, CO emissions decrease slightly compared to 80 PES. This can be explained by the increase in combustion duration (Figure 3.4). At this condition, there may also be a competition between HC and CO oxidation and HC emissions rises very rapidly while CO emission decreases. This indicates that the large amount of the fuel molecules are not being oxidized to CO and increased combustion duration (around 30 CAD) allows more CO oxidation to take place despite having a lower peak bulk temperature.

www.manaraa.com

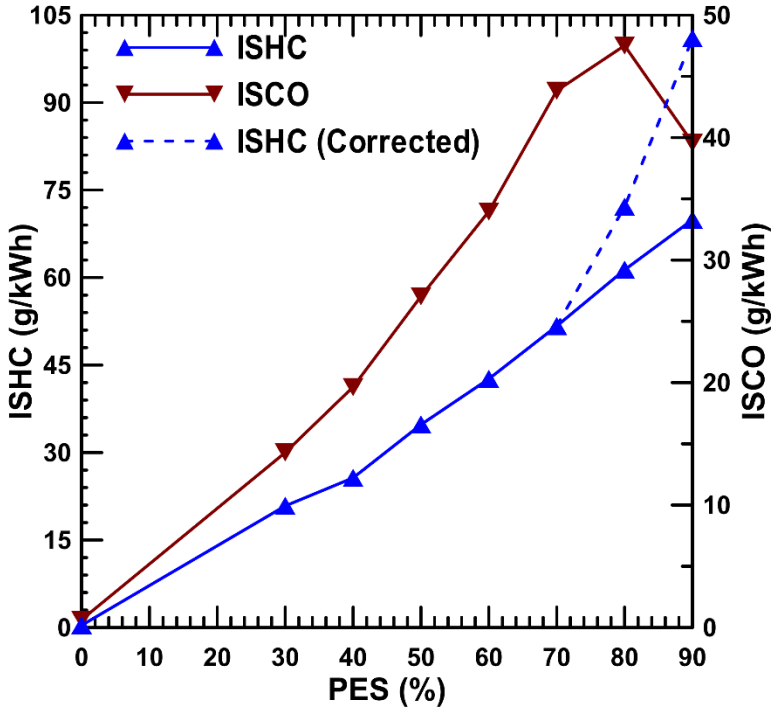

Figure 3.7 HC and CO emissions versus PES for diesel-propane

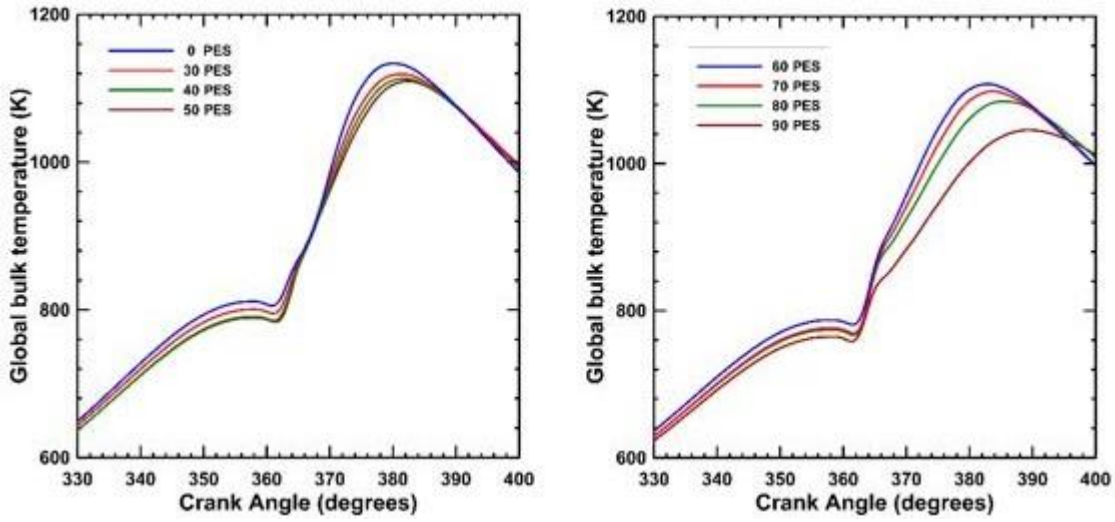

Figure 3.8 Global temperature profiles for various PES for diesel-propane

www.manaraa.com

Figure 3.9 shows the variation in measured and emissions calculated equivalence ratios for various PES. With increasing PES, both of the equivalence ratios progressively increased maintaining within ±5 percent of each other, except for two highest PES cases. At these operating conditions, HC emissions measured by emission bench exceeded operational limit of 10000 ppm resulting in an incorrect HC emissions in the exhaust. At 80 and 90 PES, the calculated ϕ and $\phi_{emissions}$ were 0.368 and 0.410 and 0.320 and 0.329, respectively. Using equations 2.8 through 2.13 and the procedures outlined in Chapter II, HC emissions were recalculated maintaining ±5 percent error limit. Corrected values of $\phi_{emissions}$were set to 0.355 and 0.395, respectively for 80 and 90 PES which were then used in reporting ISHC, IFCE and combustion efficiency.

www.manaraa.com

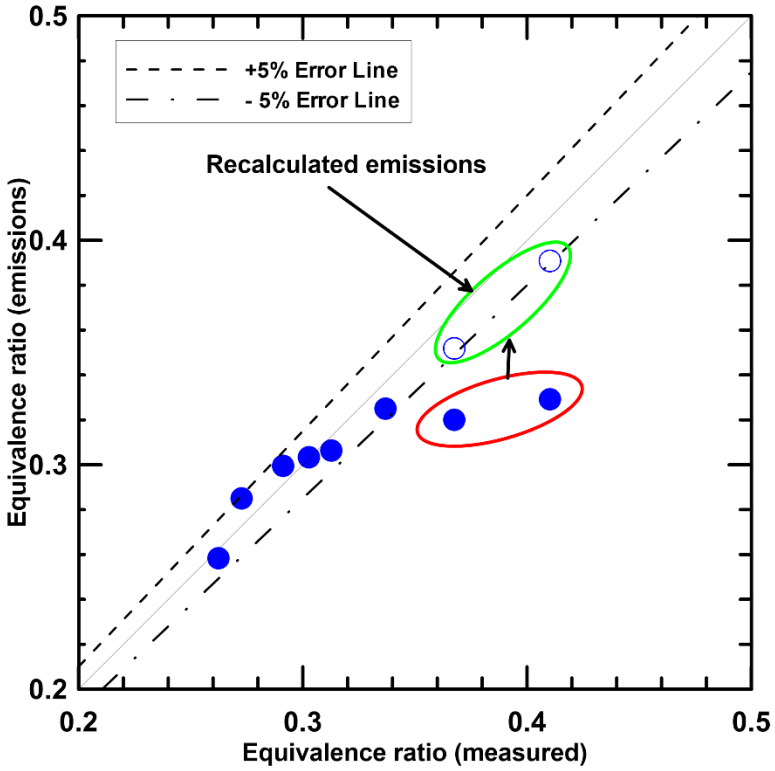

Figure 3.9 Equivalence ratio (emissions) versus equivalence ratio (measured) at various PES for diesel-propane

Figure 3.10 illustrates the effect of PES on particle number concentrations and size distributions. As PES is increased at the fixed SOI of 355 CAD, nanoparticle concentrations (less than 50 nm in diameter) decrease. Concentrations of higher diameter particles decrease slightly with increasing PES, however, relative magnitude of this decrease is order of magnitudes lower compared to nanoparticles. The trend in PM emissions is consistent with the reduced soot emissions in general which is presented earlier (Figure 3.6)

www.manaraa.com

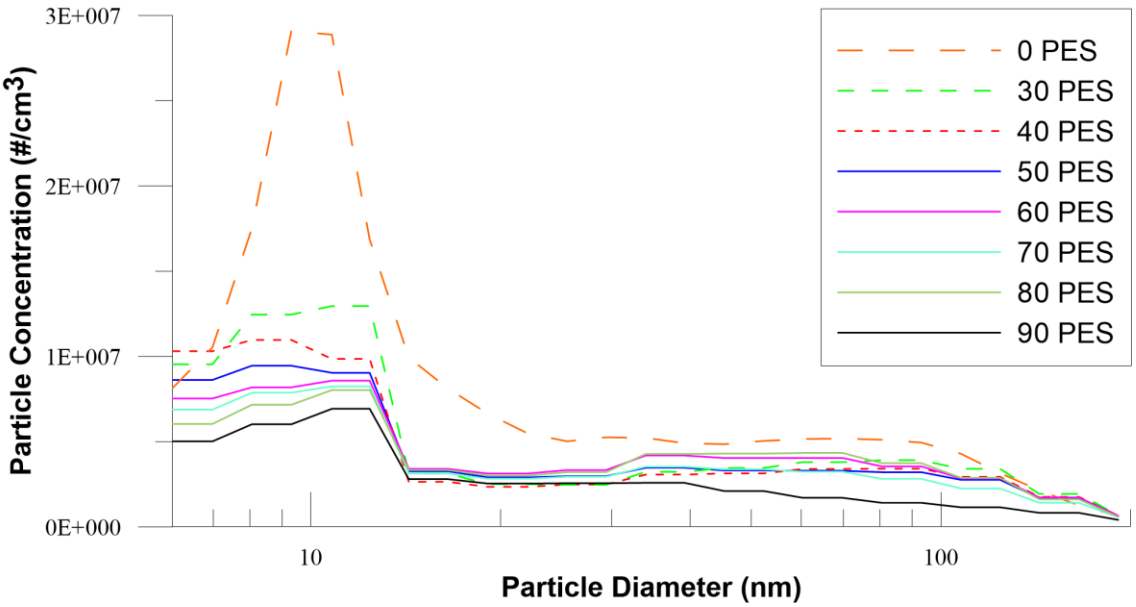

Figure 3.10 Normalized ($dN/dlogD_p$) particle number concentrations and size distribution(D_p) at various PES for diesel-propane

3.2 Injection Timing (SOI) Sweep: Performance and Emissions

For the SOI sweep, the engine was operated at 5.1 bar net IMEP, 1500 RPM and 80 percent of propane substitution while SOI was varied from 355 CAD to 280 CAD. Diesel injection pressure and intake boost pressure were kept constant at 500 bar and 1.5 bar, respectively, and no EGR was used.

3.2.1 Cylinder Pressure and Net Apparent Heat Release Rate

Figure 3.10 and 3.11 illustrate the cylinder pressure and AHRR schedules for various SOIs. As the SOI is advanced from 355 CAD to 280 CAD, the mode of combustion changes from two-stage, diesel-like combustion to single-stage combustion. As SOI is advanced from 355 CAD to 330 CAD, the magnitude of peak pressure increases and the location of peak pressure shifts towards TDC. From SOI of 320 CAD and beyond, the

www.manaraa.com

magnitude of peak pressure and the location of peak pressure start decreasing and shift away from TDC to the latter part of the expansion stroke respectively. Also, SOC advances up to an SOI of 330 CAD and then retards with further SOI advancement.

As SOI is advanced from 355 CAD to 330 CAD, two stage AHRR is observed and more pronounced for advanced SOIs. First stage heat release from the combustion process is more advanced and rises in magnitude in general except for an SOI of 350 CAD. Also, peak of second stage heat release rises in magnitude and reaches maximum for SOI of 340 CAD. For the SOI of 330 CAD, reduction in magnitude of second stage heat release can be explained by the effect earlier onset of combustion process and the combustion duration. Most of the combustion process is almost over even before the piston reaches TDC. Also, the separation between end of injection (EOI) event and SOC is around 5 CAD for an SOI of 330 CAD while for 340 CAD SOI, SOC occurs even before EOI. As a result, the time available for mixing the diesel fuel is more for 330 CAD compared to retarded SOIs which leads to an increase in the heat release during the premixed burn period, while reducing the spike of the second stage burn. Earlier onset of SOC between SOIs of 355 CAD and 340 CAD can be explained with the help of the difference between SOC and EOI and bulk gas temperature. As evident from the needle lift profiles, for retarded SOIs (330 CAD to 355 CAD) there is no or very little separation between SOC and EOI and as the fuel injection event is started and completed near TDC, in-cylinder bulk gas temperatures are high enough to support the autoignition reaction of injected diesel fuel and SOC commences after the ignition delay period. Moreover, as second stage AHRR is phased near TDC for 340 CAD compared to other advanced and retarded SOIs, the relatively higher end-of-compression temperature results in the highest second-stage peak AHRR at 340 SOI.

www.manaraa.com

As SOI is advanced further in the compression stroke, no two-stage AHRR is observed, indicating a more homogeneous combustion process at those SOIs. Also, SOC as well as the location of peak AHRR start retarding (Figure 3.14) while SOI is advanced from 320 CAD to 280 CAD. For an SOI of 320 CAD., magnitude of peak AHRR decreases and is phased before TDC, while for all other more advanced SOIs, the magnitude slightly increases. This is clearly a transition point between diesel like heterogeneous combustion at retarded SOIs and single-stage homogeneous combustion at advanced SOIs. It can be explained with the increased mixing time available to the injected diesel pilot with the surrounding lean propane-air mixture. For example, for SOI of 320 CAD, EOI and SOC occur at 330 CAD and 350 CAD respectively allows sufficient time for mixing to form a more homogenous mixture of diesel-propane-air before reaching autoignition temperature that suppresses two stage heat release representative of diesel fuel. However, it is 'not very well mixed' as proved by the presence of LTHR at that condition. LTHR is exhibited by diesel or diesel-like fuel at temperatures below 850 K (Saxena and Bedoya 2013). For the SOI of 320 CAD, diesel is injected into the cylinder at a much lower temperature and sufficient amount of stratification is still left at 340 CAD when the temperature reaches to support LTHR chemistry. Further advancement in SOI increase the residence time high enough so that the injected diesel becomes 'well-mixed' vanishing the presence of LTHR.

If SOI is advanced beyond 320 CAD, the separation between EOI and SOC increases steadily, indicating the increase in residence time of diesel fuel. Consequently, the magnitude of peak AHRR decreases and shifts towards TDC and a "well-mixed" combustion of diesel-propane is observed. The magnitudes of the peak AHRR as well as peak pressure decrease as the combustion is phased away from TDC in the expansion

www.manaraa.com

stroke due to more homogenous nature of the mixture and relatively lower in-cylinder bulk gas temperature.

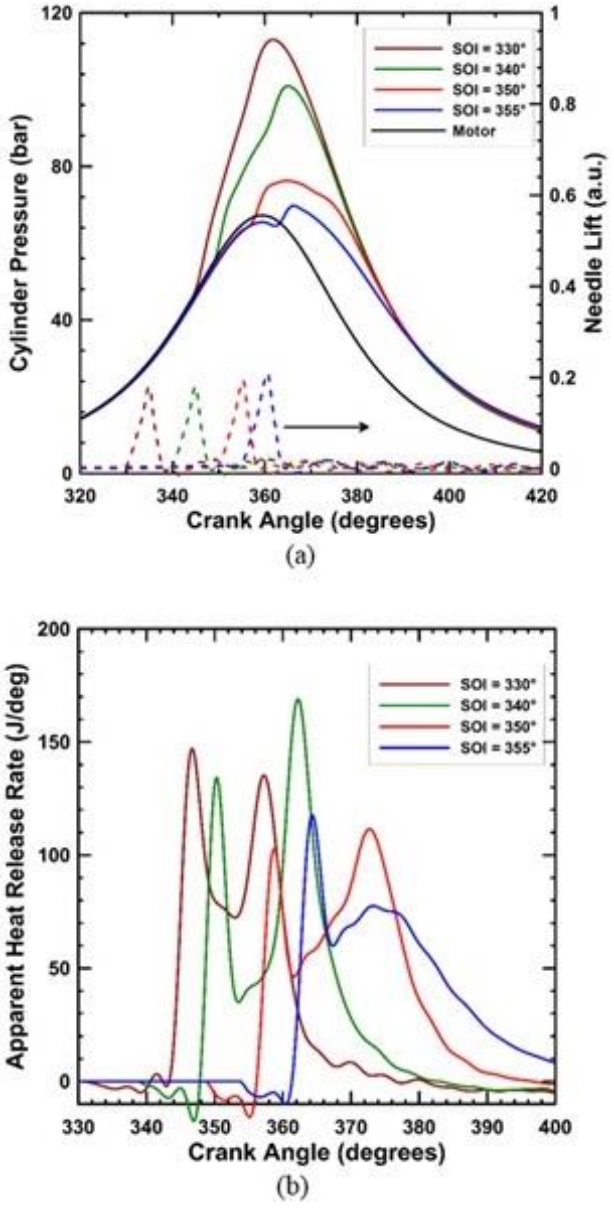

Figure 3.11 Transient data of diesel-propane dual-fueling for late SOIs

Note: (a) Cylinder pressure and needle lift profiles and (b) net AHRR profiles for late SOI at 5.1 bar net IMEP, 80 PES, 1500 RPM, P_{rail} = 500 bar

www.manaraa.com

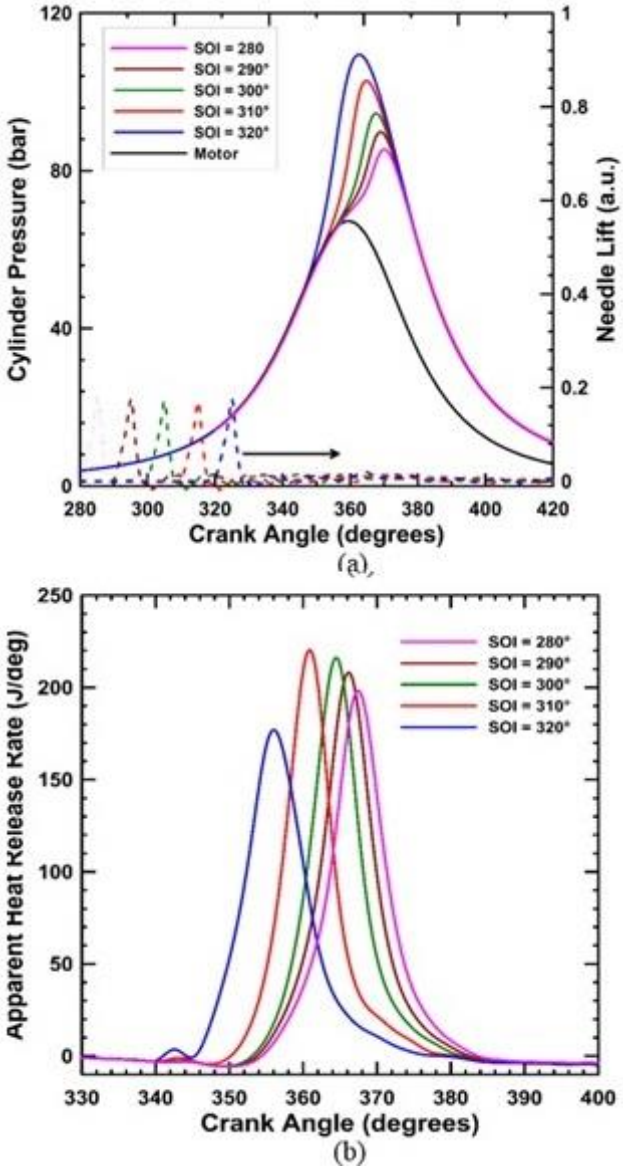

Figure 3.12 Transient data of diesel-propane dual-fueling for advanced SOIs

Note: (a) Cylinder pressure and needle lift profiles and (b) net AHRR profiles for advanced SOIs at 5.1 bar net IMEP, 80 PES, 1500 RPM, P_{rail} = 500 bar.

3.2.2 Maximum Pressure Rise Rate, Ignition Delay, Combustion Stability and Combustion Phasing

Figure 3.13 shows the ignition delay, MPRR and COV of IMEP, and Figure 3.14 shows SOC, combustion duration and combustion phasing with respect to different SOIs.

www.manaraa.com

As SOI is advanced from 355 CAD to 340 CAD, MPRR increases from 3.3 bar/CAD to 8.8 bar/CAD and decreases for any further advancement. Combustion duration (CA10-90) decreases significantly from 25.3 degrees at 355 CAD to 9.9 degrees at 310 CAD, and remains invariant beyond that. For SOIs between 355 CAD and 340 CAD, SOC occurs early in the compression stroke and phasing of combustion shifts towards TDC. Moreover, the decrease in CA10-90 along with two the aforementioned affects allow the combustion process to occur much faster, which is exhibited by the increase in magnitude of second stage AHRR. CA50 shifts from after TDC to before TDC when SOI is advanced from 360 CAD to 330 CAD and then shifts back after TDC with further SOI advancement. When SOI is advanced beyond 330 CAD, increased ignition delay allows more residence time for the diesel fuel, creating 'well mixed' conditions that eventually transform the combustion process from heterogeneous diesel-like combustion to homogeneous HCCI-like combustion. This transformation causes the shifting of SOC again towards TDC, and as CA10-90 is more or less constant at these conditions lead to relatively lower MPRR.

The combustion process becomes relatively unstable if the SOC is advanced beyond 300 CAD or retarded after 340 CAD as shown by the COV of IMEP. It may be attributed to the 'overly mixed' nature of the combustion process at advanced SOIs or relatively late combustion phasing for retarded SOIs, which increase the number of partial misfire cycles.

www.manaraa.com

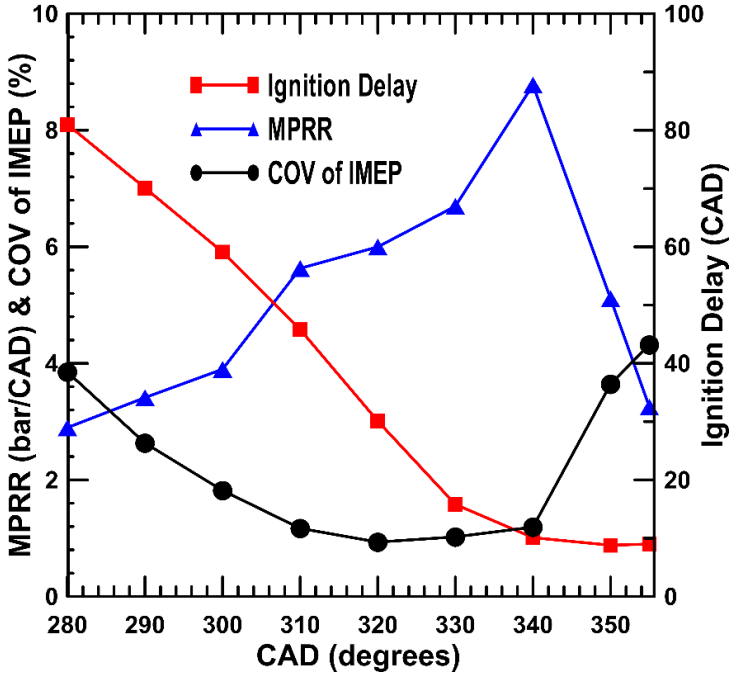

Figure 3.13 Ignition delay, MPRR and COV IMEP versus SOI for diesel-propane

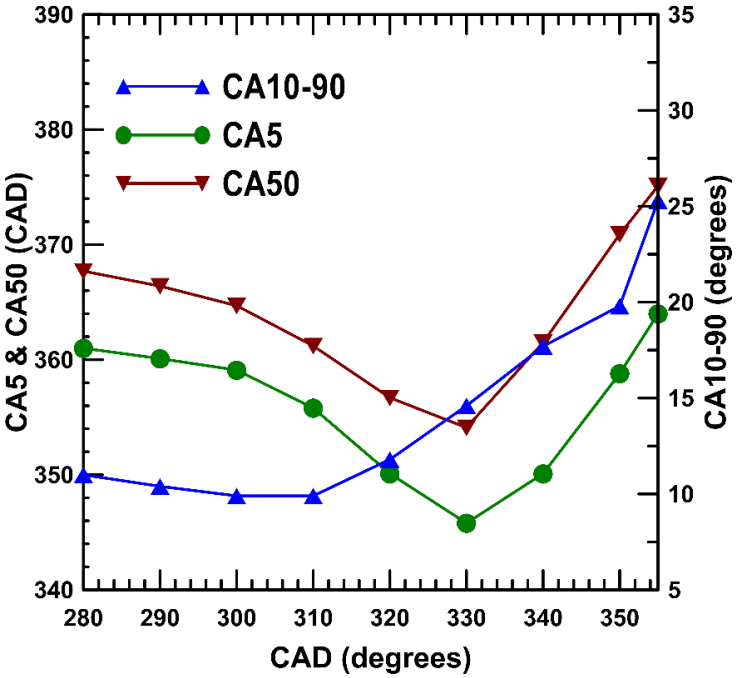

Figure 3.14 CA5, CA50, CA10-90 versus SOI for diesel-propane.

www.manaraa.com

3.2.3 Fuel Conversion Efficiency and Combustion Efficiency

IFCE and combustion efficiency sharply increase with the advancement of SOIs form 355 CAD to 340 CAD. The sharp increase in combustion efficiency and IFCE can be the attributed to the phasing of CA50 closer to TDC (Figure 3.14) and the increase in global in-cylinder temperature (Figure 3.18 a) which lead to a more complete combustion. As SOI is advanced beyond 340 CAD, combustion efficiency reaches a peak value of 92 percent at 330 CAD and slightly decreases with any further advancement in SOIs. Slight decrease in combustion efficiency and IFCE at more advanced SOIs can be caused by 'well mixed' nature of the combustion and moving away of CA50 later in the cycle.

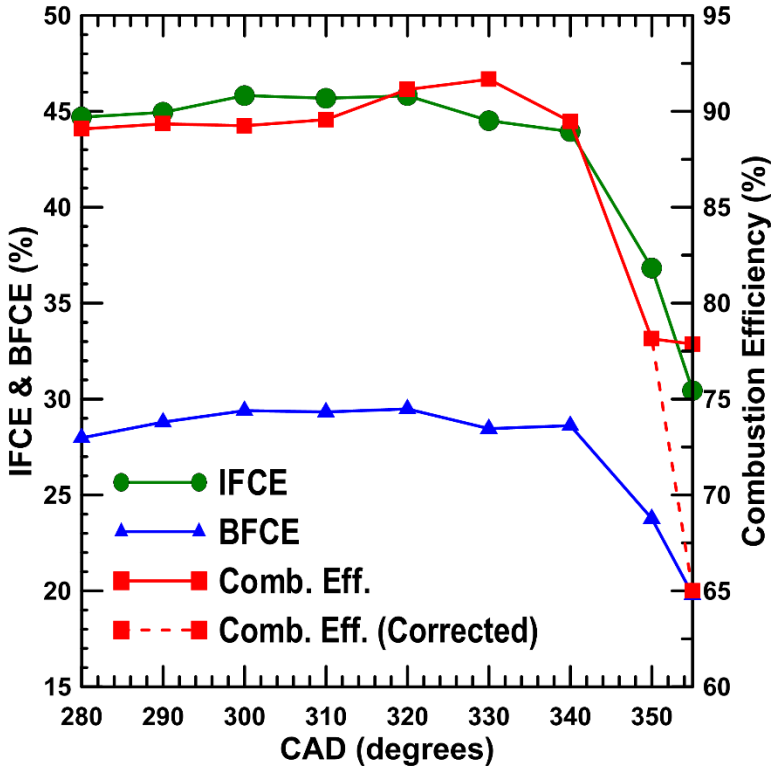

Figure 3.15 IFCE, BFCE and Combustion Efficiency versus SOI for diesel-propane

www.manaraa.com

3.2.4 Emissions, Particle Concentrations and Size Distributions

$ISNO_x$ and smoke trends are illustrated at Figure 3.16 with respect to SOIs. $ISNO_x$ increases sharply from 3.5 g/kWh at 355 CAD to 9.4 g/kWh at 340 CAD. However, further advancement in SOIs lead to a sharp decrease in $ISNO_x$ emissions reaching 0.12 g/kWh at 310 CAD and remain very low for rest of the sweep. The initial sharp increase in $ISNO_x$ can be explained by analyzing the separation between SOC and EOI and time available to injected diesel fuel for mixing with the surrounding lean propane-air mixture. For retarded SOIs (355 CAD – 340 CAD), combustion shifts earlier and very little or no separation is available between SOC and EOI. As a result, the air-fuel mixture remains stratified when combustion starts after an ignition delay period resulting in a higher local temperature. On the other hand, for SOIs of 320 CAD and beyond, enough separation between SOC and EOI create relatively homogeneous lean air-fuel mixture. Near-zero ISNOx levels for sufficiently early SOIs are the cumulative effects of increased residence times, separation between EOI and SOC, and more complete fuel-air mixing, all of which lead to low local temperatures.

Smoke emissions gradually decrease from 0.1 FSN to 0.02 FSN with the advancement of SOIs. The reduction in smoke emissions at advanced injection timings is the direct consequence of high PES of propane substitution coupled with more homogenous nature of predominantly lean air-fuel mixture under these operating conditions.

www.manaraa.com

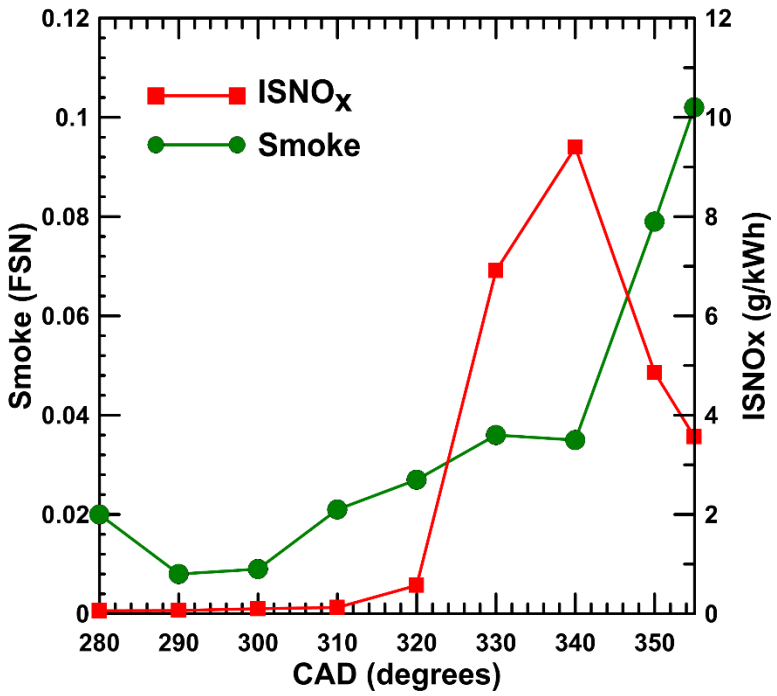

Figure 3.16 Smoke and $ISNO_x$ versus SOI for diesel-propane.

Figure 3.17 shows the variations in ISHC and ISCO emissions as well as peak bulk temperature versus SOI. Except for the SOI of 350 CAD, ISHC and ISCO emissions both decrease up to an SOI 0f 330 CAD. ISHC emissions decrease from 77 g/kWh to around 15 g/kWh while ISCO decreases from 46 g/kWh to around 11 g/kWh. Any further advancement in SOIs, does not yield any significant variation in ISHC emissions; however, ISCO emissions increase again to around 33 g/kWh at 280 CAD SOI. The trends can be explained by analyzing the residence times of high temperature regions (due to combustion) and bulk temperature profiles,

As the entire timing sweep is performed at high propane substitution of 80 percent, unburned propane trapped in the crevices is likely one of the major sources of HC emissions. Residence time and bulk temperature play important roles to oxidize HC and

www.manaraa.com

CO formed during the combustion process. As mentioned earlier, CO is an intermediate combustion species formed from the oxidation of HC molecules and rate of CO oxidation is directly proportional to the formation of OH radicals which can only be formed in high temperature regions. For complete oxidation of CO to CO_2, local temperatures of at least 1500 K are needed (Sjöberg & Dec 2005) along with sufficient residence times. This critical CO oxidation temperature is independent of the nature of the hydrocarbon fuel because the reaction chemistry ($CO + OH \rightarrow CO2 + H$) is fuel independent.

Now, the peak bulk gas temperatures for different SOIs between 355 CAD and 330 CAD are 1050 K (355 CAD), 1135 K (350 CAD), 1253 K (340 CAD) , 1342 K (330 CAD) and decreases with further advancement and reaches the value of 1200 K at 280 CAD. As the peak temperature significantly increases between 355 CAD and 330 CAD, a steep decrease in ISCO is observed except for 355 CAD. Despite having higher peak temperatures at 350 CAD than 355 CAD, the increase in ISCO emission is due to the competing effect of peak bulk temperature and residence time. CA10-90 decreases significantly from 25.3 CAD to around 20 CAD, and this counteracted the effect of higher bulk temperature at that operating point and is manifested by higher CO emissions in the exhaust.

For SOIs between 330 and 280 CAD, ISCO emissions increase as a direct consequence of the decrease in peak bulk temperature from 1342 K to 1200 K for the advanced SOIs. However, ISHC emissions remain more or less invariant.

Figure 3.19 compares equivalence ratios estimated from the emissions measurements and flow rate measurements. This plot is a measure of the relative consistency of the presented data as equivalence ratio is calculated using two completely

www.manaraa.com

different methods employing different set of instruments. Similar to PES sweep, the THC emissions at only one operating point (355 CAD) exceeded operational limits of emission bench. So, THC emissions are recalculated (shown by the dotted curve in the Figure 3.19) keeping equivalence ratio of emissions within ±5 percent of the equivalence ratio measured from the flow rates of air and fuel. This also affects the combustion efficiency and ISHC emissions and are presented with dotted lines as well in their respective figures. *It must be emphasized that the recalculation of THC emissions (only where needed) from equivalence ratio is done to present a better estimation of THC emissions and may vary significantly from actual ones.*

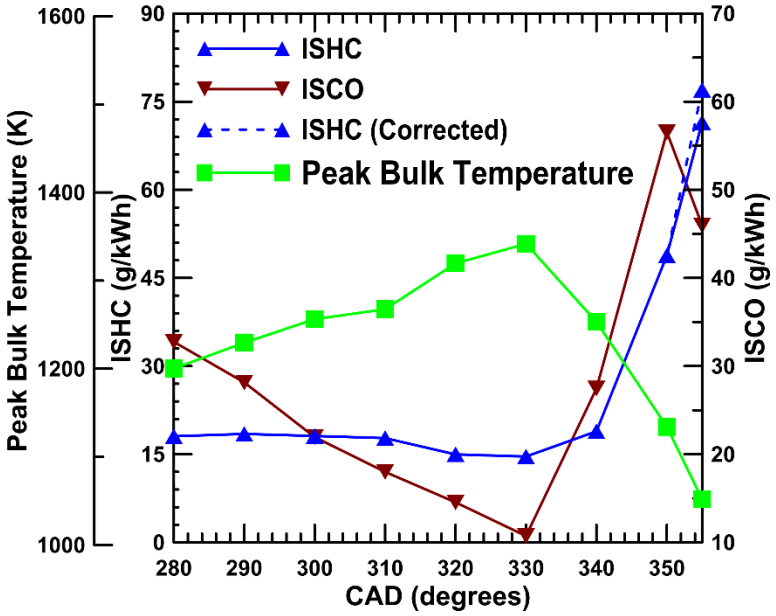

Figure 3.17 ISHC ,ISCO and peak bulk temperature versus SOI for diesel-propane

www.manaraa.com

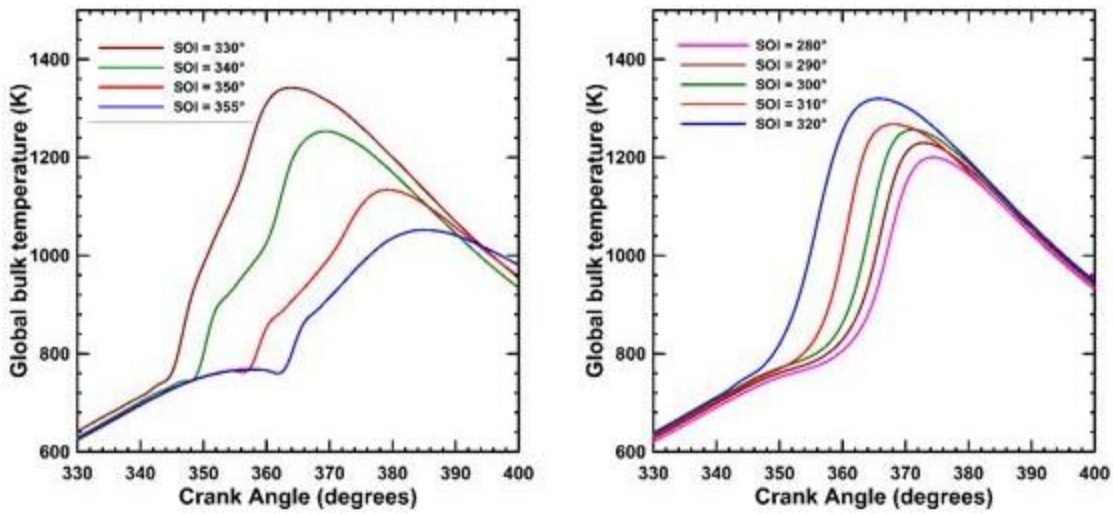

Figure 3.18 Global temperature profiles at various SOIs for diesel-propane

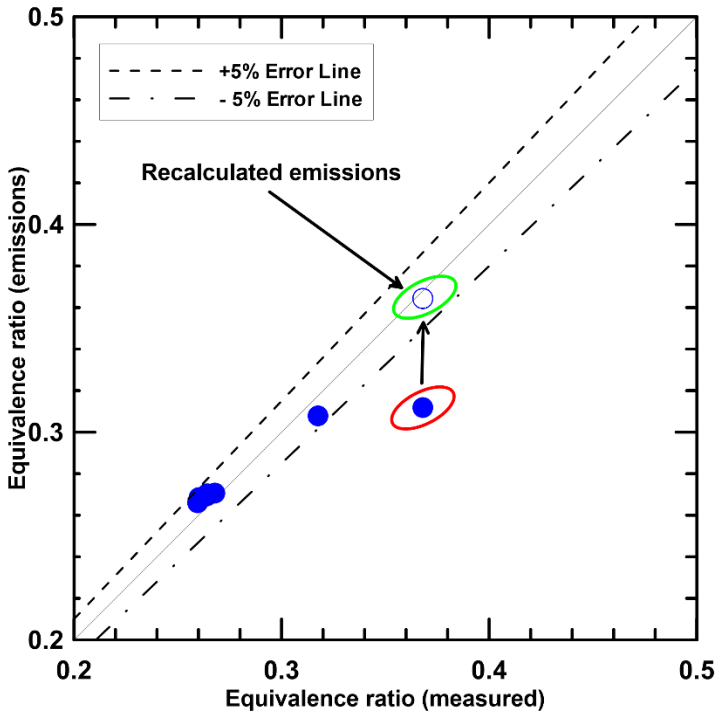

Figure 3.19 Equivalence ratio (emissions) versus equivalence ratio (measured) at various SOIs for diesel-propane

www.manaraa.com

Figure 3.20 illustrates the effect of SOIs on particle number concentration and size distribution. It is evident from the figure that nanoparticles having diameters between 5 nm to 20 nm have the highest concentrations and fewer particles form with higher diameters. It is likely due to the higher percentage of propane substitution and relatively simpler molecular structure of propane compared to diesel. In general, as SOI is advanced, particle concentrations in the aforementioned nanoparticle zones decrease due to more homogeneous nature of the combustion while particles having higher diameters exhibit more complex trend. The only exception to this decreasing trend is shown at an SOI of 350 CAD which needs further investigation. The trend is consistent with the reduced smoke emissions trends presented earlier in Figure 3.16.

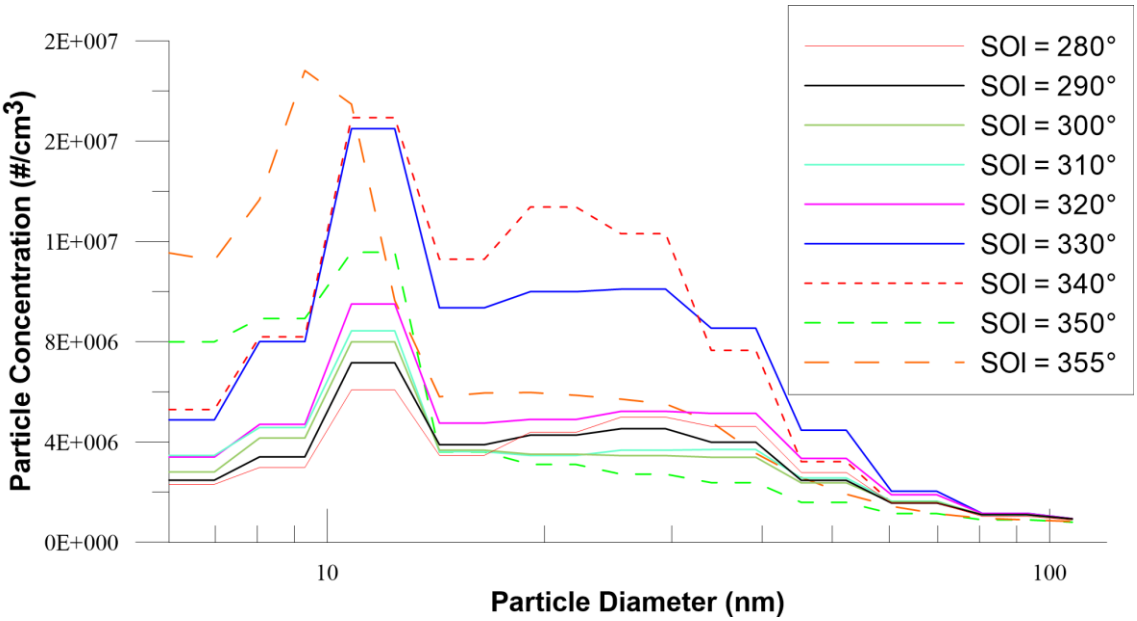

Figure 3.20 Normalized particle number ($dN/dlogD_p$) concentrations and size distribution (D_p) at various SOIs for diesel-propane.

www.manaraa.com

3.3 Rail Pressure Sweep: Performance and Emissions

Rail pressure is another important engine parameters which is being successfully used to optimize the nature of emissions in a diesel engine. To isolate and better understand the effects of rail pressure in LTC conditions, an SOI of 310 CAD and 80 percent of propane substitutions were chosen, as in this operating condition both NO_x and smoke emissions are lower indicative of LTC. Boost pressure was set to 1.5 bar while the injection pressure was varied from 200 bar to 1300 bar.

3.3.1 Cylinder Pressure and Net Apparent Heat Release Rate

Cylinder pressure and AHRR profiles are presented in Figure 3.21 and Figure 3.22 along with needle lifts for a range of rail pressure between 200 bar and 1300 bar. As rail pressure is increased, peak pressure reduces in magnitude and shifts away from TDC. The AHRR profiles show interesting trend by exhibiting two stage heat release from premixed and mixing controlled burn, respectively, only at 200 bar of rail pressure. Further increase in rail pressure changes the combustion to be predominantly premixed as exhibited by single stage heat release. When rail pressure is increased from 200 to 600 bar, magnitude of AHRR increases while shifting away to the latter part of the combustion cycle. However, increasing rail pressures from 800 bar and 1300 bar, a reverse trend is observed.

Ignition delay time progressively increases with the increase of rail pressure (Figure 3.23) and very low values of COV of IMEP indicates the stability of the combustion process. As diesel pilot is injected at 310 CAD and sufficient amount of mixing time is available for all operating conditions. The only contributing factor that can govern the mixing rate of diesel fuel with surrounding propane-air charge is the value of rail pressure. The rate of entrainment of the charge into the diesel jet is proportional to the fuel jet exit

www.manaraa.com

velocity, the nozzle orifice diameter, the axial distance of the liquid length from the injector tip and densities of the fuel and air (Siebers 1999). In this particular set of experiment, only velocity of the affects the rate of entrainment as parameters control the nozzle orifice diameter (same injector) and density (SOI) were kept constant and axial distance of liquid length is invariant to the rail pressures of 200 bar and above. So, as the rail pressure is increased from 200 bar to 1300 bar, the rate of entrainment increases due to jet induced turbulence resulted from higher injection velocities. This enhances the vaporization of diesel jet at a faster rate, and also allows better mixing. As a result, the mixture of air-fuel becomes increasingly homogenous and affects the rate of combustion. Moreover, rail pressure of 1300 bar has relatively less mixing time compared to 1300 bar. As it is seen from the needle lift profiles, the difference in EOI between these two points is almost 7 CAD (323 CAD for 200 bar while 316 CAD for 1300 bar). So, availability of increased mixing at 1300 bar favors more homogeneity, and therefore, affects the nature of combustion.

In light of this above discussion, the trends in AHRR can be explained as follows. As injection pressure is increased from 200 bar to 600 bar, entrainment rate increases significantly resulted from the jet induced momentum and is supported by the relatively steeper increase in ignition delay period. The combustion also phases towards TDC and reaches just after TDC at the rail pressure of 600 bar (Figure 3.24). Upon further increase of rail pressure, enhancement in the entrainment is still there but may not affect the nature of combustion that much, and as a result variation in SOC (CA5) becomes marginal. The lowest entrainment rate along with residence time lead to a 'relatively heterogeneity' in the

www.manaraa.com

mixture and start the combustion process much earlier than any other operating points exhibited by the two stage heat release.

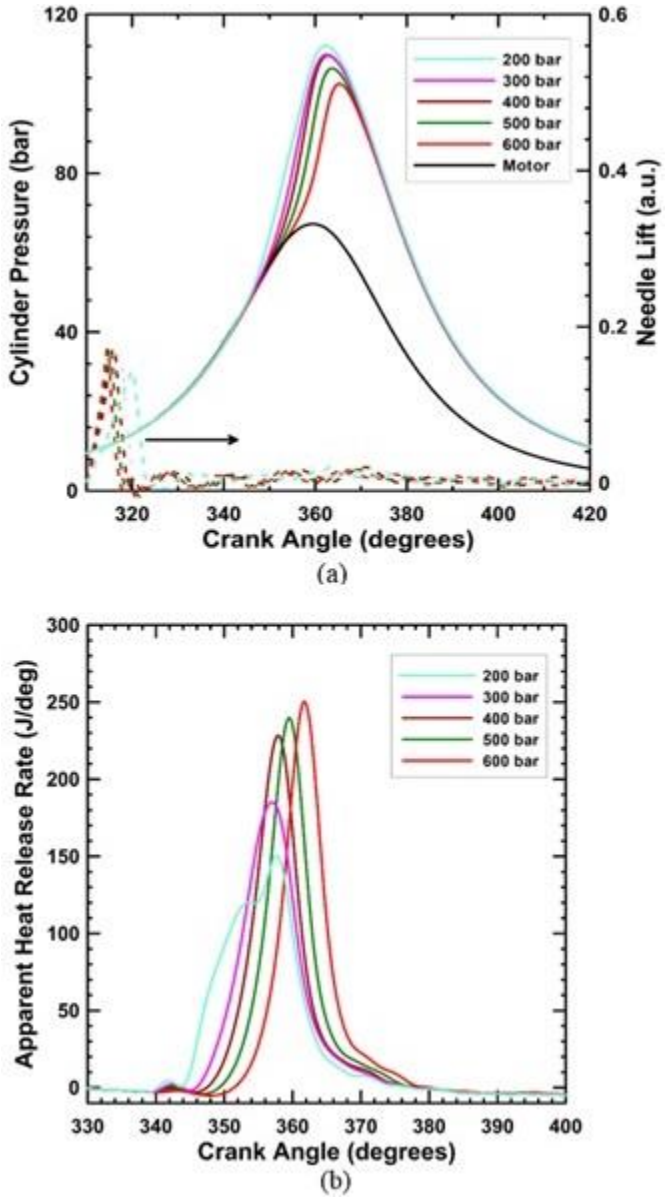

Figure 3.21 Transient data of diesel-propane dual fueling at lower injection pressures

Note: (a) Cylinder pressure and needle lift profiles and (b) net AHRR profiles for 200 to 600 bar of rail pressure at 5.1 bar net IMEP, 80 PES, 1500 RPM, SOI = 310 CAD

www.manaraa.com

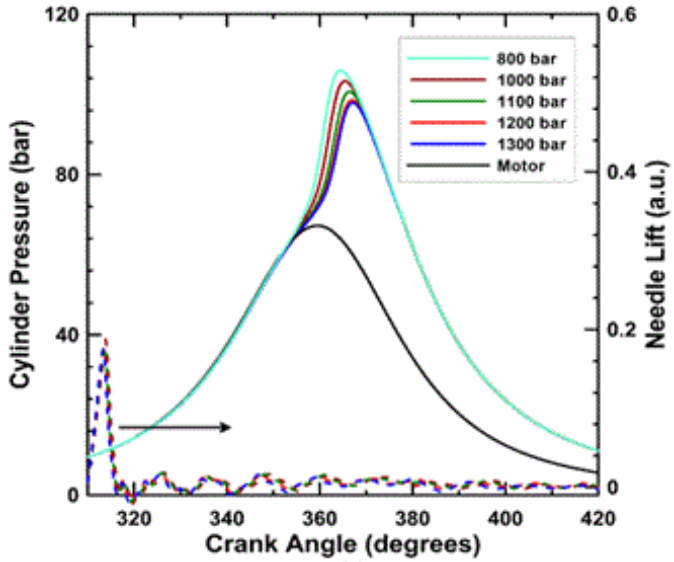

(a)

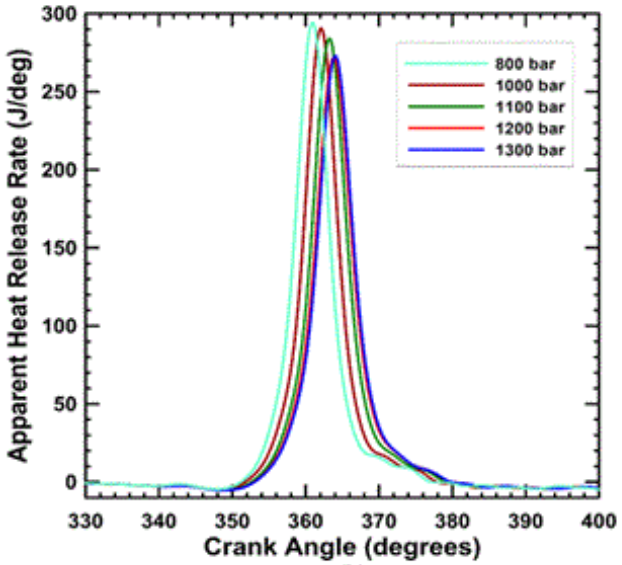

(b)

Figure 3.22 Transient data of diesel-propane dual fueling at higher injection pressures

Note: (a) Cylinder pressure and needle lift profiles and (b) net AHRR profiles for 800 – 1300 bar of rail pressure at 5.1 bar net IMEP, 80 PES, 1500 RPM, SOI = 310 CAD

3.3.2 Maximum Pressure Rise Rate, Ignition Delay, Combustion Stability and Combustion Phasing

MPRR attains a maximum value of 7.6 bar/CAD at a rail pressure of 800 bar, and generally decreases if deviates from this operating point. This is also reflected in the

www.manaraa.com

AHRR profiles exhibiting the highest peak heat release rate. This increase in AHRR are the cumulative effects of CA5 and CA50 moving closer to TDC and just after TDC, respectively. Ignition delay increases sharply from 37.5 CAD at 200 bar to almost 48 CAD at 600 bar, after which rate of increase becomes marginal. The reason behind this trend is already explained in the previous paragraphs.

CA5 and CA50 occur later part of the cycle with any increase in the rail pressure due to presence of more homogeneity in the mixture. However, CA10-90 decreases sharply from 13.2 CAD at 200 bar to 7.5 CAD at 800 bar of rail pressure. This can be explained by analyzing SOC, combustion phasing and bulk temperature. Between 200 to 600 bar, CA5 and CA50 shifts towards TDC and bulk temperature from compression are relatively higher. This trend with increased homogeneity in the mixture forces the combustion to release energy at a much faster rate, hence, a sharp decrease in combustion duration. After that, as discussed earlier, the increase in homogeneity becomes minimal, and as SOC is already very near to TDC and CA50 shifts latter in the expansion stroke, CA10-90 becomes invariant to rail pressure.

www.manaraa.com

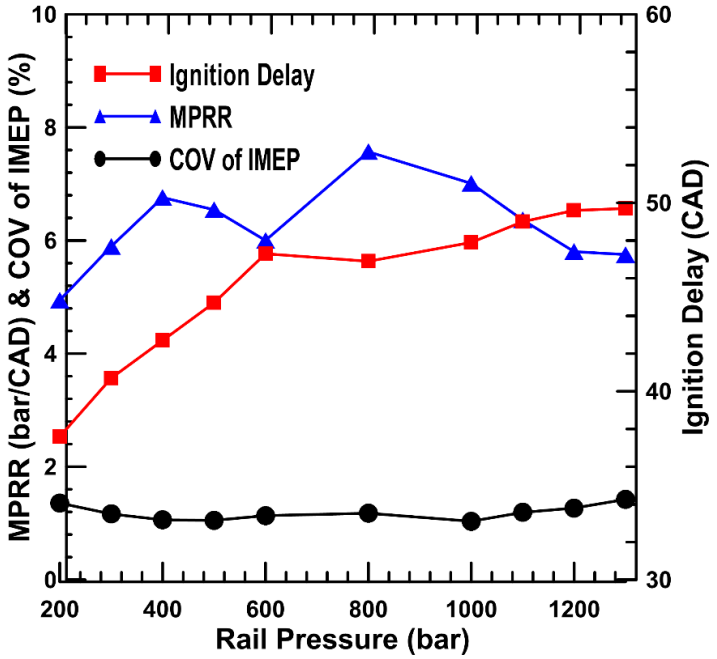

Figure 3.23 Ignition delay, MPRR and COV IMEP versus rail pressures for diesel-propane

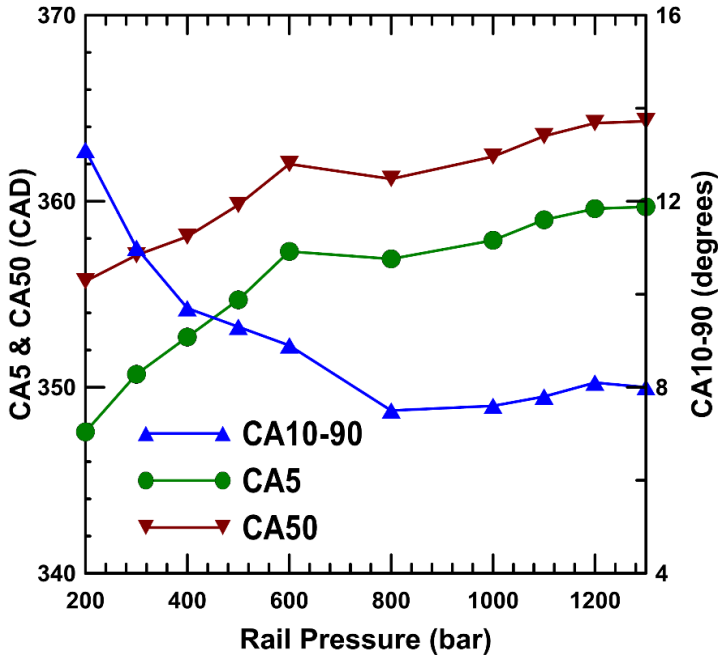

Figure 3.24 CA5, CA50, CA10-90 versus rail pressures for diesel-propane

www.manaraa.com

3.3.3 Fuel Conversion Efficiency and Combustion Efficiency

As shown Figure 3.25 variation IFCE is marginal with increased injection pressure. IFCE varies from 45.9 percent at 200 bar to 46.9 percent at 1300 bar while the highest IFCE of 47.5 percent was achieved for 1000 bar of rail pressure. This trend can be explained by analyzing combustion phasing and combustion duration. Combustion is accompanied by the retardation of CA50 before TDC to after TDC, and also by the steep reduction of combustion duration. As a result, lesser amount of work are required during compression for higher rail pressures. Moreover, as explained earlier, IFCE generally increases with the decrease in combustion duration and phasing of CA50 near TDC. For the rail pressure of 1000 bar, CA50 appears to be the closest to TDC and has lowest combustion duration, therefore, a slight increase in IFCE is observed. CA10-90 becomes more or less constant for rail pressures over 1000 bar and combustion is phased slightly latter resulted in losing some of the work being produced in the expansion stroke, and hence, a slight reduction in IFCE.

Combustion efficiency varies between 88 percent and 91 percent, and the lowest value of 88.4 percent is observed for 600 bar rail pressure. As the combustion efficiency, is a direct consequence of HC and CO emissions in the exhaust, the trends, if there is any, will be explained in conjunction with ISHC and ISCO emissions.

www.manaraa.com

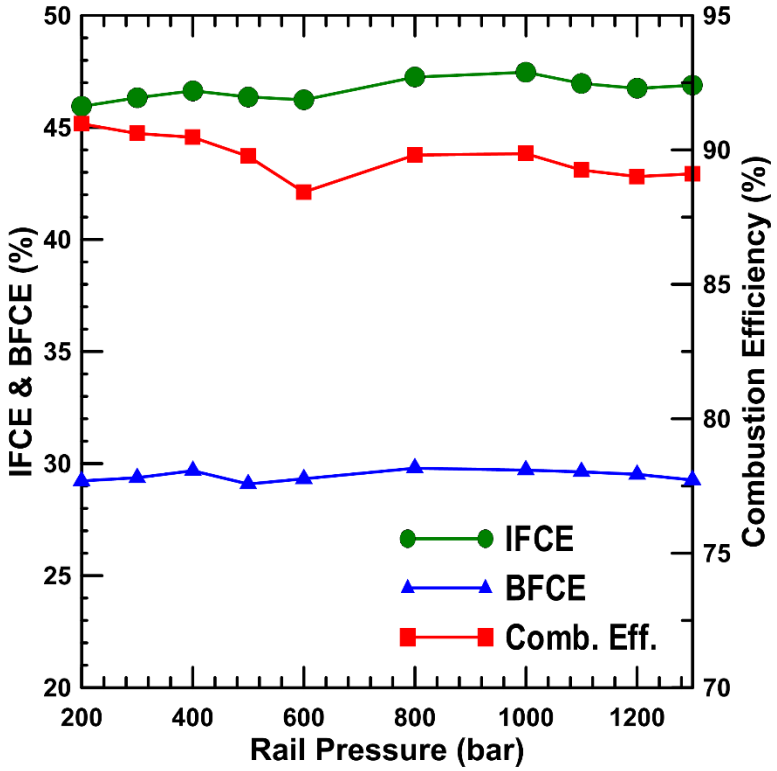

Figure 3.25 IFCE, BFCE and Combustion Efficiency versus rail pressures for diesel-propane.

3.3.4 Emissions, Particle Concentrations and Size Distributions

ISNO$_x$ decreases almost exponentially from 2.4 g/kWh at 1300 bar to near-zero level (0.12 g/kWh) at 500 bar satisfying the US EPA limit of 0.268 g/kWh, as mentioned earlier. Further increase in rail pressures helped to lower the ISNO$_x$ emissions even further, even though, only a slight decrease is noticeable. Extremely high level of ISNO$_x$ at 200 bar can be attributed to the lower rate of entrainment and decreased separation time between SOC and EOI at that condition which in turn allow more heterogeneity in the air-fuel mixture. As a result, the combustion is probably more stratified and characterized by high local temperatures that favor thermal NO$_x$ formation. On the other hand, as injection

www.manaraa.com

pressure increases, the separation between EOI and SOC increases, and enhanced rate of entrainment allows the diesel pilot to mix more completely with the surrounding propane-air mixture before the onset of combustion. As a result, the ignition delays are longer and combustion becomes increasingly homogeneous which inhibits thermal NO_x formation.

Smoke emissions also show a progressively decreasing trend again due to more homogeneous nature of combustion. However, it must be kept in mind that the smoke numbers are already significantly lower than straight diesel operation having a value of FSN of 0.85 (0 PES), and therefore, this may not be an actual trend due to very low magnitudes of these reported emissions

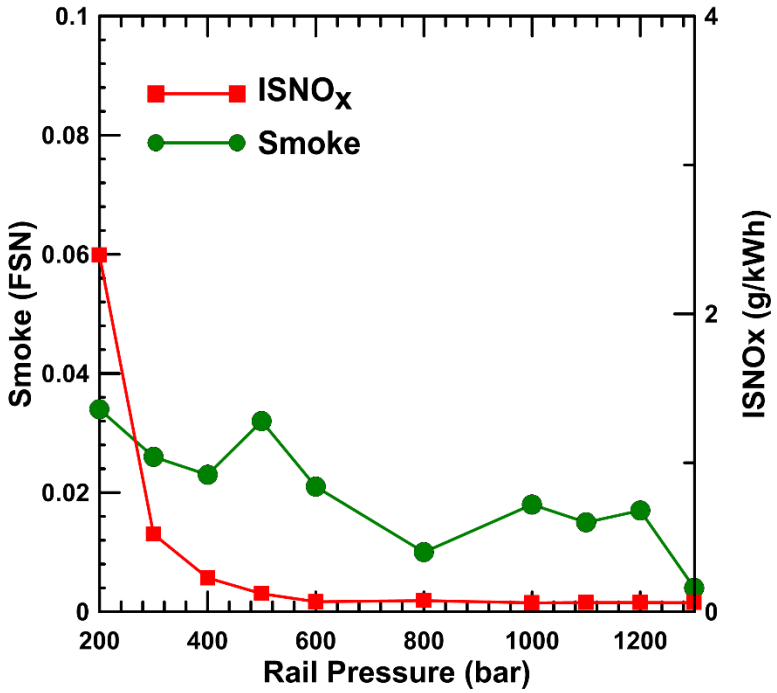

Figure 3.26 Smoke and $ISNO_x$ versus rail pressures for diesel-propane.

www.manaraa.com

ISHC and ISCO emissions as well as variation in peak bulk temperature are plotted against rail pressures in Figure 3.27. In general, both of the ISHC and ISCO emissions slightly decrease with decreasing rail pressures. The only exception of this trend is shown by the operating point having a rail pressure of 600 bar. The increasing and decreasing trend in ISHC and ISCO emissions can be explained by analyzing the residence time and peak bulk temperatures. As it is mentioned earlier, higher peak bulk temperature and longer residence time favor HC and CO oxidation. However, peak bulk temperature has more significant effects than residence time and increase or decrease in HC and CO emissions are governed by the relative dominance of these two parameters. From Figure 3.24 and 3.27, as rail pressure is increased from 200 bar to 600 bar, peak bulk temperature and CA10-90 decrease resulted in a higher HC and CO emissions. At 800 bar, though the residence time decreases compared to 600 bar, relatively higher value of peak bulk temperature helps to oxidize more HC and CO at this condition. For rail pressures above 800 bar, CA10-90 is more or less constant and rate of oxidation mostly depends on the peak bulk temperature and decreases slightly increasing the emissions once again.

Combustion efficiency is a product of HC and CO emissions and flow rates of air and fuels and directly affected by the trends exhibited by these two emissions. In this particular set of experiments, ISHC and ISCO offer the same kind of increasing or decreasing trends, and as a result, combustion efficiency exhibits a direct inverse trend reporting the lowest value of 89 percent at a rail pressure of 600 bar.

www.manaraa.com

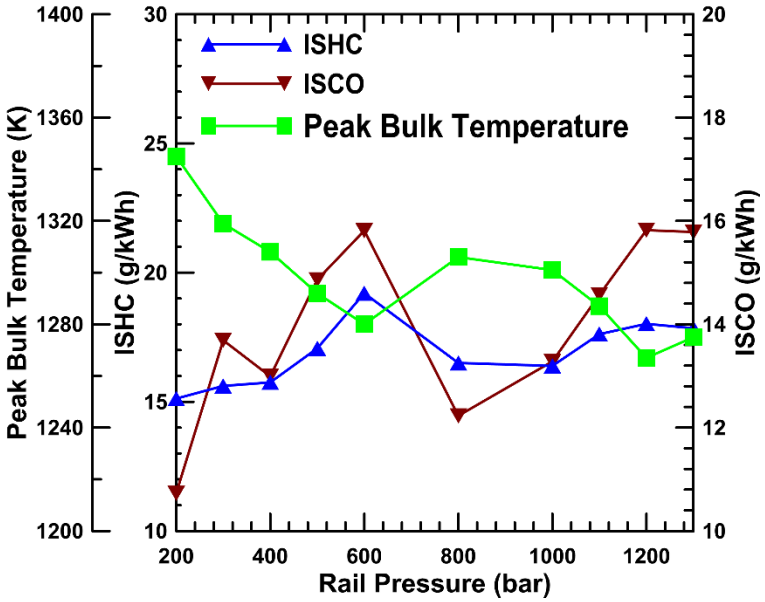

Figure 3.27 ISHC ,ISCO and peak bulk temperature versus rail pressures for diesel-propane

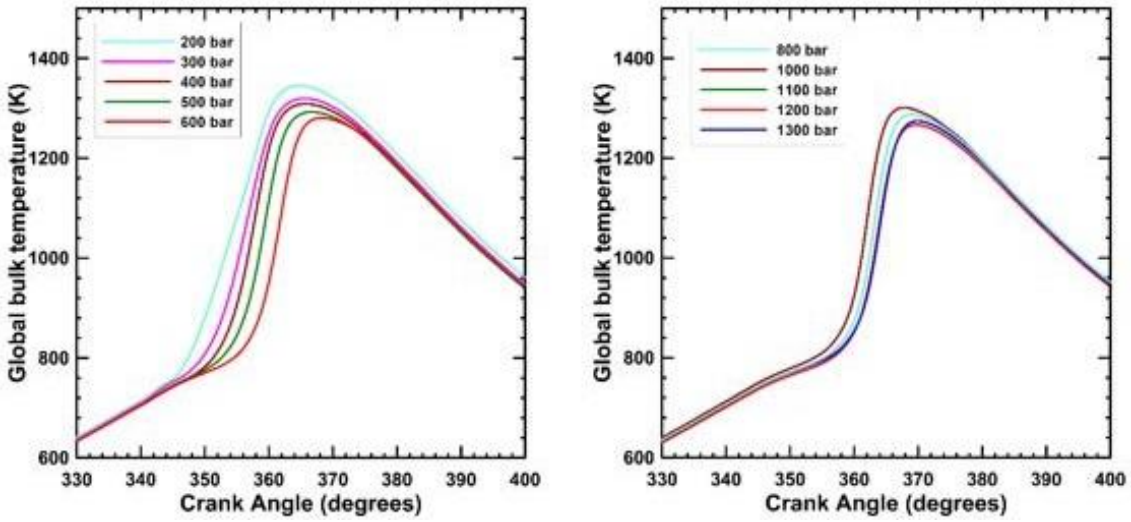

Figure 3.28 Global temperature profiles for various rail pressures for diesel-propane

www.manaraa.com

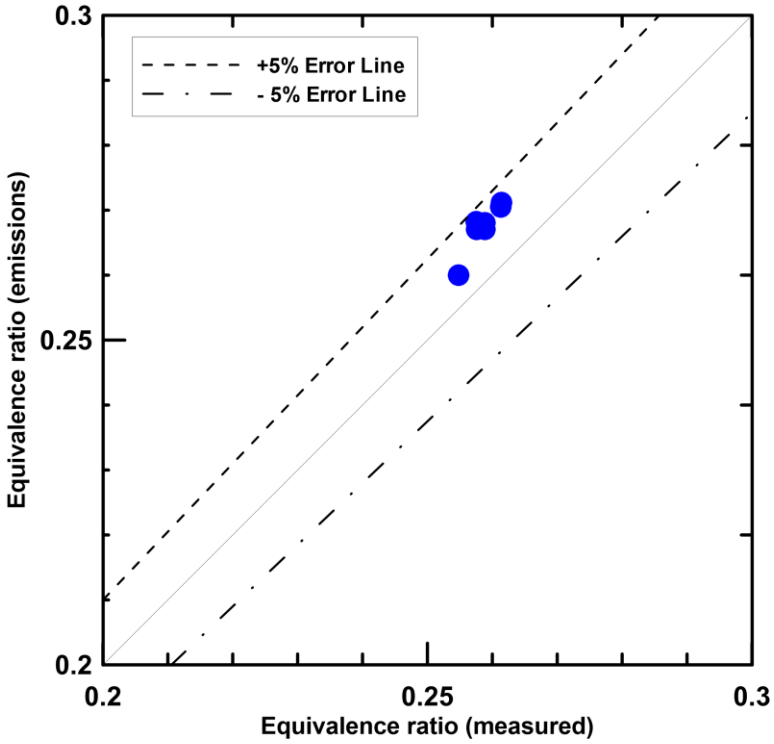

Figure 3.29 Equivalence ratio (emissions) versus equivalence ratio (measured) at various rail pressures for diesel-propane.

Figure 3.30 illustrates the effect of rail pressures on particle number concentration and size distribution. Concentration of nanoparticles (less than 50 nm in diameter) are the highest for all rail pressures. Relative concentration and distribution of particles with increasing rail pressures do not show any definite kind of trend. However, it must be kept in mind that concentration of particles is almost an order of magnitude lower, and as mentioned earlier, smoke emissions are significantly lower than straight diesel operation (Figure 3.10; 0 PES).

www.manaraa.com

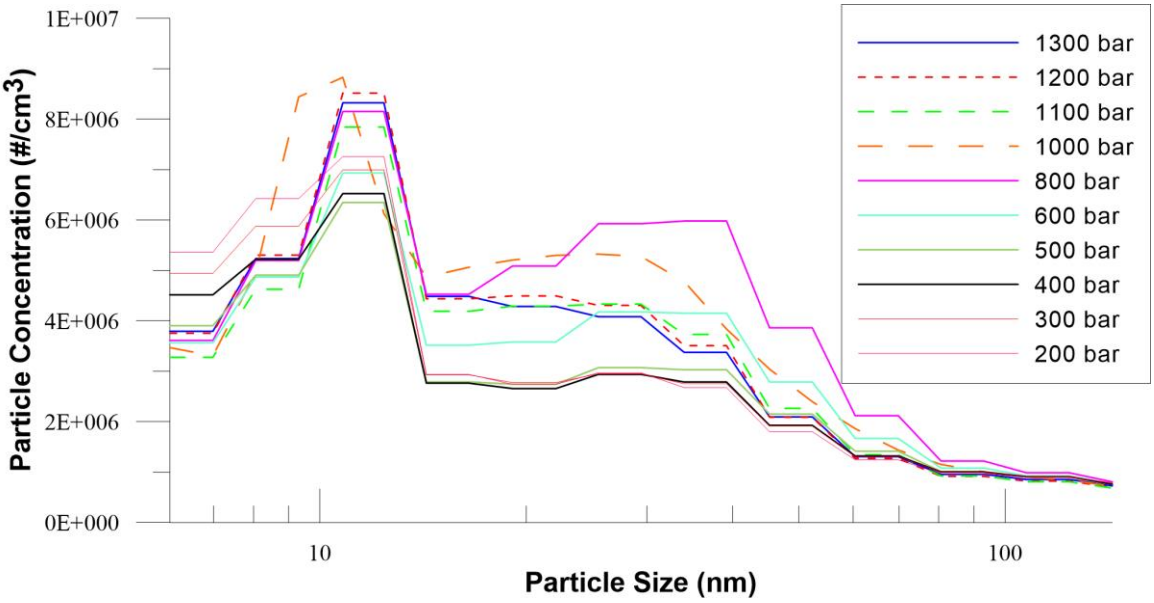

Figure 3.30 Normalized particle number ($dN/dlogD_p$) concentrations and size distribution (D_p) at various rail pressures for diesel-propane

3.4 Intake Boost Pressure Sweep: Performance and Emissions

All of the three sweeps mentioned earlier were performed to attain LTC conditions at a constant intake boost pressure (intake air pressure) of 1.5 bar. The next set of experiments are designed to quantify the effects of boost pressure variations (from 1.1 bar to 1.8 bar in steps of 0.1 bar) at 5.1 bar net IMEP, 1500 RPM, 80 PES, SOI = 310 CAD, and maintaining constant injection pressure of 500 bar. SOI of 310 CAD and a rail pressure of 500 bar was selected due to very low NO_x emissions (less than EPA regulation) at those operating conditions, as reported earlier.

3.4.1 Cylinder Pressure and Net Apparent Heat Release Rate

Cylinder pressure and AHRR profiles are plotted in Figure 3.31 and Figure 3.32 along with needle lifts for a range of boost pressure between 1.1 bar and 1.8 bar. As boost

www.manaraa.com

pressure is increased, peak pressure increases in magnitude and shifts towards TDC indicative of early onset of combustion. Moreover, pressure during the compression stroke is also higher for higher boost pressure The AHRR profiles show a decreasing trend, then an increasing trend with increasing boost pressure reporting the highest magnitude of peak heat release at 1.4 bar. Furthermore, combustion phasing shifts from before TDC to after TDC with increasing boost pressure.

AHRR profiles exhibit single stage sinusoidal profiles which proves the fact that the HCCI like combustion mode is dominant at all operating conditions, though varies in rate and magnitude. As the PES, rail pressure and SOI are kept constant, surrounding premixed propane-air mixture is predominantly lean and residence time of diesel pilot and jet induced momentum do not affect the rate of entrainment, leaving only one variable to consider. As the boost pressure increases, mass of air trapped during compression also increases proportionately. As a result, equivalence ratio of intake charge (propane-air) as well as total equivalence ratio (diesel-propane-air) gradually decrease in magnitude (Figure 3.39).

In light of this above discussion, the trends in AHRR can be explained as follows. As boost pressure is increased from 1.1 bar to 1.8 bar, more and more air entrain into the diesel jet during the ignition delay period forming a leaner homogeneous mixture. This trend insinuates a shift of combustion phasing latter part of the cycle (like during the rail pressure sweep), while only a complete opposite trend is visible. Cylinder pressure during compression increases with the increase of boost pressure, which in turn also rises the global in-cylinder temperature. Though the mixture of air-fuel is more lean and homogeneous for higher boost pressures, this increase in compression temperature forces

www.manaraa.com

the mixture to attain the autoignition temperature earlier and earlier part in the cycle. For higher boost pressures (1.5 to 1.8 bar), as combustion start much earlier in the compression stroke, part of the energy coming from fuel is lost to overcome the compression effect and hence, decrease the magnitude in heat release rate. Between 1.5 and 1.8 bar of boost pressure, the same decreasing trend is observed as combustion is phased latter in the expansion stroke.

www.manaraa.com

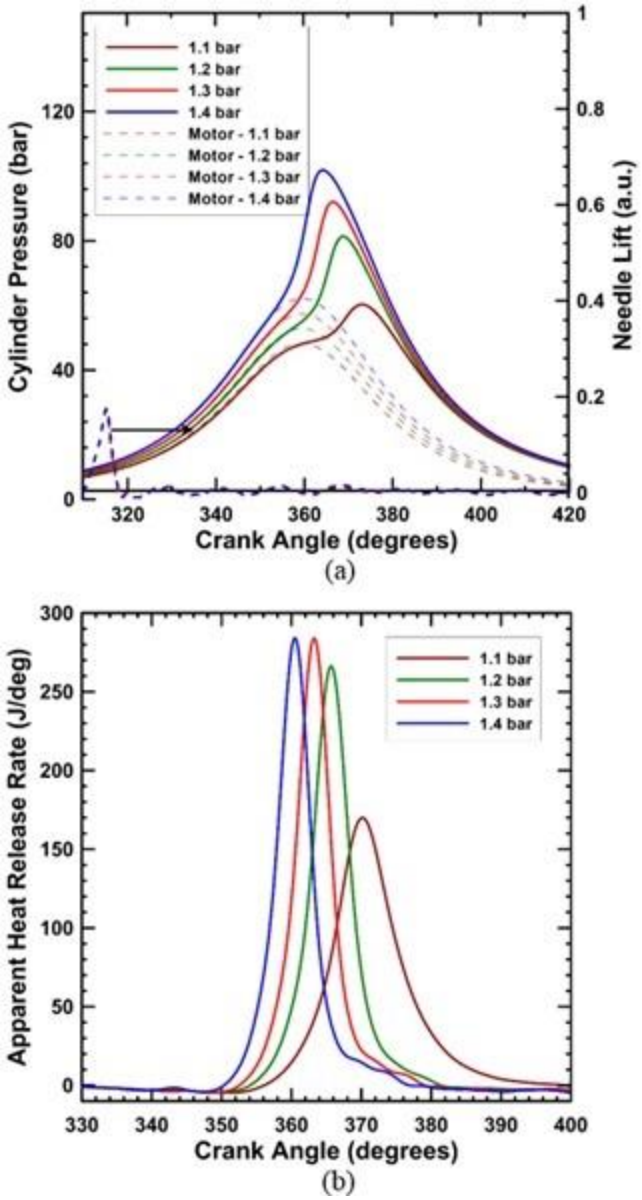

Figure 3.31 Transient data of diesel-propane dual fueling for boost pressure of 1.1 to 1.4 bar

Note: (a) Cylinder pressure and needle lift profiles and (b) net AHRR profiles at 5.1 bar net IMEP, 80 PES, 1500 RPM, SOI = 310 CAD, P_{rail} = 500 bar

www.manaraa.com

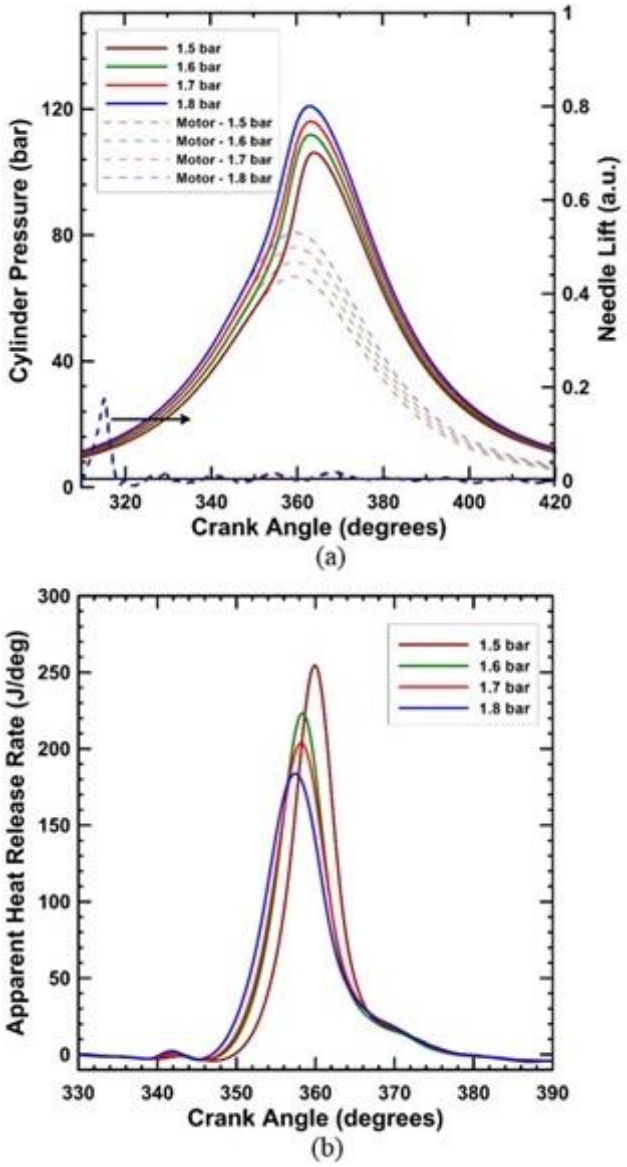

Figure 3.32 Transient data of diesel-propane dual fueling for boost pressure of 1.5 to 1.8 bar

Note: (a) Cylinder pressure and needle lift profiles and (b) net AHRR profiles at 5.1 bar net IMEP, 80 PES, 1500 RPM, SOI = 310 CAD, P_{rail} = 500 bar

3.4.2 Maximum Pressure Rise Rate, Ignition Delay, Combustion Stability and Combustion Phasing

Figure 3.33 shows the ignition delay, MPRR and COV of IMEP, and Figure 3.34 presents SOC, combustion duration and combustion phasing with respect to different boost

www.manaraa.com

pressures. The trends in ignition delay, CA5 and CA50 have already been discussed in the heat release section. Combustion duration becomes minimum (7.8 CAD) at a boost pressure of 1.4 bar and increases if boost pressure is increased or decreased, however, an opposite trend is observed for MPRR. Combustion is phased just after TDC for 1.4 bar, and advances or retards based on the direction in deviation. Retardation of CA50 in the expansion cycle causes a decrease and an increase in MPRR and CA10-90, respectively.

A very high value of COV of IMEP (10.7 percent) is observed for 1.1 bar of boost pressure indicating misfire limits, while all other operating points lie within the acceptable limit. This might be due to the fact that, at 1.1 bar, combustion starts after TDC and bulk of the combustion happen in the expansion stroke. Phasing of the combustion very late in the expansion stroke along with high equivalence ratio lead to a sharp increase in number of misfire cycles.

www.manaraa.com

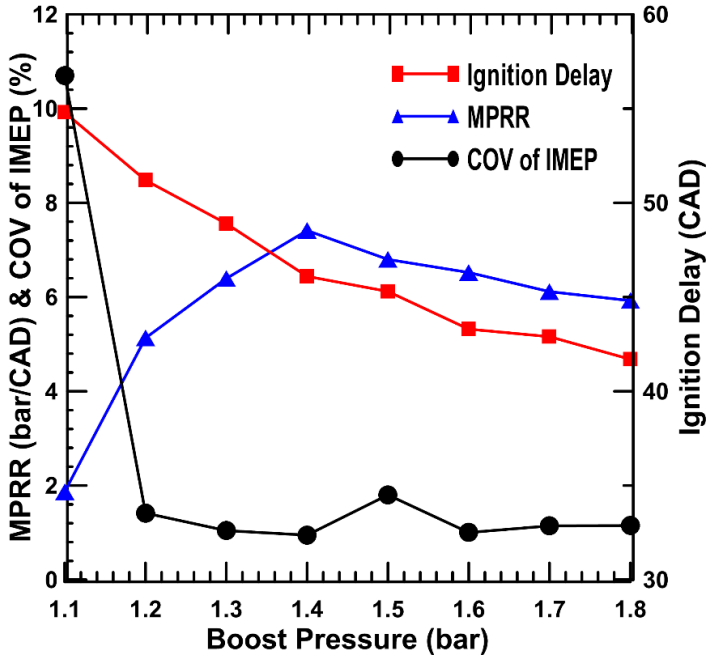

Figure 3.33 Ignition delay, MPRR and COV IMEP versus boost pressures for diesel-propane.

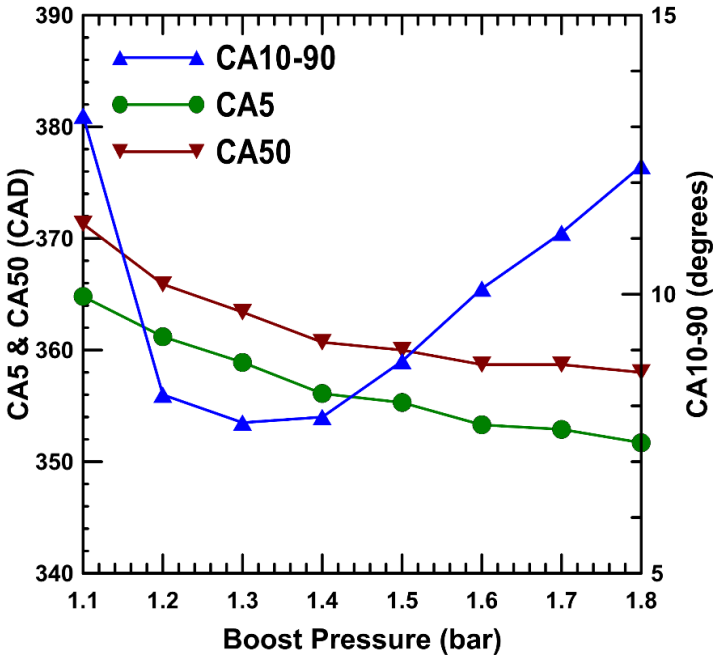

Figure 3.34 CA5, CA50, CA10-90 versus boost pressures for diesel-propane.

www.manaraa.com

3.4.3 Fuel Conversion Efficiency and Combustion Efficiency

IFCE, BFCE and combustion efficiency are plotted against boost pressures in Figure 3.35. . IFCE increases from 46.8 percent at 1.2 bar to 48.7 percent at 1.8 bar, and obviously much lower (43.6 percent) at 1.1 bar due to misfire conditions. This slightly increasing trend at higher boost pressures (1.5 to 1.8 bar) is counterintuitive to the trends portrayed by the combustion phasing and combustion duration. Phasing of combustion shifts before TDC along with increased combustion duration at these conditions should create a negative impact on IFCE. However, after careful examination, it has been found that, IMEP calculated from in-cylinder pressure data slightly increases with the increase of boost pressures reaching almost 5.3 bar at 1.8 bar boost pressure (not presented) despite having higher pumping losses. This might be due to very large increases in peak pressures (from 60 bar to 120 bar), and again, as equivalence ratios are lower, IFCE increases.

Combustion efficiency slightly increases from 88 percent to around 91 percent with increasing boost pressures and will be explained with ISHC and ISCO emissions.

www.manaraa.com

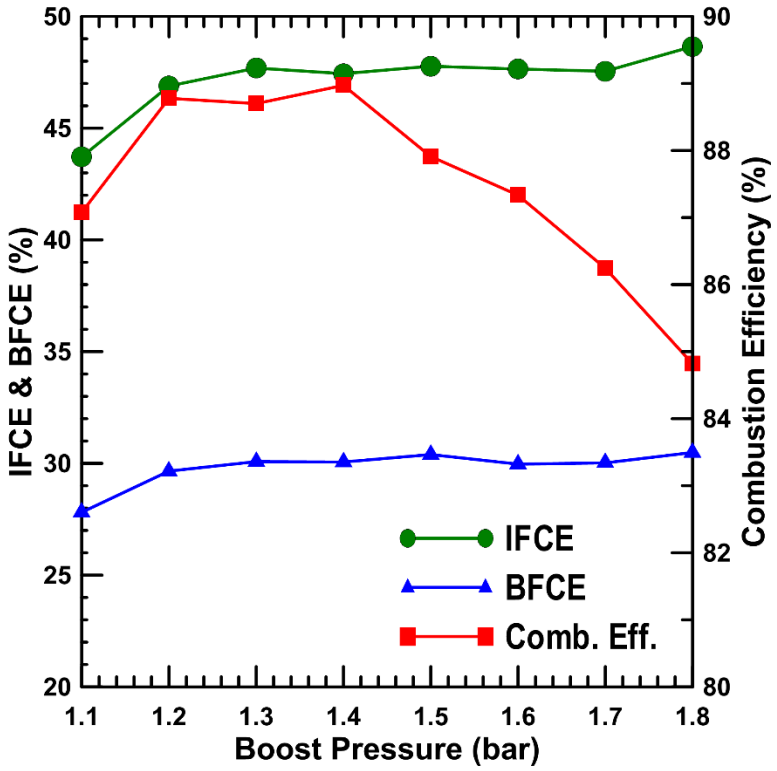

Figure 3.35 IFCE, BFCE and Combustion Efficiency versus boost pressures for diesel-propane.

3.4.4 Emissions, Particle Concentrations and Size Distributions

ISNO$_x$ slightly decreases from 0.2 g/kWh at 1.1 bar to near-zero level (0.07 g/kWh) at 1.8 bar. It is possible that higher ϕ values at increasing boost pressures lead to an increase in the local temperature that favor thermal NO$_x$ formation.

Smoke emissions remain invariant except for 1.1 bar. Instability in combustion process sharply increases the number of misfire cycles leading to a very slight increase in smoke.

www.manaraa.com

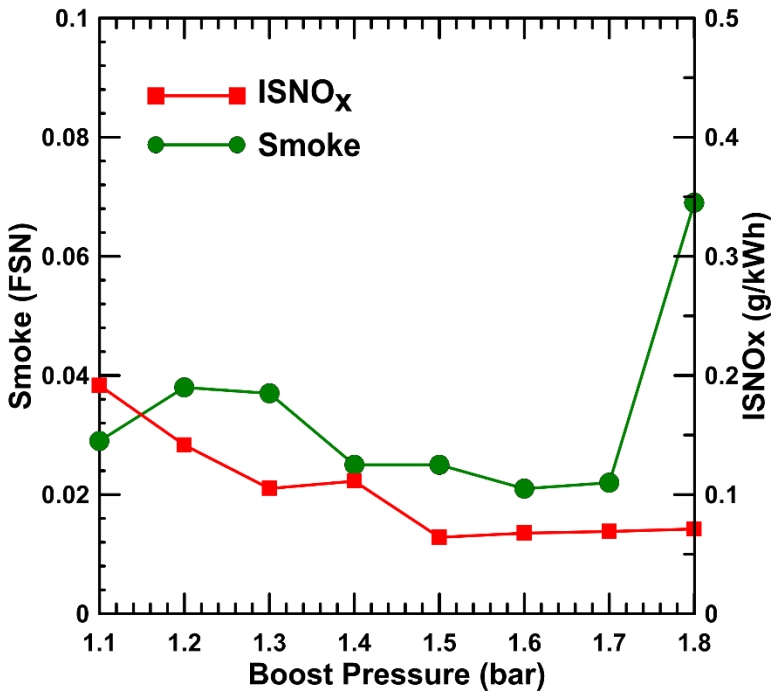

Figure 3.36 Smoke and $ISNO_x$ versus boost pressures for diesel-propane

ISHC, ISCO emissions and peak bulk temperatures are presented in Figure 3.37. Interestingly, ISHC and ISCO show opposite trends with respect to boost pressure. At 1.1 bar, misfire conditions are prevalent and ISHC emissions are the highest. It indicates that increased amount of fuels are left unburnt due to very high variations in global temperatures. Apart from 1.1 bar, as the boost pressure increases, ISCO increases sharply from 6.7 to 30 g/kWh while ISHC remains somewhat invariant. It seems that reduction in peak bulk temperatures affect the rate of CO →CO2 oxidation, and in turn, decreases the combustion efficiency.

www.manaraa.com

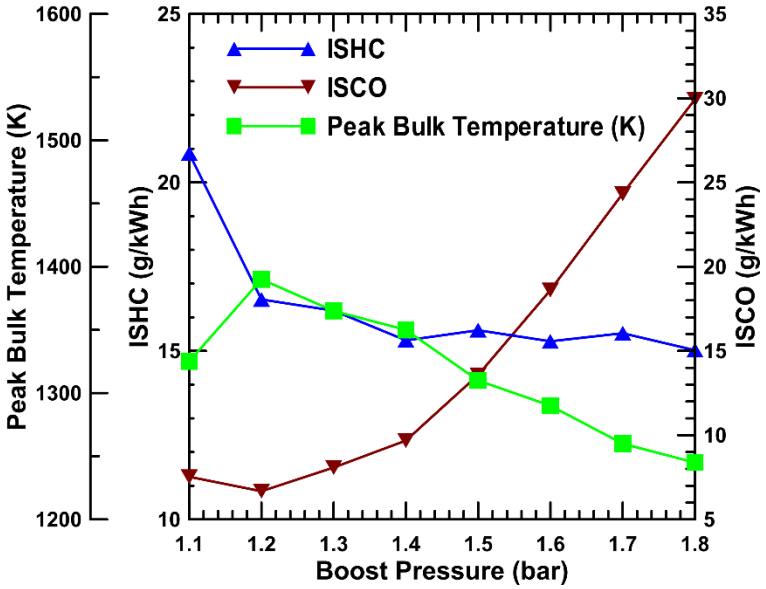

Figure 3.37 ISHC ,ISCO and peak bulk temperature versus boost pressures for diesel-propane

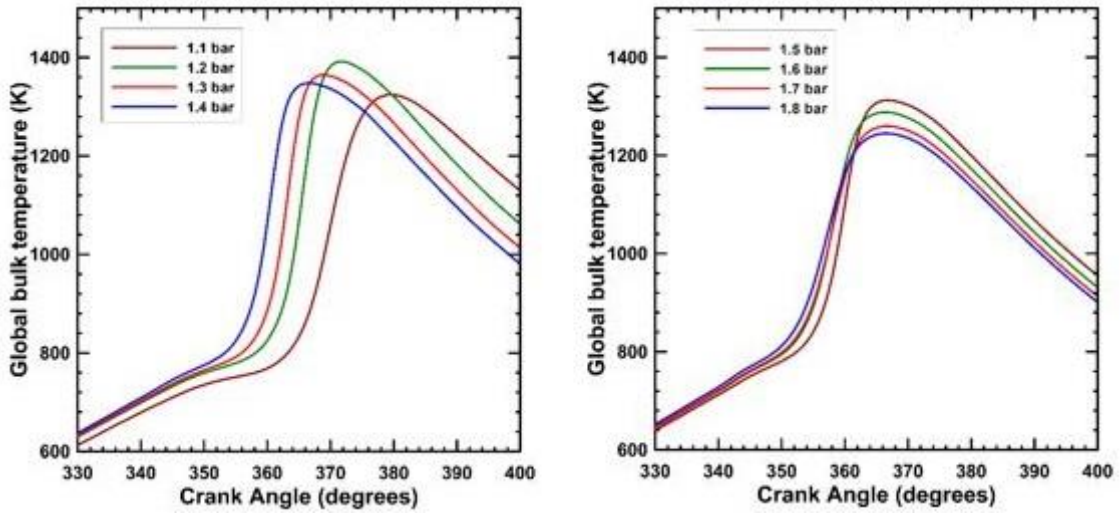

Figure 3.38 Global temperature profiles for various boost pressures for diesel-propane

www.manaraa.com

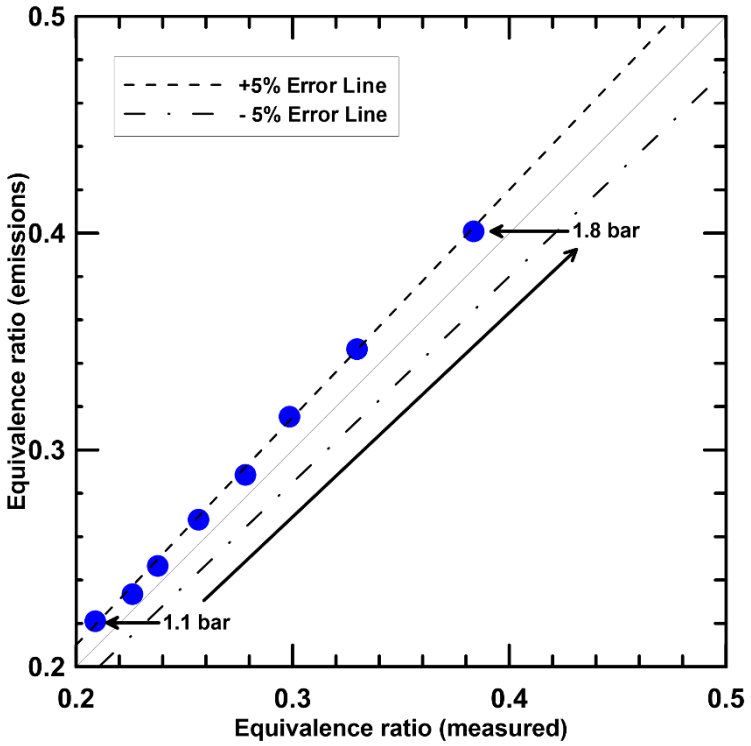

Figure 3.39 Equivalence ratio (emissions) versus equivalence ratio (measured) at various rail pressures for diesel-propane

Figure 3.40 depicts the boost pressure effects on particle number concentrations and size distribution. Again, significantly highest number of particles form in the nanoparticles zone (less than 50 nm) for all boost conditions. However, two distinguishable zones are present within these nanoparticles showing opposite trends. As boost pressure is increased, in general, concentrations of particles in the lower spectrums of these nanoparticles increase, while an opposite is true for the higher ones. The reasons behind these trends are not clear and requires further investigation. However, these opposite trends countermand the effect of each other and smoke emissions remain very low and are almost invariant with respect to boost pressure.

www.manaraa.com

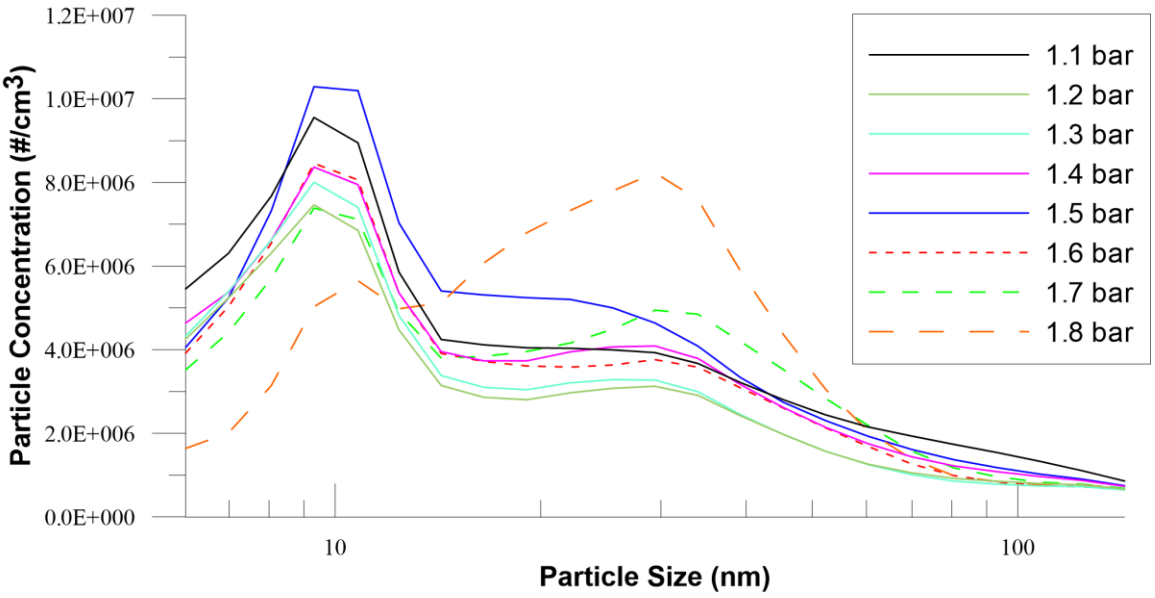

Figure 3.40 Normalized particle number concentrations ($dN/dlogD_p$) and size distribution (D_p) at various boost pressures for diesel-propane

www.manaraa.com

CHAPTER IV

DIESEL-METHANE DUAL FUEL LOW TEMPERATURE COMBUSTION

Natural gas engines have attracted a lot of attentions in the past decades mainly due to their improved reliability, fuel economy and lower fuel costs. Also, improvement of technology like "fracking" has increased the availability of natural gas enormously making the price of natural gas extremely cheap. This makes natural gas a very attractive options as a fuel source in mobile applications in many countries in the world. Again, this study focuses on the effects of critical engine control parameters on performance and emissions of a compression ignition engine in light load employing two different fuels. As a result, for diesel-ignited methane dual fuel combustion, efforts are made to maintain engine control parameters similar to the diesel-propane case in order to present a comparative analysis between these two fuels. A portion of the present study of diesel-methane dual fuel combustion has already been published in a peer-reviewed journal article (Raihan et al. 2014):

"*Raihan, M., Guerry, E., Dwivedi, U., Srinivasan, K., and Krishnan, S. (2014). "Experimental Analysis of Diesel-Ignited Methane Dual-Fuel Low-Temperature Combustion in a Single-Cylinder Diesel Engine." ASCE Journal of Energy Engineering, 10.1061/(ASCE)EY.1943-7897.0000235 , C4014007.*"

www.manaraa.com

4.1 PES Sweep: Performance and Emissions

PES sweep for diesel-methane dual fuel combustion was performed at an engine speed of 1500 RPM, a net IMEP of 5.1 bar and rail pressure, intake boost pressure and injection timing was set at 500 bar, 1.5 bar and 355 CAD, respectively. The substitution rate of methane was varied from 0 percent (pure diesel operation) to 90 percent, and no EGR was used.

4.1.1 Cylinder Pressure and Net Apparent Heat Release Rate

Figure 4.1 and 4.2 show cylinder pressure profiles and net AHRR profiles for diesel ignited methane dual fuel combustion for various PES. For AHRR between 0 percent and 70 percent PES, as PES is increased, magnitudes of first stage peak increase while second stage peak decrease in magnitude. For PES of 80 percent and 90 percent, both of the peak decrease in magnitude corresponding to 70 percent PES. As described earlier, first stage of AHRR comes from the premixed burn which is determined by the amount of fuel mixture prepared during the ignition delay period. The second spike occurs from the mixing controlled burn resulted from the standing premixed flame and depends on the spatial area of diffusion flame and mixing rate of air and fuel inside the combustion chamber.

AS PES is increased from 0 percent to 70 percent, equivalence ratio of the intake premixed charge becomes higher and higher and entrains into the diesel jet to form a combustible mixture. Some amount of this premixed air-methane mixture take part in the premixed burn period, while most of the methane ignite during the second phase of the burn. With increasing PES, air-methane mixture with higher equivalence ratio entrains into the jet and it is possible that this intake charge create more ignition point during the

www.manaraa.com

ignition delay period. This causes an increase in the first stage heat release. On the other hand, with increasing PES, quantity of pilot diesel decreases and percentage of energy provided by the methane increases. Diffusion flame created at the end of the first stage burn decreases in size significantly. This decrease in the size of diffusion flame may inhibit the burning of the remainder air-methane mixture present in the combustion chamber and heat release rate decreases.

If PES is increased beyond 70 percent, both of the magnitudes of first and second stage heat release starts decreasing slightly. Also, combustion shifts further away in the expansion stroke having higher combustion duration. It may be possible that, at these high PES, as the equivalence ratios of the intake charge are even higher form non-combustible mixture with very rich equivalence ratios (diesel-methane-air). Moreover, smaller size of the diesel jet may not capable enough to create and sustain a diffusion flame to burn the air-fuel mixture completely. Consequently, significant amount of unburned fuels are present in the exhaust as engine is operated at these two high PES.

www.manaraa.com

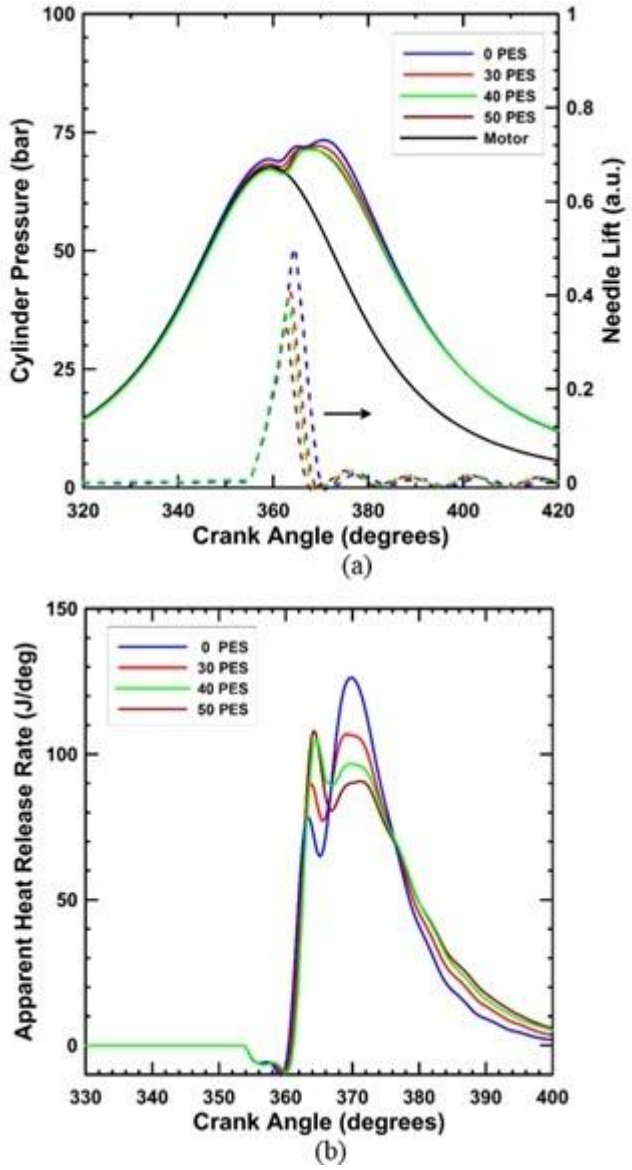

Figure 4.1 Transient data of diesel-methane dual-fueling for 0 to 40 PES

Note: (a) Cylinder pressure and needle lift profiles and (b) net AHRR profiles for 0 to 50 PES at 5.1 bar net IMEP, 1500 RPM, SOI = 355 CAD, P_{rail} = 500 bar.

www.manaraa.com

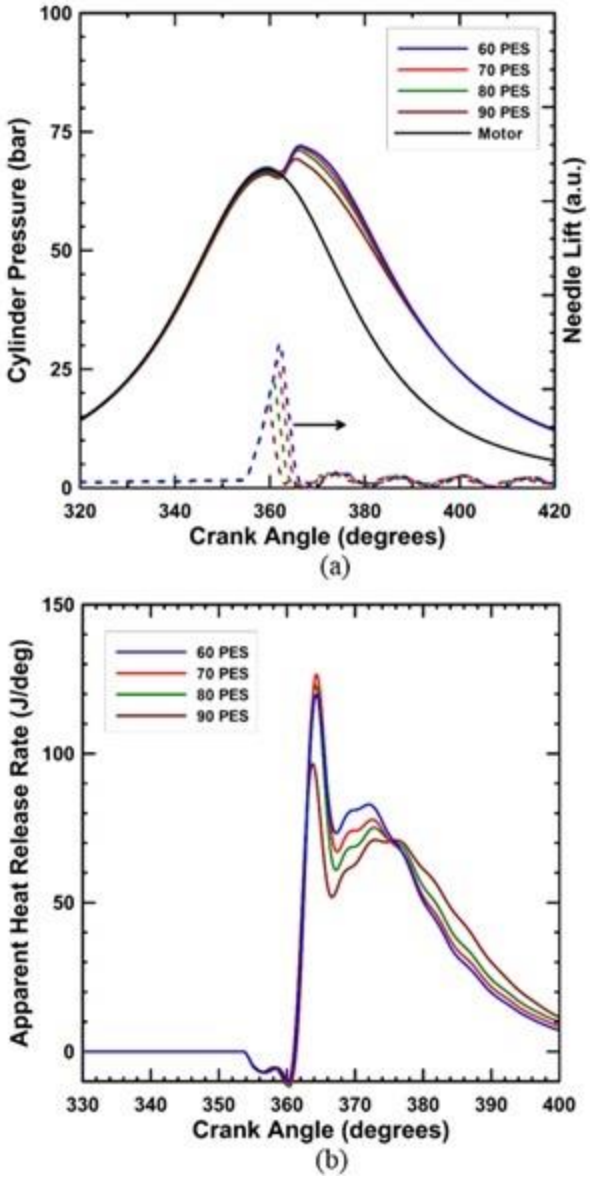

Figure 4.2 Transient data of diesel-methane dual fueling for 60 to 90 PES.

Note: (a) Cylinder pressure and needle lift profiles and (b) net AHRR profiles 60 to 90 PES at 5.1 bar net IMEP, 1500 RPM, SOI = 355 CAD, P_{rail} = 500 bar.

4.1.2 Maximum Pressure Rise Rate, Ignition Delay, Combustion Stability and Combustion Phasing

Figure 4.3 illustrates the variation of Ignition delay, MPRR and COV of IMEP with the variation of PES. As the ignition timing is set very close to TDC and combustion starts

www.manaraa.com

and finishes in the expansion stroke, MPRR remains low through-out the whole sweep. Ignition delay slightly increases with increasing PES. The slight increase in ignition delay can be attributed to the change in specific heat of the intake air-methane mixture due to variation in PES. AS PES is increased, specific heat of the air-methane mixture increases, which decreases the mean in-cylinder temperature during compression. This is also supported by Figure 4.8 showing a decrease in bulk in-cylinder temperature profile for higher PES. As a result, autoignition temperature occurs later part in the cycle, hence, an increase in ignition delay.

COV of IMEP shows an increasing trend and rises sharply for PES over 70 percent. It indicates that combustion at higher PES SOI are relatively less stable. This is due to the very low percentage of diesel amount which is not sufficient to burn much larger amount of air-methane mixture.

Figure 4.4 represents the variation of CA5, CA50, and CA10-90 with PES. CA5 and CA50 shift slightly away from TD with increasing PES indicating that more and more energy are being released in the later part of the cycle. Combustion duration progressively increases with the increasing PES. It indicates that at higher PES, rate of heat release decreases due to insufficient amount of ignition fuel. Also, as bulk of the combustion is happening very late of the expansion stroke, variations in cylinder temperature and pressure are also very high. This leads to a very high COV at highest PES of 90 percent depicting the onset of misfire at that operating condition

www.manaraa.com

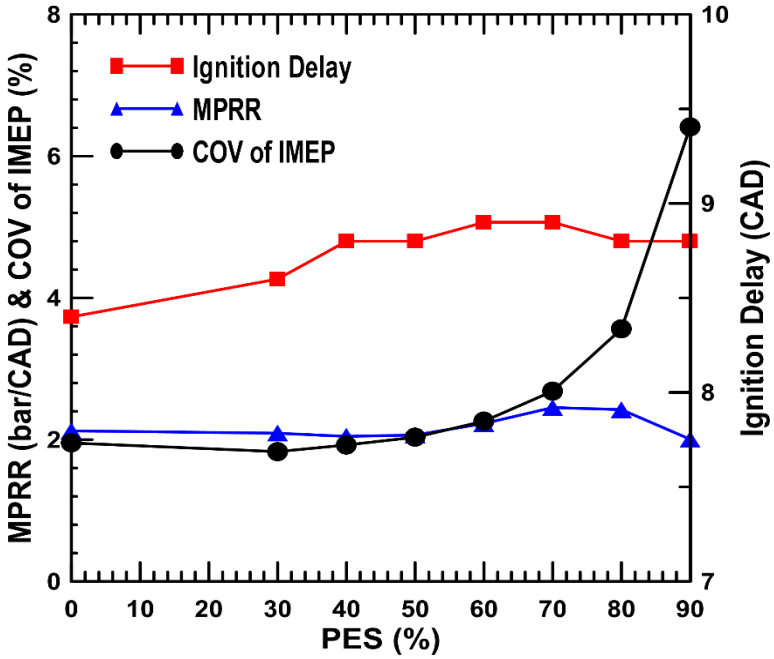

Figure 4.3 Ignition delay, MPRR and COV IMEP versus PES for diesel-methane.

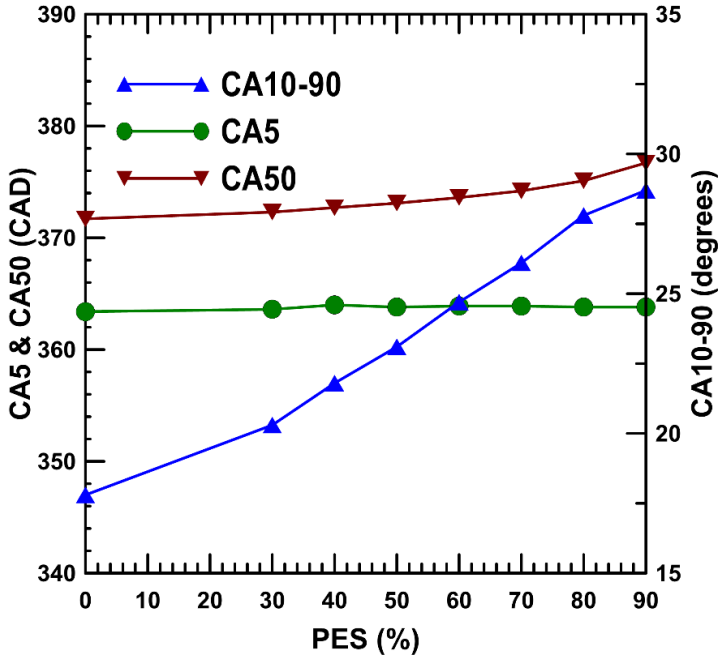

Figure 4.4 CA5, CA50, CA10-90 versus PES for diesel-methane

www.manaraa.com

4.1.3 Fuel Conversion Efficiency and Combustion Efficiency

BFCE, IFCE and combustion efficiency trends are plotted in Figure 4.5. All of the presented parameters showed a progressively decreasing trend with increasing PES. It may be worth noting that, for PES of 70 percent, 80 percent and 90 percent, HC emissions were recalculated from measured equivalence ratio using the equations described earlier.

Combustion efficiency varies from almost 100 percent for pure diesel to nearly 50 percent for 90 percent PES. It indicates that as PES is increased, combustion process becomes very inefficient in burning the diesel-methane mixture, as most of the diesel pilot are consumed during the burn. Again, this is due to the phasing of combustion later part in the expansion stroke and higher combustion duration associated with higher PES.

As the amount of unburned fuel in the exhaust increases rapidly at higher PES, more and more fuel are needed to produce the same amount of power. This hurts both the IFCE and BFCE very badly decreasing to almost half of the values reported for pure diesel operation.

www.manaraa.com

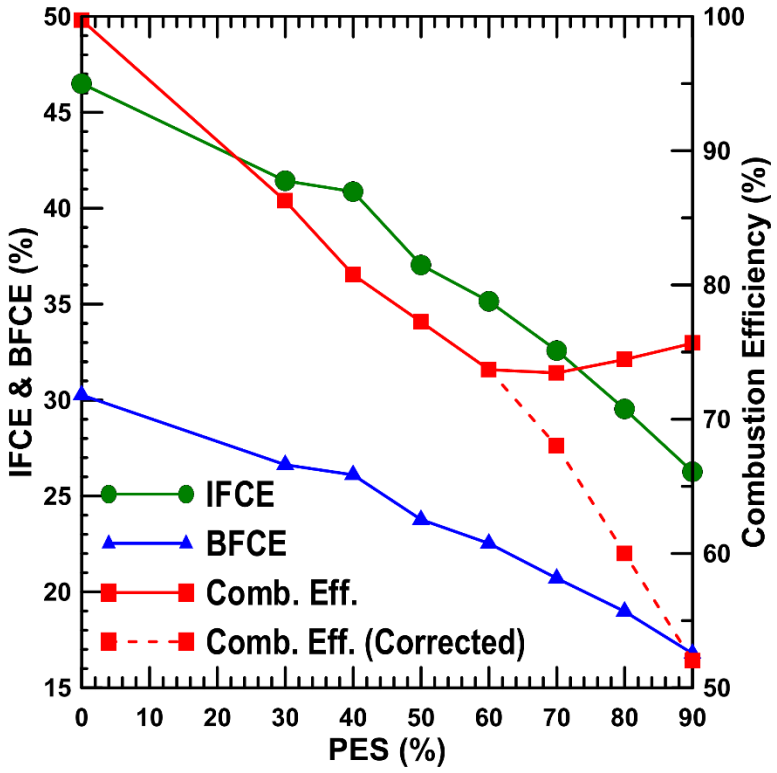

Figure 4.5 IFCE, BFCE and combustion efficiency versus PES for diesel-methane.

4.1.4 Emissions, Particle Concentrations and Size Distributions

Figure 4.6 shows indicated specific oxides of nitrogen ($ISNO_x$) and Smoke emissions versus PES at 355 CAD injection timing. As PES is increased, $ISNO_x$ emission decreases. The value of $ISNO_x$ reduces from 6.6 g/kWh at 0 PES to 2.95 g/kWh at 90 PE. As described earlier in the chapter of diesel-propane dual-fueling, NO_x primarily forms in the hot, near-stoichiometric mixtures of the diffusion fame surrounding the diesel jet and spatial area of the diffusion flame reduces as less diesel is injected into the combustion chamber with increasing PES. Thus, increased homogeneity with increasing PES reduces the peak local temperature favorable for thermal NO_x formation.

www.manaraa.com

In general, smoke emissions decrease with the increase of PES, Soot forms in the rich premixed areas with higher equivalence ratios. As described earlier, formation of soot can be avoided by keeping the local temperature of the rich premixed regions below 1800K (Akihama et al. 2001). Lean premixed mixture of air and methane surrounding the diesel jet has significantly lower adiabatic equilibrium temperature, and thus do not take part in producing soot. With increasing PES, more and more energy are supplied by the lean premixed mixture and less heterogeneity from diesel pilot is produced during combustion, resulted in a decrease in soot emissions.

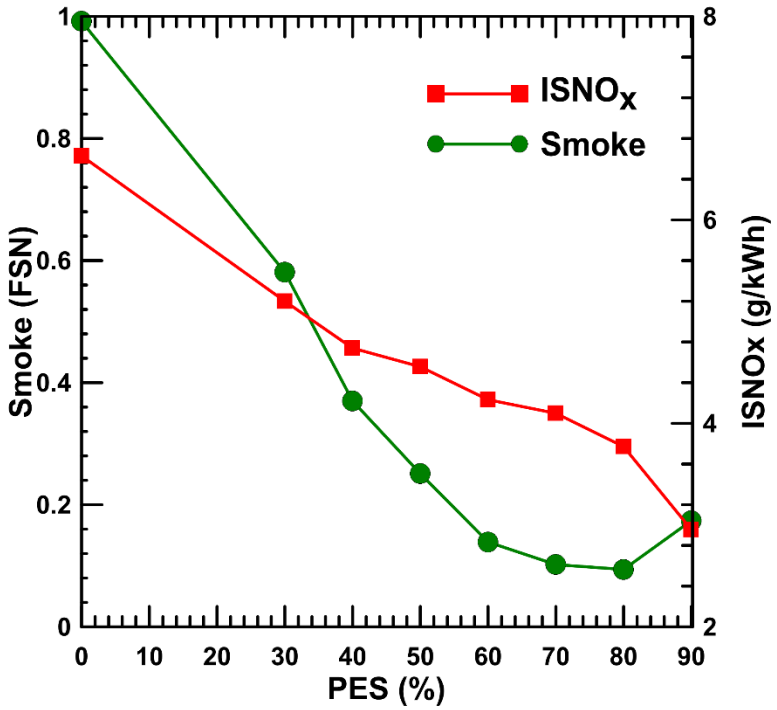

Figure 4.6 $ISNO_x$ and Smoke emissions versus PES for diesel-methane.

ISHC and ISCO emissions are presented in Figure 4.7. As PES is increased, both ISHC and ISCO emissions increase rapidly except for ISCO emissions at 90 PES. It is

www.manaraa.com

evident that ISHC and ISCO emissions are very low for straight diesel operation demonstrating the efficiency and suitability of diesel fuel for this type of engine. ISHC increases from 0.49 g/kWh at 0 PES to around 141 g/kWh at 90 PES while ISCO increases from 0.62 g/kWh at 0 PES to 22 g/kWh at 80 PES. However, the actual concentration of ISHC emissions couldn't be quantified for 70, 80 and 90 PES because the emissions level were beyond the upper limit of the analyzer and were recalculated from equivalence ratios (Figure 4.9).

Very low of ISHC emissions for straight diesel operation compared to dual fuel combustion indicate that most of the intermediate hydrocarbon species formed during the combustion process are oxidized in the relatively hotter bulk temperatures (Figure 4.8) and no or very little unburned fuel escapes the diffusion flame. Also, peak bulk temperature is the highest for straight diesel operation.

As described earlier, for dual fuel combustion, high HC emissions are correlated to incomplete flame propagation (Karim 1991). As PES is increased, the flame initiated by the diesel ignition fuel becomes progressively smaller and smaller and can't spread far enough or fast enough into the surrounding lean methane-air mixture leading to higher HC emissions. Also, as fuel molecules trapped in the crevices is a significant source of HC emissions in the exhaust, and amount of methane trapped in the crevices increase with increasing PES lead to higher concentration of unburned fuel in the exhaust.

In addition, bulk in-cylinder temperature during combustion and post combustion and also, residence time play a significant role on oxidation of HC and CO molecules. Peak bulk temperature of 1500K is needed to oxidize the HC and CO molecules completely and is irrespective of the nature or composition of the fuel. As shown in Figure 4.7, peak

www.manaraa.com

bulk temperature gradually decreases with the increase of PES and bulk of the combustion is happening latter part of the expansion stroke for higher PES (Figure 3.4). This reduction in bulk in-cylinder temperature may lead to lower oxidation rate of fuel molecules to intermediate HC species, as well as complete combustion of these intermediate species. Increased amount of unburned fuel molecules and partial oxidation of fuel molecules at higher PES stemmed from aforementioned affects lead to an increase in engine-out HC emissions.

CO is in intermediate combustion species formed during the oxidation process of any hydrocarbon fuel and then converted to CO_2 reacting with available OH radicals. This CO oxidation reaction ($CO + OH \rightarrow CO2 + H$) is strongly dependent on bulk in-cylinder temperature and relatively slow at temperature below 1100 K (Glassman 1996). With increasing PES, peak bulk in-cylinder temperature decreases. Moreover, the spatial area of the diffusion flame reduces in size, in turn, decreases the availability of OH radicals for CO oxidation, as PES is increased.

At the highest PES of 90 percent, there may be a competing effect going on between HC and CO oxidation. HC emissions increases tremendously at that operating condition indicating that significant amount of methane fuel remain. As HC oxidation rate was lower than 80 PES, the combustion process was actually producing lower CO molecules compared to 80 PES. As a result, ISCO emissions decrease slightly, while there a rapid rise in ISHC emissions is observed.

www.manaraa.com

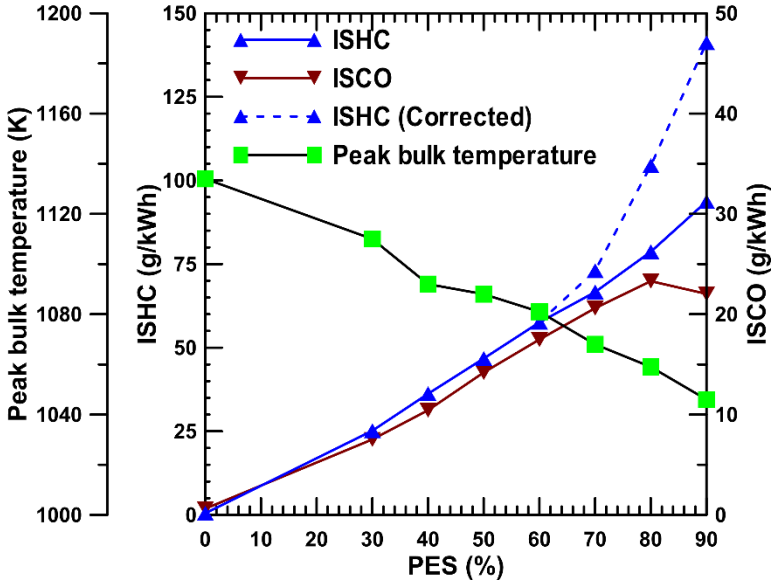

Figure 4.7 HC and CO emissions versus PES for diesel-methane.

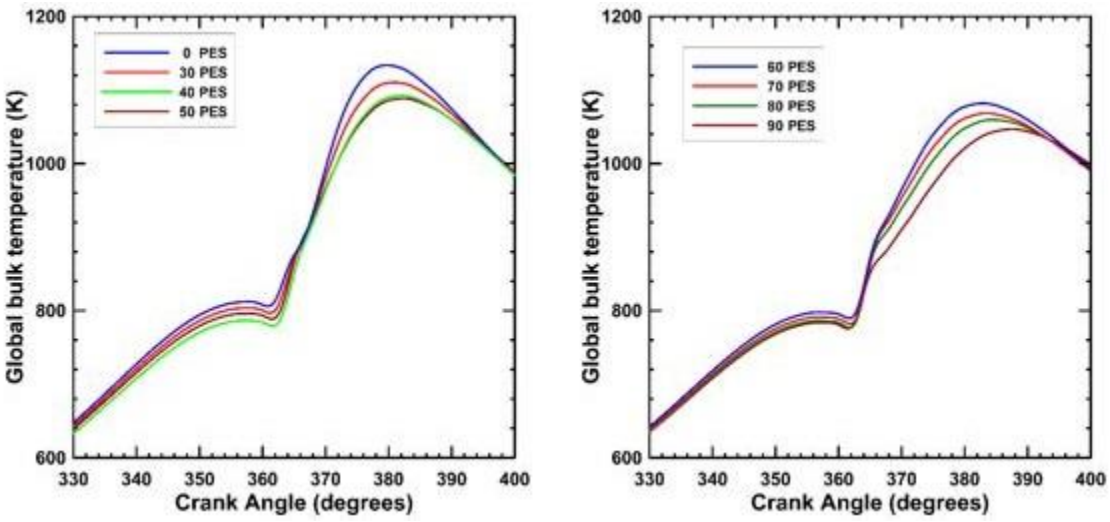

Figure 4.8 Global temperature profiles for various PES for diesel-methane.

www.manaraa.com

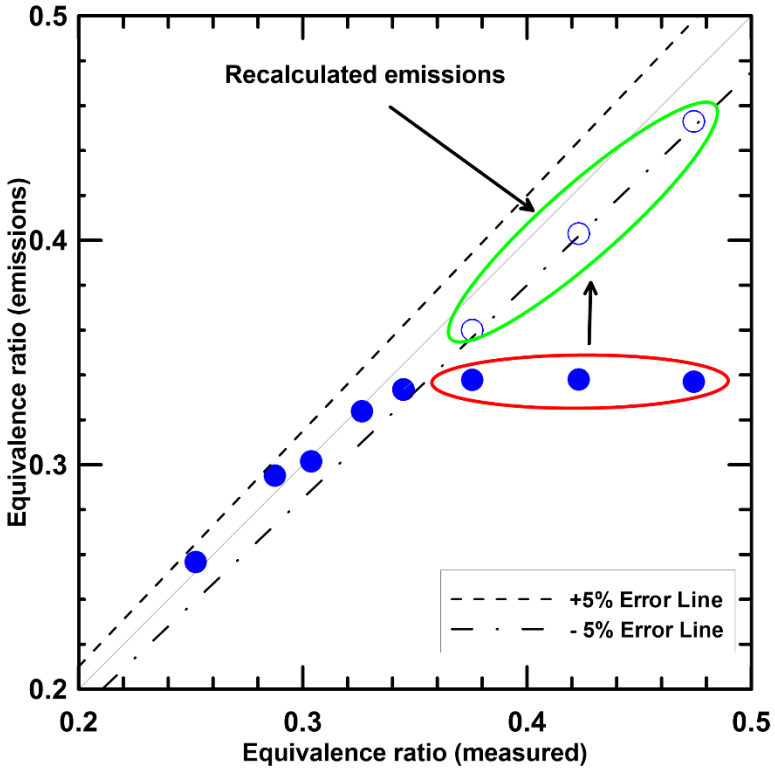

Figure 4.9 Equivalence ratio (emissions) versus equivalence ratio (measured) at various PES for diesel-methane

Figure 4.10 illustrates the effect of PES on particle number concentration and size distribution. Significant number of particles form having a diameter of 50 nm or less at all PES conditions. For straight diesel operation, the particle concentrations are the highest for almost all diameters. Particle concentrations exhibit a decreasing trend with increasing PES, in general, but exceptions are also available, and thus, require further study.

www.manaraa.com

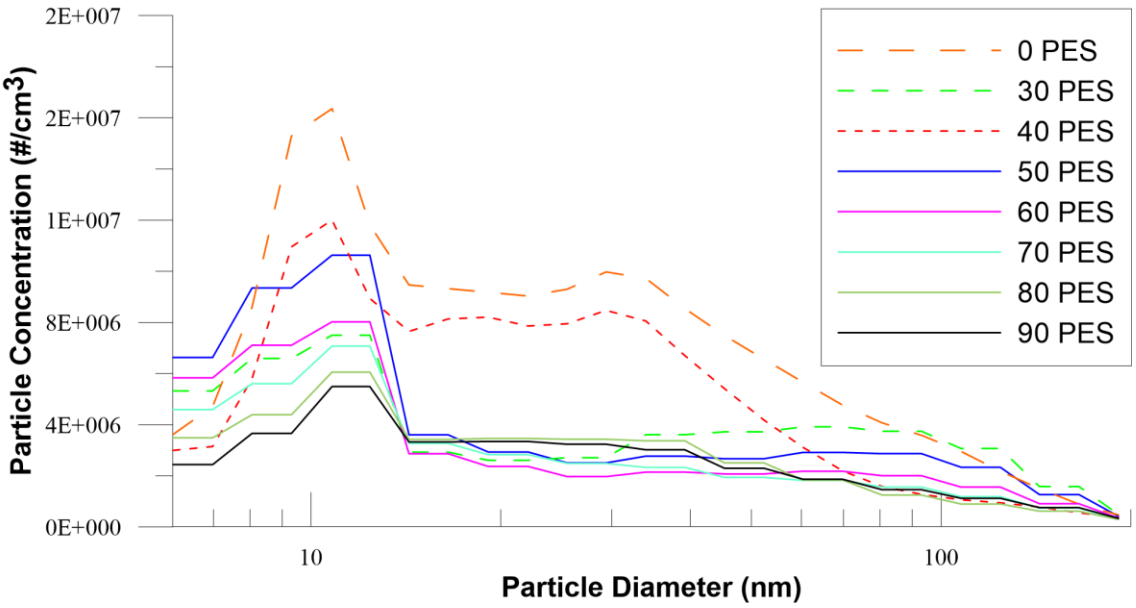

Figure 4.10 Normalized particle number ($dN/dlogD_p$) concentrations and size distribution (D_p) at various PES for diesel-methane

4.2 Injection Timing (SOI) Sweep: Performance and Emissions

For the SOI experiments, the engine was operated at 5.1 bar net IMEP, 1500 RPM and 80 PES while SOI was varied from 355 to 280 CAD. Diesel injection pressure and intake boost pressure were kept constant at 500 bar and 1.5 bar, respectively, and no EGR was used.

4.2.1 Cylinder Pressure and Net Apparent Heat Release Rate

Figures 4.10 and 4.11 present cylinder pressure profiles and AHRR curves at different SOIs. As SOI is advanced from 350 CAD to 280 CAD, the shapes of the AHRR curves and combustion characteristics change significantly. For convenience and better understanding of the results, cylinder pressure profiles and AHRR are plotted separately for early and late SOIs. As SOI is advanced from 350 CAD to 330 CAD, peak AHRR

www.manaraa.com

values increase. The AHRR curves also exhibit two distinct stages and no significant low temperature heat release (LTHR) peak because of relatively high in-cylinder temperatures for late SOIs. Another feature to be noted is that there was very little or no separation between the end of injection (EOI) and start of heat release for these SOIs. For example, for the SOI of 340 CAD, the difference between SOC and where heat release rate becomes positive is about 0 CAD as both of the fuel injection finishes and combustion starts at 348 CAD. For the other two SOIs of 350 CAD and 355 CAD, heat release starts even before EOI.

As SOI is advanced further in the compression stroke, the separation between EOI and SOC increases. For the SOI of 320 CAD, the separation between SOC and EOI is about 16 CAD. As SOI is advanced to 280 CAD, the peak magnitude of AHRR decreases and the peak AHRR is phased beyond TDC. Also as SOI is advanced from 310 CAD to 280 CAD, the LTHR vanishes and a smooth AHRR curve that may represent "well mixed" diesel-ignited methane LTC is observed.

Figure 4 shows trends for maximum pressure rise rate (MPRR), ID, and COV of IMEP versus SOI. It is evident from Fig. 4 that while ID increases when SOI is advanced beyond 330 CAD, MPRR peaks near 330 CAD and is reduced for earlier and later SOIs. Also, as SOI is advanced, COV of IMEP decreases at first from 4.0 percent at 350 CAD to 1.6 percent at 320 CAD, and increased with further SOI advancement. The highest COV of IMEP of 9 percent occurred at the SOI of 250 CAD, indicating that combustion becomes increasingly unstable due to increasing homogeneity (and presumably weaker ignition centers) as SOI is advanced. Figure 5 shows that the combustion duration (CA10-90) decreases from about 23 CAD to about 12 CAD between SOIs of 350 CAD 310 CAD, and

www.manaraa.com

increases slightly for more advanced SOIs. Also, CA50 shifts from after TDC to before TDC as SOI is advanced from 350 CAD to 320 CAD and again swings back to after TDC upon further SOI advancement. These trends can be traced to the transition from two-stage AHRR curves at late SOIs to smooth single-stage AHRR curves that are progressively retarded with respect to TDC as SOI is advanced.

www.manaraa.com

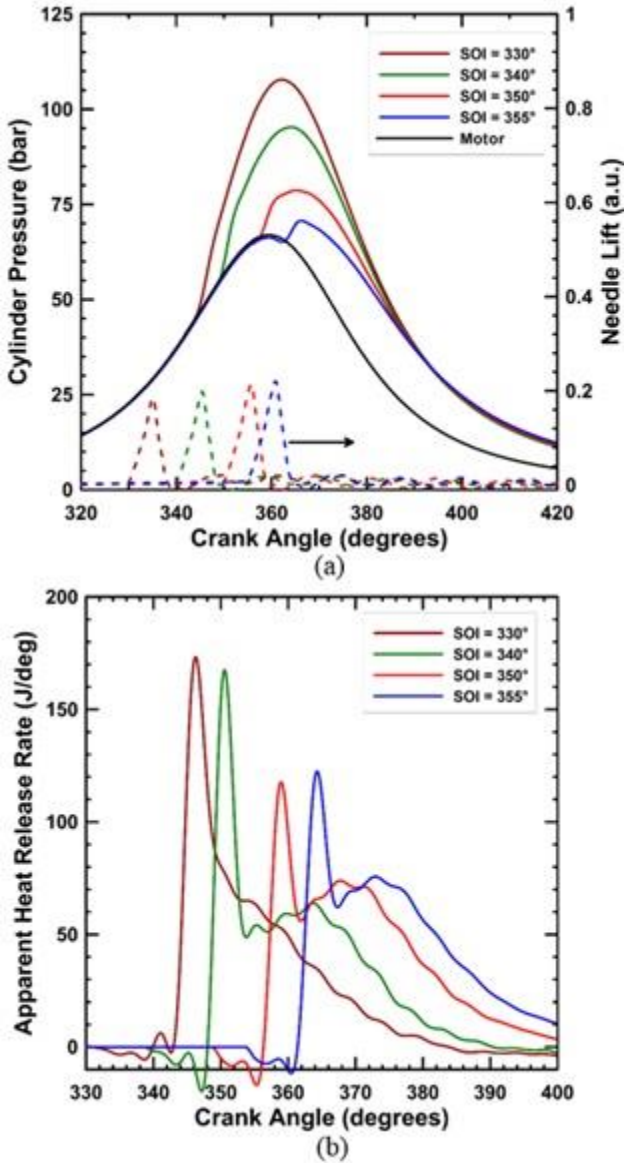

Figure 4.11 Transient data of diesel-methane dual-fueling for late SOIs

Note: (a) Cylinder pressure and needle lift profiles and (b) net AHRR profiles for late SOIs at 5.1 bar net IMEP, 80 PES, 1500 RPM, P_{rail} = 500 bar

www.manaraa.com

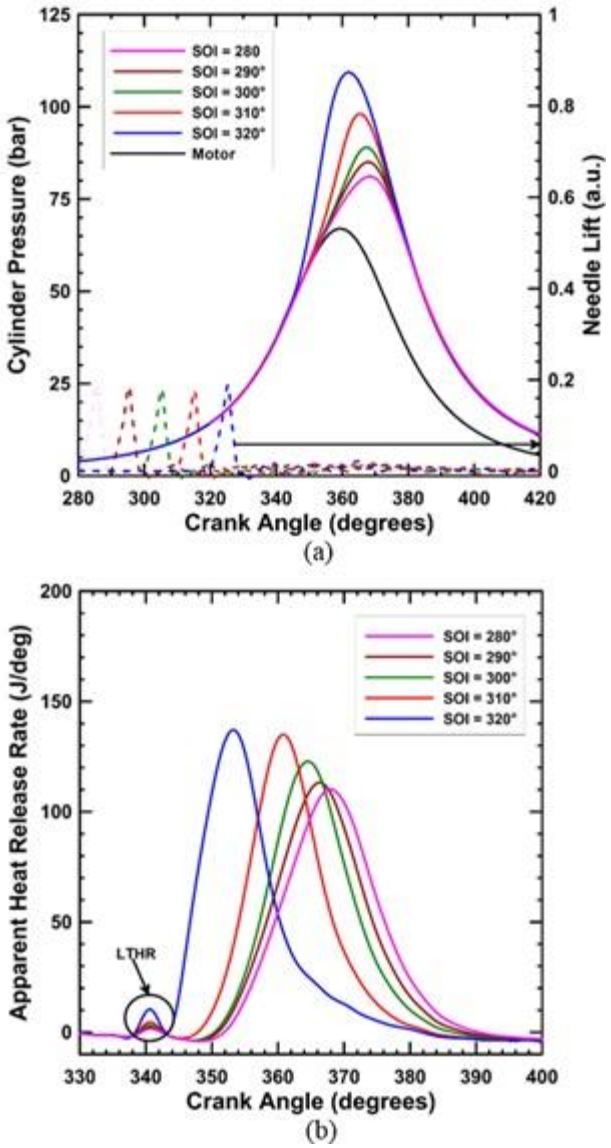

Figure 4.12 Transient data of diesel-methane dual-fueling for advanced SOIs

Note: (a) Cylinder pressure and needle lift profiles and (b) net AHRR profiles for advanced SOIs at 5.1 bar net IMEP, 80 PES, 1500 RPM, P_{rail} = 500 bar

4.2.2 Maximum Pressure Rise Rate, Ignition Delay, Combustion Stability and Combustion Phasing

Figure 4.13 shows trends for maximum pressure rise rate (MPRR), ID, and COV of IMEP versus SOI. It is evident from Fig. 4.13 that while ID increases when SOI is advanced beyond 330 CAD, MPRR peaks near 340 CAD and is reduced for earlier and

www.manaraa.com

later SOIs. Also, as SOI is advanced, COV of IMEP decreases at first from around 4.0 percent at 355 CAD to 1.7 percent at 330 CAD, and increases with further advancement in SOI. The highest COV of IMEP of 9.5 percent occurred at the SOI of 280 CAD, indicating that combustion becomes increasingly unstable due to increased homogeneity (and presumably weaker ignition centers) as SOI is advanced.

Figure 4.14 shows that the combustion duration (CA10-90) decreases from about 27.5 CAD to about 14.5 CAD between SOIs of 355 CAD and 310 CAD, and increases slightly for more advanced SOIs. Also, CA50 shifts from after TDC to before TDC as SOI is advanced from 350 CAD to 330 CAD and again swings back to after TDC upon further SOI advancement. These trends can be traced to the transition from two-stage AHRR curves at late SOIs to smooth single-stage AHRR curves that are progressively retarded with respect to TDC as SOI is advanced.

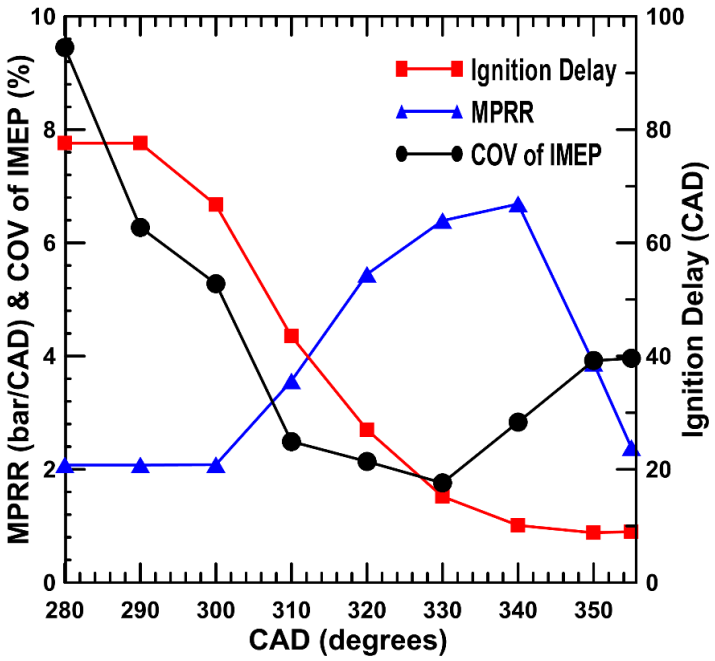

Figure 4.13 Ignition delay, MPRR and COV IMEP versus SOI for diesel-methane.

www.manaraa.com

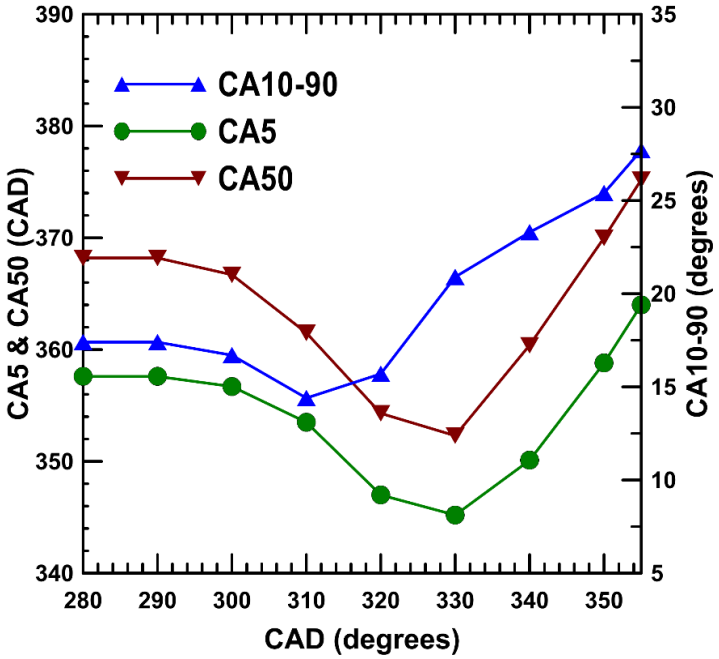

Figure 4.14 CA5, CA50, CA10-90 versus SOI for diesel-methane

4.2.3 Fuel Conversion Efficiency and Combustion Efficiency

Figure 4.15 shows the effects of SOIs on IFCE and combustion efficiencies at 5.1 bar IMEP and 80 PES. Combustion efficiency increases with SOI advancement from 355 CAD to 290 CAD and reaches the highest value of 81 percent, indicating that the HC and CO emissions are near the lowest levels at this SOI (see Fig. 4.17). Also, IFCE increases from 29 percent to 44 percent as SOI is advanced from 355 CAD to 320 CAD. This increase in IFCE can be related to the AHRR, CA50, and CA10-90 trends as well as the increased combustion efficiencies at the advanced SOIs. For further SOI advancement from 320 CAD to 280 CAD, both combustion efficiency and IFCE decrease due to retarded CA5 and CA50 and sharply increasing HC and CO emissions.

www.manaraa.com

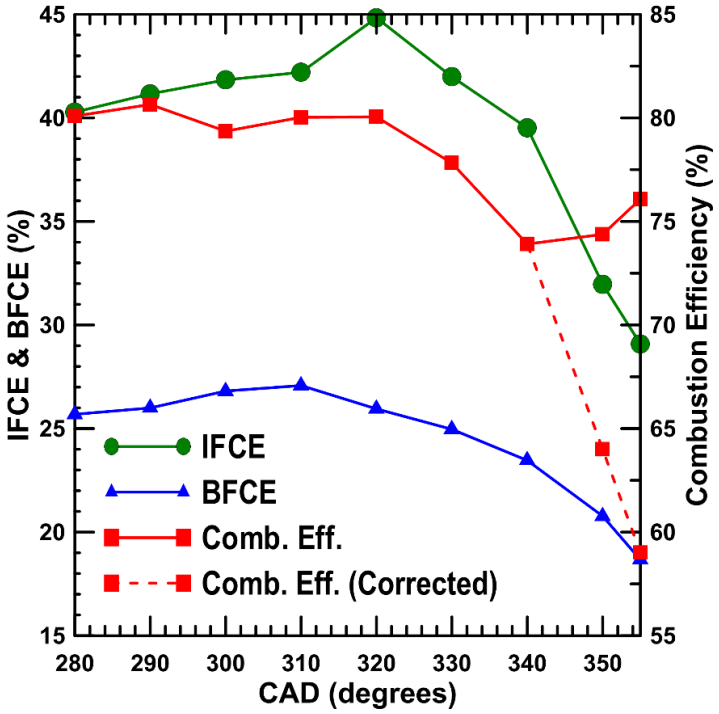

Figure 4.15 IFCE, BFCE and Combustion Efficiency versus SOI for diesel-methane

4.2.4 Emissions, Particle Concentrations and Size Distributions

Figure 4.16 shows $ISNO_x$ and smoke trends for different SOIs. As SOI is advanced from 355 CAD to 340 CAD, $ISNO_x$ sharply increases from about 5.5 g/kWh to about 11.6 g/kWh. However, on further SOI advancement to 330 CAD and beyond, $ISNO_x$ decreases significantly from 11.6 g/kWh to near zero levels (0.02 g/kWh). Near-zero $ISNO_x$ levels for sufficiently early SOIs are the cumulative effect of increased residence times, separation of EOI and SOC, and more complete fuel-air mixing leading to lean homogeneous fuel-air mixtures, all of which lead to low local temperatures.

The smoke emissions, which were less than 0.1 FSN for the entire SOI sweep, remain low due to the relatively high PES of methane (80 percent) coupled with the fact that the combustion process occurs in predominantly lean regions within the cylinder under

www.manaraa.com

these operating conditions. Simultaneous reductions in $ISNO_x$ and smoke emissions indicate that dual fuel LTC has been attained for SOIs at and beyond 310 CAD.

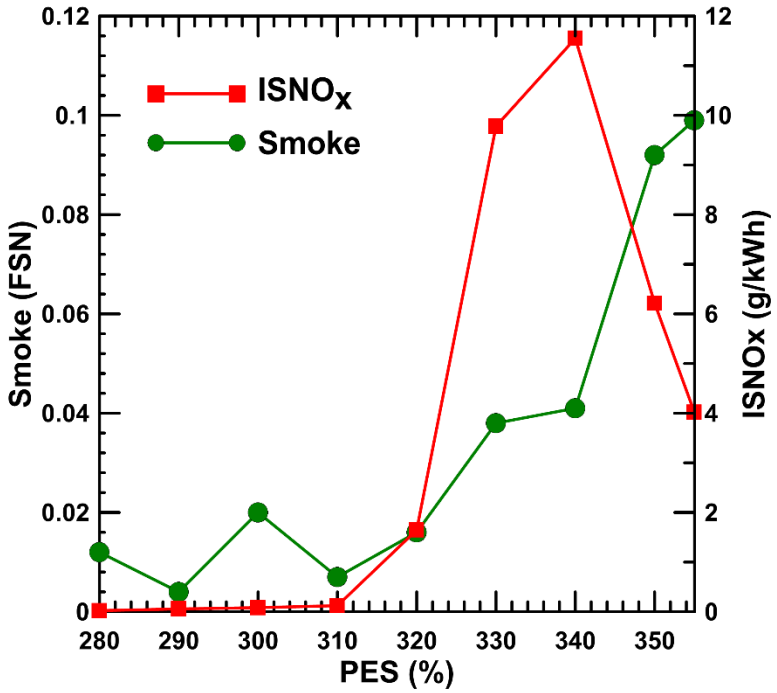

Figure 4.16 Smoke and $ISNO_x$ versus SOI for diesel-methane

Figure 4.17 shows the ISCO and ISHC emissions trends along with peak bulk temperature between SOIs of 355 CAD and 280 CAD. The ISCO decreases from about 23.6 g/kWh at 355 CAD SOI to 6.2 g/kWh at 320 CAD SOI and then increases to 41 g/kWh at the most advanced SOI of 280 CAD. A very sharp decrease in ISHC is also observed from 108 g/kWh to 35 g/kWh when SOI is advanced from 350 CAD to 280 CAD.

The manifestation of very high ISHC at the SOIs of 355 CAD and 350 CAD can be explained by analyzing the CA50 and CA10-90 trends along with bulk peak temperature. At the outset, it must be recognized that combustion chamber crevices are

www.manaraa.com

likely significant sources of HC in the present scenario where methane is fumigated into the intake manifold. On the other hand, bulk quenching due to mixing of hotter post-combustion gases with cooler surroundings may also lead to CO as well as HC formation. At the retarded SOIs of 355-340 CAD and the very advanced SOIs of 300 CAD – 280 CAD, the CA50 occurs at nearly 18 CAD after TDC, and consequently, the bulk of the combustion process occurs during the expansion stroke. Oxidation of CO and HC are significantly influenced by the in-cylinder temperatures as well as the residence times of hot post-combustion gases in the combustion chamber. Since the bulk of the combustion occurs after TDC, peak in-cylinder temperatures for these retarded SOIs are relatively lower but increase in magnitude as SOI is advanced, thereby leading to high engine-out ISHC emissions under these conditions.

The CO emissions attain the lowest levels for the SOI of 320 CAD. This is because of the fact that CA50 is phased before TDC and the peak bulk gas temperature is the highest at this particular SOI which favors CO oxidation during the expansion process. On further advancement of SOIs from 320 CAD to 280 CAD, it is possible that competition between HC and CO oxidation reactions resulted in high CO emissions. Since HC oxidation rates are much faster than CO, HC is oxidized and CO increases. The decreasing trend of peak bulk temperatures as SOI is advanced 320 CAD and beyond also supports this theory. It is evident that for very advanced or very retarded SOIs, the overall bulk gas temperatures are lower than those of intermediate SOIs. This reduction in peak bulk gas temperature likely reduced the availability of OH radicals in the lean premixed diesel-methane-air mixture surrounding the diesel jet. Also, as CO oxidation occurs later in the combustion process after the oxidation of the original fuel molecules, it is possible that HC is oxidized

www.manaraa.com

early in the combustion process but late-cycle CO oxidation is perhaps inhibited by lower bulk gas temperatures at these advanced or retarded SOIs.

Figure 4.19 is plotted to present the variation of equivalence ratio and also a measure of the authenticity of the presented data as equivalence ratios are calculated by two completely different methods using different set of instruments. Similar to PES sweep, THC emissions at two operating point (355 CAD and 350 CAD) exceeded operational limits of emission bench. So, THC emissions are recalculated (shown by the dotted curve in the Figure 4.19) keeping equivalence ratio of emissions within ±5 percent of the equivalence ratio measured from the flow rates of air and fuel. This also affects the combustion efficiency and ISHC emissions significantly and are presented with dotted lines as well in their respective figures.

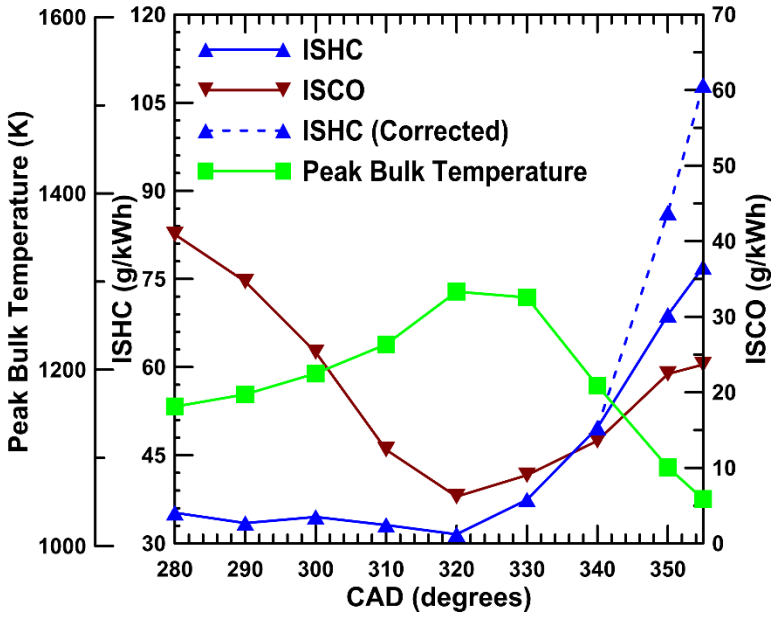

Figure 4.17 ISHC ,ISCO and peak bulk temperature versus SOI for diesel-methane

www.manaraa.com

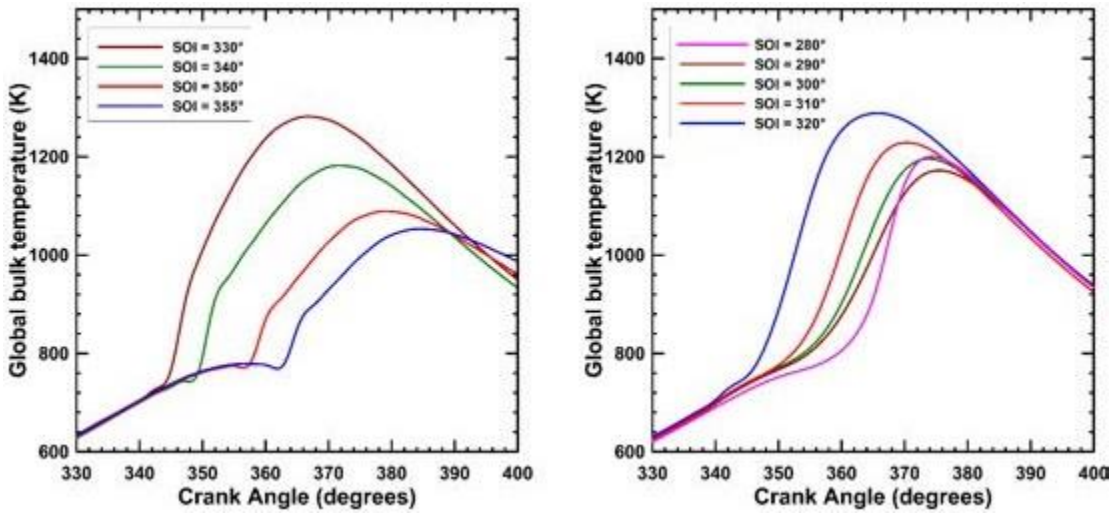

Figure 4.18 Global temperature profiles at various SOIs for diesel-methane

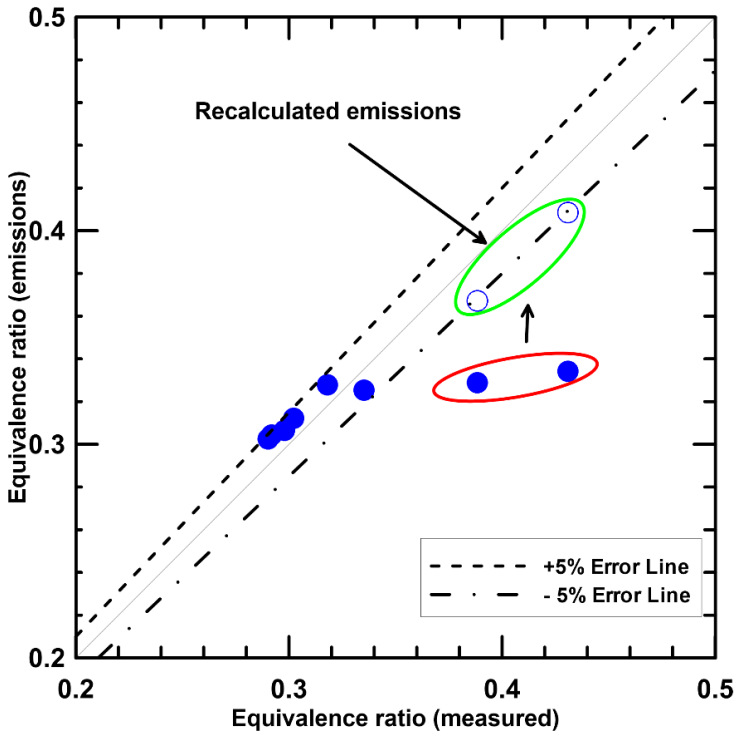

Figure 4.19 Equivalence ratio (emissions) versus equivalence ratio (measured) at various SOIs for diesel-methane

www.manaraa.com

Figure 4.20 illustrates the effect of SOIs on particle number concentration and size distribution. Very high concentration of nanoparticles are present for 355 SOIs of CAD and 350 CAD indicating comparatively higher soot emissions at these conditions. As SOI is advanced from 355 CAD to 320 CAD, particles concentrations decrease, only to increase again slightly with further advancement in SOIs. Also from Figure 4.16, it is evident that soot emissions are invariant for SOIs of 320 and beyond and significantly higher at two most retarded SOIs further validate the trends observed in particle concentrations.

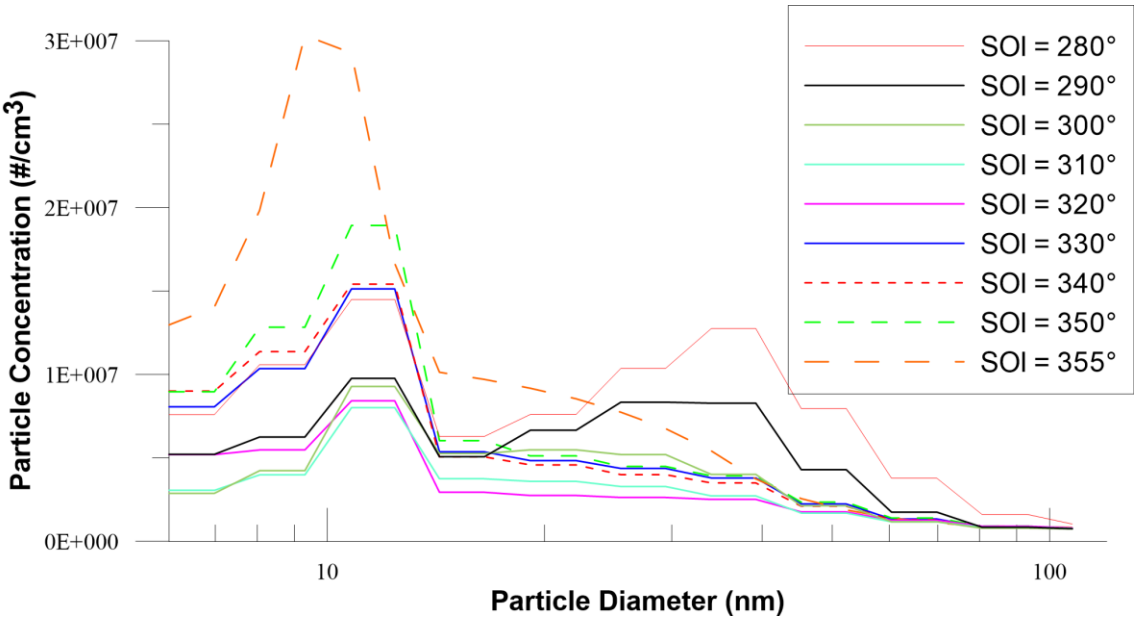

Figure 4.20 Normalized particle number ($dN/dlogD_p$) concentrations and size (D_p) distribution at various SOIs for diesel-methane

4.3 Rail Pressure Sweep: Performance and Emissions

For the rail pressure sweep, the engine was operated at 5.1 bar IMEP, 1500 RPM, 80 PES, 310 CAD SOI, and an intake boost pressure of 1.5 bar while injection pressure was varied from 200 bar to 1300 bar.

www.manaraa.com

4.3.1 Cylinder Pressure and Net Apparent Heat Release Rate

Figures 4.21 and 4.22 present cylinder pressure and AHRR profiles for injection pressures ranging from 200 to 1300 bar. As injection pressure increases from 200 bar to 1300 bar, the cylinder pressure profile shifts away from TDC. From the needle lift profiles shown in Fig. 4.21, it is evident that the injection duration for 200 bar injection pressure is approximately 15 CAD. The separation between EOI (325 CAD) and SOC (345 CAD) is about 25 CAD. A distinct LTHR is present for all injection pressures at around 339 CAD. The LTHR is related to the SOI and the in-cylinder residence time of the pilot diesel fuel before SOC. Since SOI was kept constant at 310 CAD for the range of injection pressures, the magnitude of LTHR is slightly suppressed with increasing injection pressure whereas the location of LTHR with respect to TDC remains almost constant. The magnitude of peak AHRR increases and the SOC shifts toward TDC (Figure 4.24) as the injection pressure is increased. As the SOC is shifted toward TDC, the diesel sprays have more time to mix with the surrounding methane-air mixture. Consequently, a more premixed combustion process occurs and this facilitates faster overall burn rates. Moreover, as the diesel is injected at higher pressures, enhanced entrainment and turbulent mixing due to high jet momentum ensure availability of more prepared diesel-methane-air mixture when the in-cylinder temperature and pressure are high enough to support autoignition. Simultaneous autoignition of higher amounts of prepared diesel-air mixture also resulted in high peak AHRR at high injection pressures.

www.manaraa.com

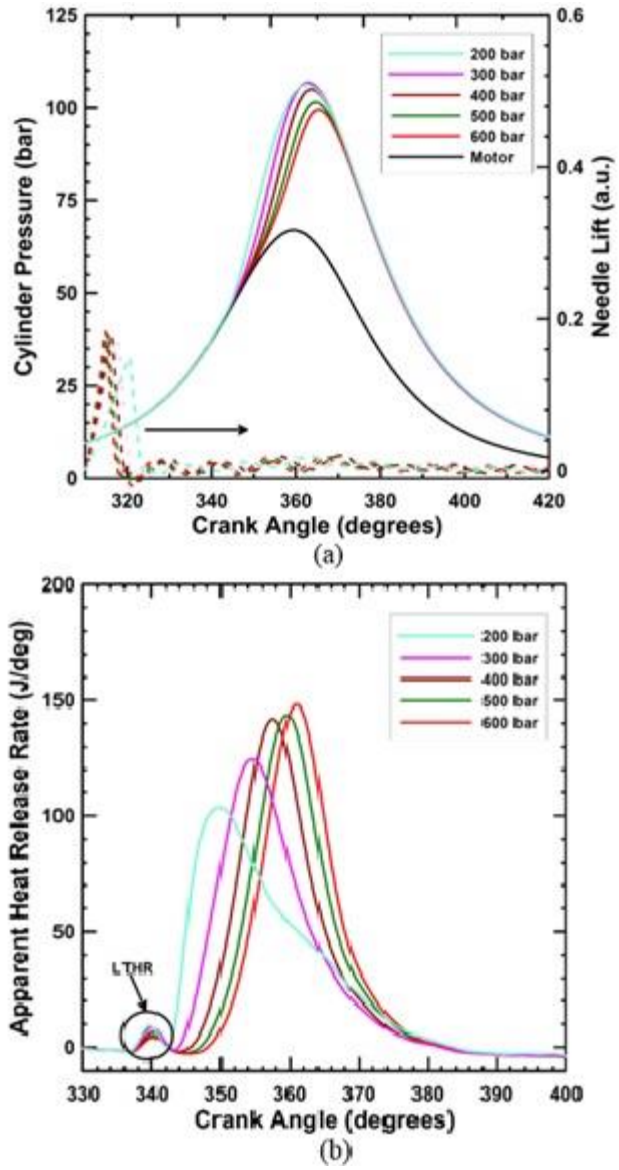

Figure 4.21 Transient data of diesel-methane dual fueling at lower injection pressures

Note: (a) Cylinder pressure and needle lift profiles and (b) net AHRR profiles for 200 to 600 bar of rail pressure at 5.1 bar net IMEP, 80 PES, 1500 RPM, SOI = 310 CAD, P_{in} = 1.5 bar

www.manaraa.com

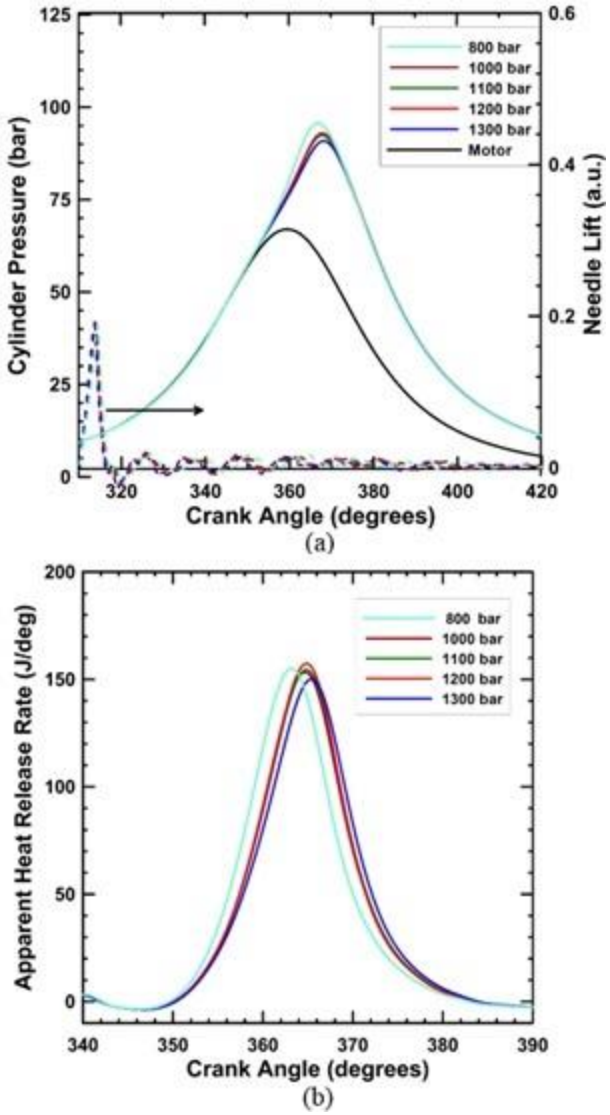

Figure 4.22 Transient data of diesel-methane dual fueling at higher injection pressures

Note: (a) Cylinder pressure and needle lift profiles and (b) net AHRR profiles for 800 – 1300 bar of rail pressure at 5.1 bar net IMEP, 80 PES, 1500 RPM, SOI = 310 CAD, P_{in} = 1.5 bar

4.3.2 Maximum Pressure Rise Rate, Ignition Delay, Combustion Stability and Combustion Phasing

As shown in Figure 4.23, MPRR decreases and ID increases with increasing injection pressure. These trends further support the reasons discussed earlier for CA50 and CA10-90 behavior. The increase in ID with increasing injection pressure leads to longer

www.manaraa.com

residence times for the diesel to mix with the methane-air mixture, thereby creating a "well mixed" mixture at high injection pressures. Further, the probability of spray impingement on the cylinder walls is increased with increasing injection pressure, especially for the early SOI of 310 CAD for these experiments. These factors combined to delay the CA50 as rail pressure is increased, thereby decreasing the MPRR. The COV of IMEP for the rail pressure sweep remained nearly invariant between 2.1 percent to 2.5 percent, except for the case of 200 bar rail pressure.

Figure 4.24 shows the SOC (i.e., CA5), combustion phasing (CA50), and combustion duration (CA10-90) over the range of injection pressures investigated. The CA50 is phased progressively closer to TDC as the injection pressure is increased from 200 bar to 1300 bar while the CA10-90 decreases with increased injection pressure. The combustion process is phased closer to TDC at higher injection pressures due to enhanced turbulent mixing of diesel with the surrounding methane-air mixture, which is caused by the greater jet momentum at higher injection pressures.

www.manaraa.com

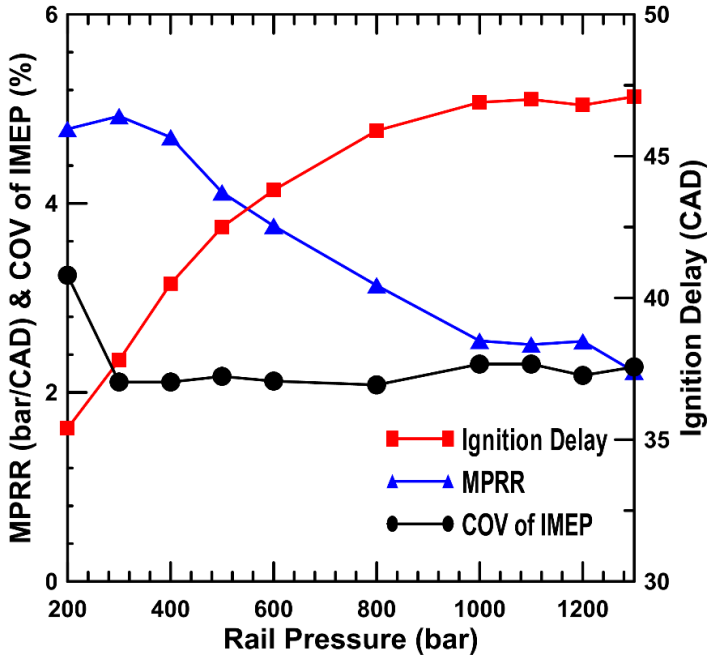

Figure 4.23 Ignition delay, MPRR and COV IMEP versus rail pressures for diesel-methane

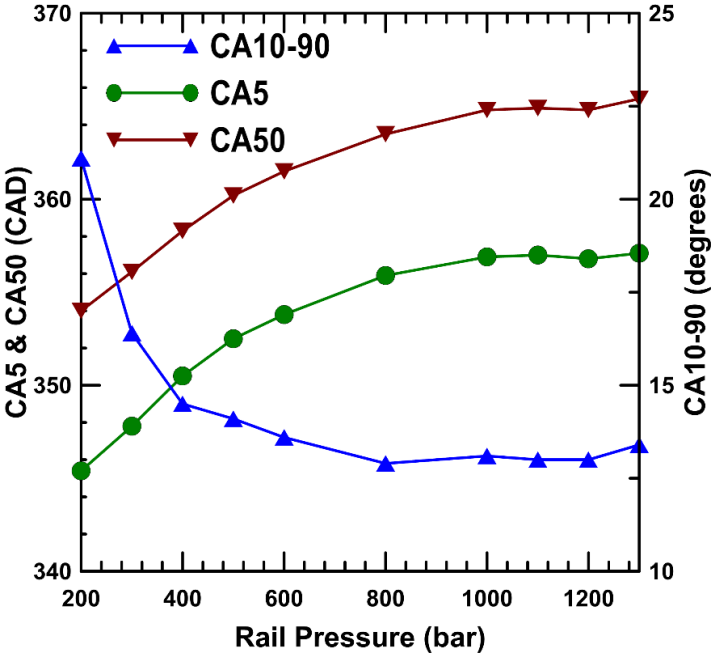

Figure 4.24 CA5, CA50, CA10-90 versus rail pressures for diesel-methane

www.manaraa.com

4.3.3 Fuel Conversion Efficiency and Combustion Efficiency

Figure 4.25 shows the combustion efficiency and IFCE trends with injection pressures. Combustion efficiency increases slightly as the injection pressure is increased from 200 to 1300 bar. Combustion at 1300 bar is characterized by CA50 phased after TDC and shorter combustion durations; therefore, the IFCE and combustion efficiency are slightly higher.

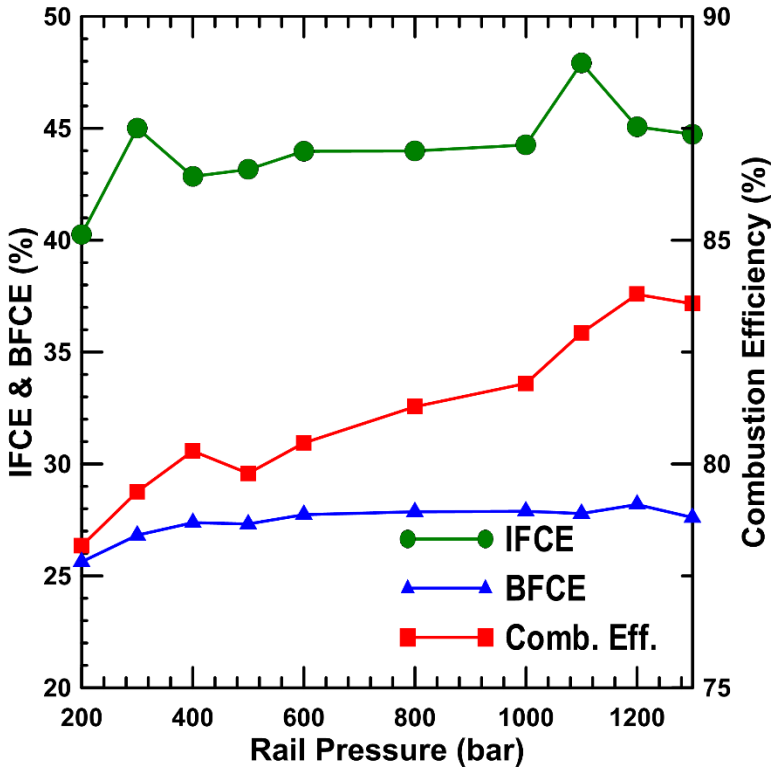

Figure 4.25 IFCE, BFCE and Combustion Efficiency versus rail pressures for diesel-methane

4.3.4 Emissions, Particle Concentrations and Size Distributions

Figure 4.26 represents $ISNO_x$ and smoke emissions with injection pressure variations. As injection pressure is increased from 200 bar to 1300 bar, $ISNO_x$ emissions

www.manaraa.com

decrease significantly from 5.4 g/kWh to near-zero levels (0.034 g/kWh) while the smoke emissions levels remain constant (less than 0.1 FSN). The high value of NO_x at 200 bar injection pressure is likely due to the fact that the injection duration is longer to keep the same diesel injected quantity as evident from the needle lift profile shown in Figure 4.21. As a result, the combustion is probably more stratified and characterized by high local temperatures that favor thermal NO formation. On the other hand, as injection pressure increases, the injection duration decreases, the separation between EOI and SOC increases, and most importantly, diesel fuel is mixed more completely with the surrounding methane-air mixture before the onset of combustion. Figure 4.21 and Figure 4.22 show that with increasing injection pressure, the cylinder pressure profiles are shifted away from TDC. As a result, the ignition delays are longer and combustion is increasingly homogeneous and occurs at low local temperatures thus alleviating thermal NO_x formation. From Fig. 4.26, it is evident that the "optimum" injection pressure vis-à-vis $ISNO_x$ emissions is 500 bar (*only* under the present conditions), beyond which there is very little change in the $ISNO_x$ levels (0.14 g/kWh at 500 bar). Engine-out smoke emissions are low throughout the injection pressure sweep due to the high PES of methane (80 percent) and the overall lean combustion process in the methane-air mixture, regardless of injection pressure.

www.manaraa.com

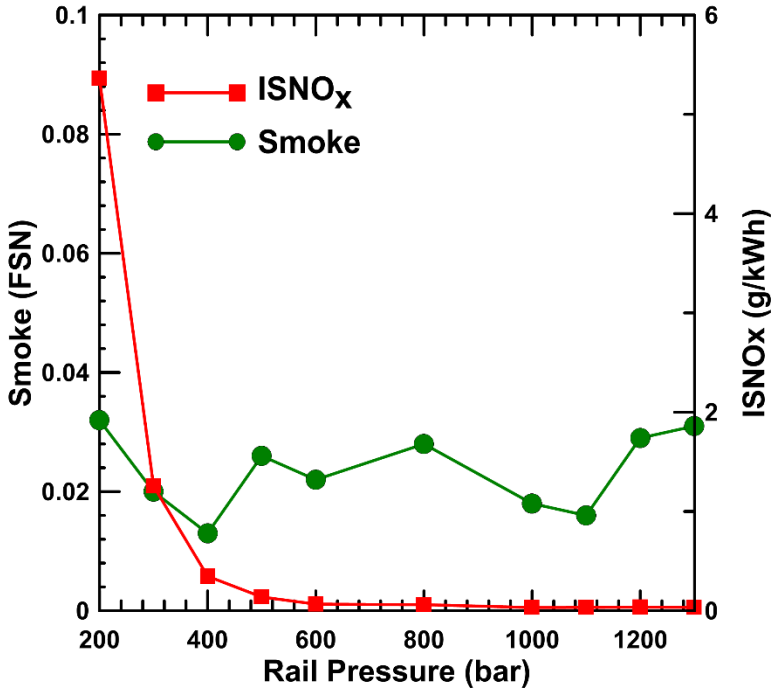

Figure 4.26 Smoke and $ISNO_x$ versus rail pressures for diesel-methane.

Figure 4.27 shows the ISHC and ISCO emissions trends with injection pressures. The ISHC emissions steadily decrease from about 37 g/kWh at 200 bar to about 25 g/kWh at 1300 bar injection pressure. This trend also indicates the higher combustion efficiencies at higher injection pressures. Higher injection pressures lead to better fuel-air mixing and a more homogeneous combustion process, which also facilitates better mixing of high-temperature diesel combustion zones with leaner, low-temperature methane combustion zones, and consequently, better HC oxidation. On the other hand, only a slight increase in ISCO emissions is observed with increasing injection pressure. At higher injection pressures, better fuel-air mixing can cause mixture "overleaning" that leads to lower peak bulk temperatures, which inhibit the CO $\rightarrow$ CO_2 conversion. Combined with better HC oxidation and potential mixture overleaning, the shorter CA10-90 durations at higher

www.manaraa.com

injection pressure reduce the time available for CO oxidization as post-combustion gases cool, thereby increasing the CO emissions.

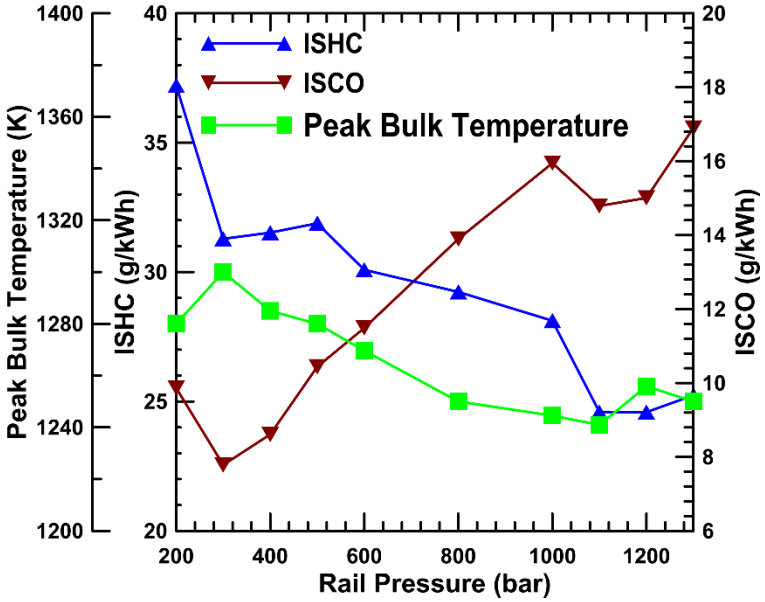

Figure 4.27 ISHC ,ISCO and peak bulk temperature versus rail pressures for diesel-methane..

www.manaraa.com

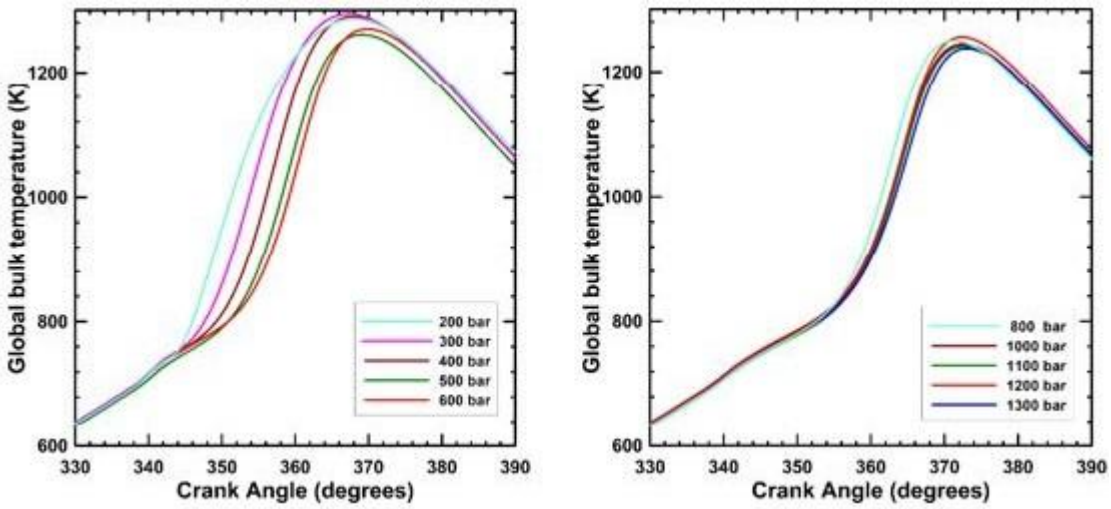

Figure 4.28 Global temperature profiles for various rail pressures for diesel-methane

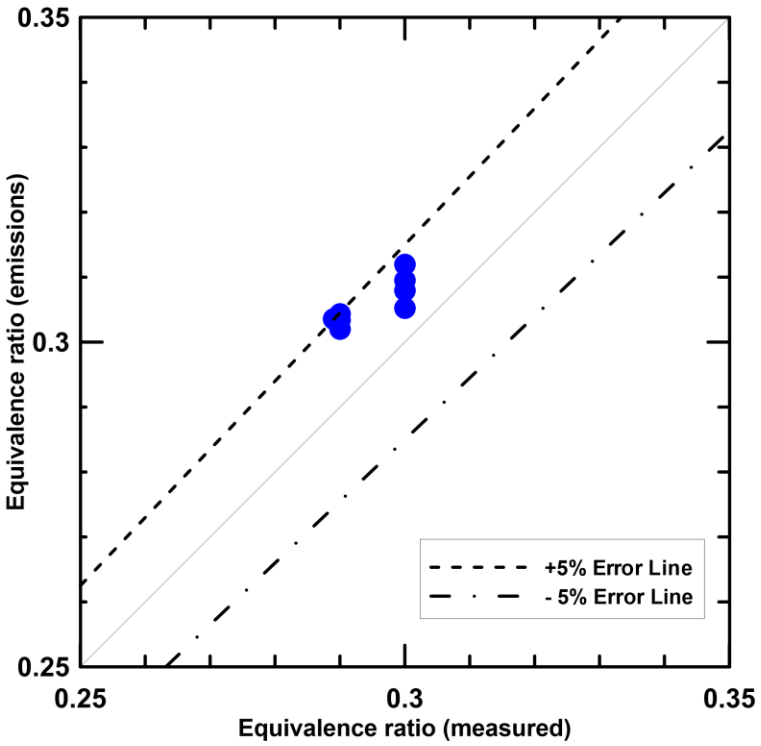

Figure 4.29 Equivalence ratio (emissions) versus equivalence ratio (measured) at various rail pressures for diesel-methane

www.manaraa.com

Figure 4.30 presents the effect of rail pressures on particle number concentration and size distribution. No definite trend is observed in particle concentrations Overall, it can be said that more nanoparticles form at higher injection pressures due to more homogenous nature of the mixing and combustion process. The relative magnitudes of the particle concentrations exhibit more complex trends and need extensive study to fully understand the effects of injection pressures at these operating conditions.

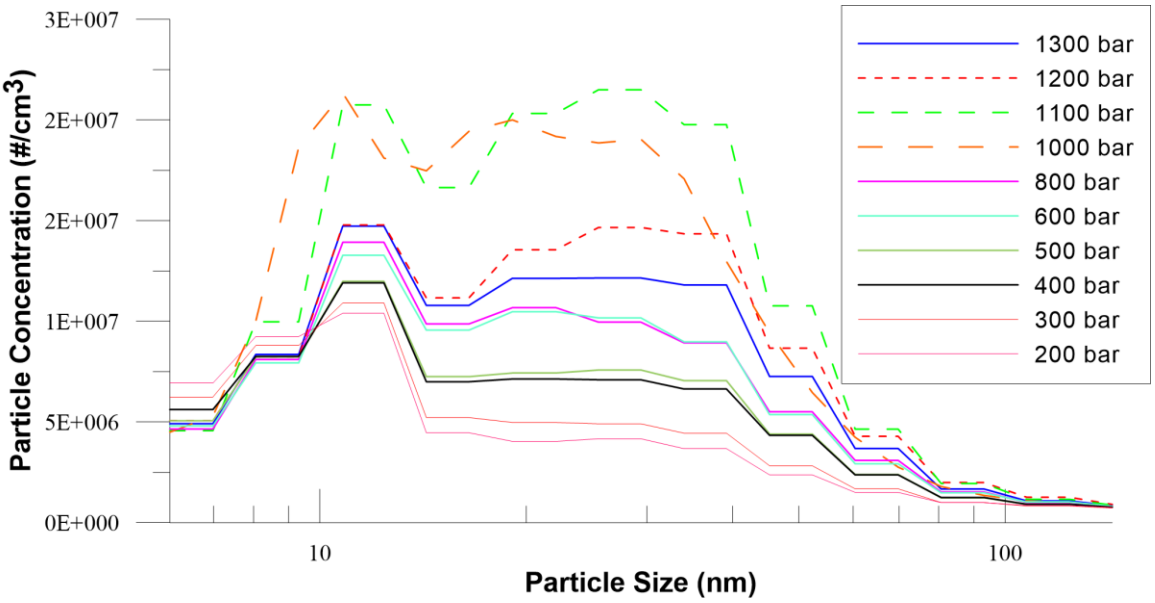

Figure 4.30 Normalized particle number ($dN/dlogD_p$) concentrations and size (D_p) distribution at various rail pressures for diesel-methane

4.4 Intake Boost Pressure Sweep: Performance and Emissions

The effect of intake boost pressure variations (from 1.1 bar to 1.8 bar) were studied at 5.1 bar IMEP, 1500 RPM, 80 PES, 310 CAD SOI, an injection pressure of 500 bar.

www.manaraa.com

4.4.1 Cylinder Pressure and Net Apparent Heat Release Rate

Figure 4.31 shows cylinder pressure and AHRR profiles for intake boost pressures ranging from 1.1 to 1.8 bar. As the intake boost pressure is increased, peak cylinder pressure is also increased as expected due to the greater charge mass trapped within the cylinder. Also, the SOC as well as the location of peak pressure occur earlier with increasing boost pressure. However, the AHRR profiles exhibit a different trend. Peak AHRR decreases and the location of peak AHRR advances with increasing intake boost pressure. As intake boost pressure increases, the in-cylinder pressures and temperatures both before and during combustion are higher; consequently, combustion occurs earlier. In addition, the advancement of SOC with increasing boost pressure can be attributed to the increase in the magnitude of LTHR as well as a slight advancement of the LTHR profile, which can lead to higher pre-combustion temperatures and faster pre-ignition reactions. Another related aspect of these intake boost pressure experiments is that the overall equivalence ratio is also allowed to vary with boost pressure (since the engine load is fixed at 5.1 bar IMEP); the equivalence calculated from measured fuel and air mass flow rates decreased from 0.41 at 1.1 bar to 0.27 at 1.8 bar boost pressure. Clearly, the temporal phasing of the AHRR curves is also affected by the overall equivalence ratios.

www.manaraa.com

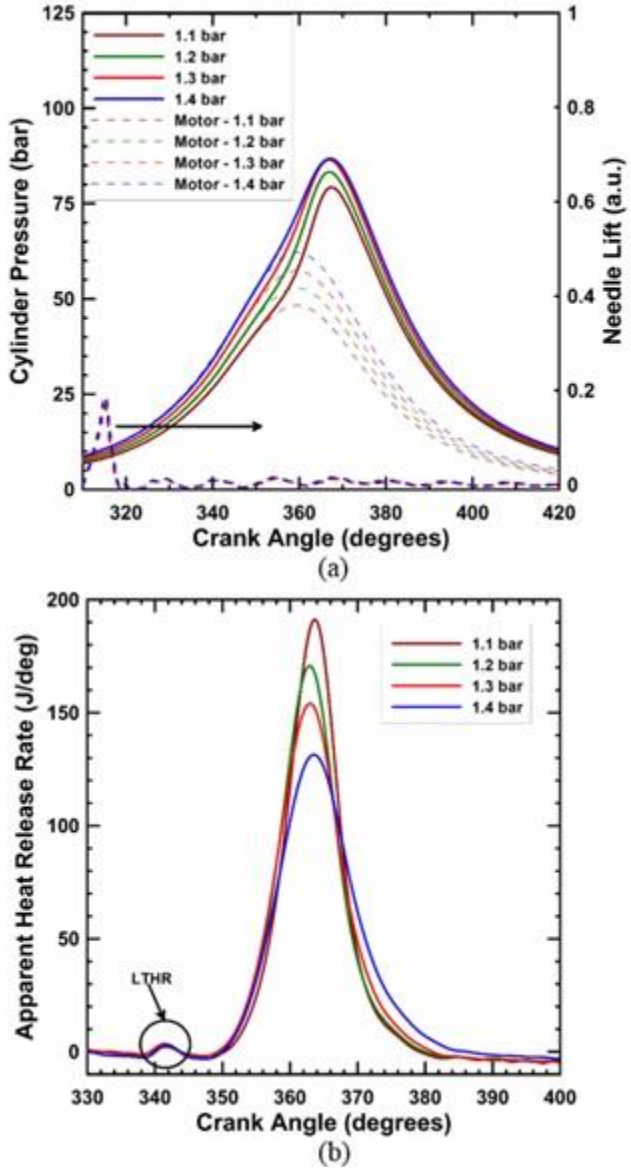

Figure 4.31 Transient data of diesel-methane dual fueling for boost pressure of 1.1 to 1.4 bar

Note: (a) Cylinder pressure and needle lift profiles and (b) net AHRR profiles at 5.1 bar net IMEP, 80 PES, 1500 RPM, SOI = 310 CAD, P_{rail} = 500 bar

www.manaraa.com

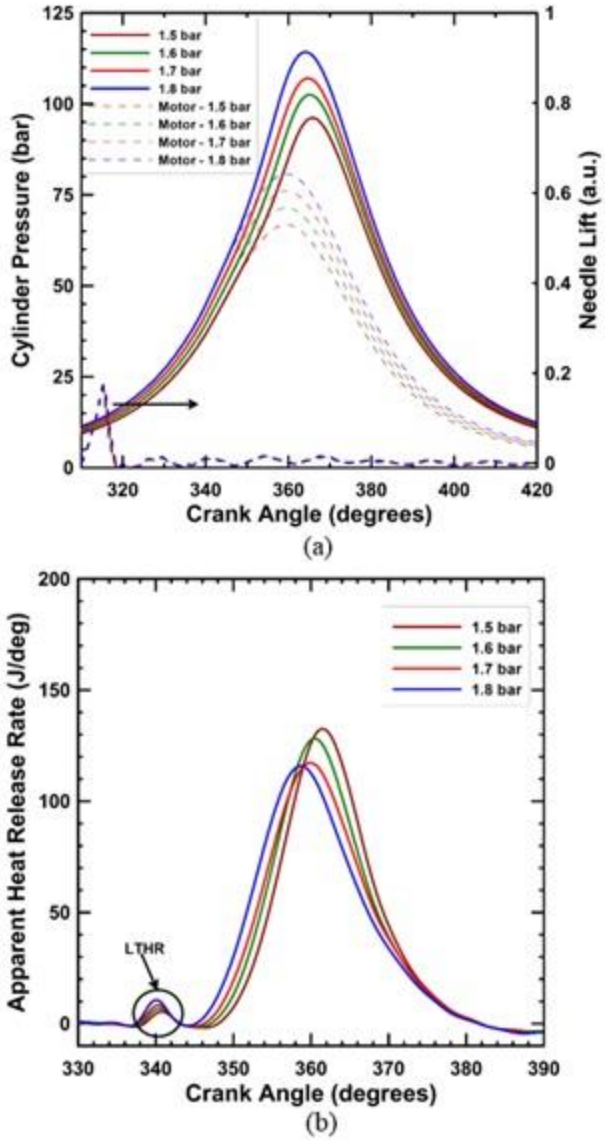

Figure 4.32 Transient data of diesel-methane dual fueling for boost pressure of 1.5 to 1.8 bar

Note: (a) Cylinder pressure and needle lift profiles and (b) net AHRR profiles at 5.1 bar net IMEP, 80 PES, 1500 RPM, SOI = 310 CAD, P_{rail} = 500 bar

4.4.2 Maximum Pressure Rise Rate, Ignition Delay, Combustion Stability and Combustion Phasing

Figure 4.33 presents MPRR and ID trends while Figure 4.34 shows trends for CA5, CA50, and CA10-90 for different intake boost pressures. MPRR shows an increasing trend

www.manaraa.com

followed by a decreasing trend with increasing boost pressure, ID decreases from 46 CAD at 1.1 bar boost to about 39 CAD at 1.8 bar boost. A decrease in intake boost pressure reduces in-cylinder pressures and temperatures, thus increasing the ID period. In addition, the CA50 shifts from before TDC to after TDC and CA10-90 decreases from 17 CAD to 11 CAD as the boost pressure is reduced. Finally, since the overall equivalence ratio also increases as boost pressure is decreased, the combustion process occurs more rapidly, resulting in higher peak AHRR and slightly higher MPRR. Additionally, the COV of IMEP increases slightly from 2 percent at 1.1 bar to 3 percent at 1.8 bar of boost pressure.

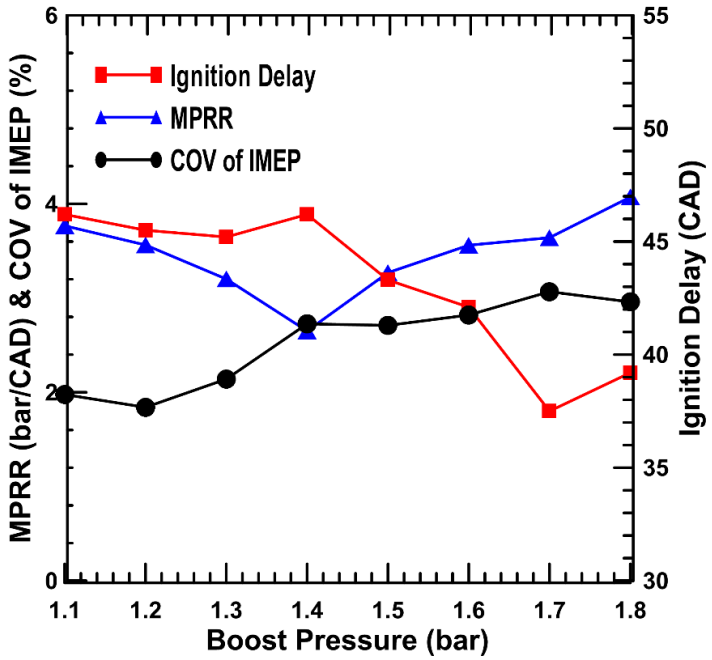

Figure 4.33 Ignition delay, MPRR and COV IMEP versus boost pressures for diesel-methane

www.manaraa.com

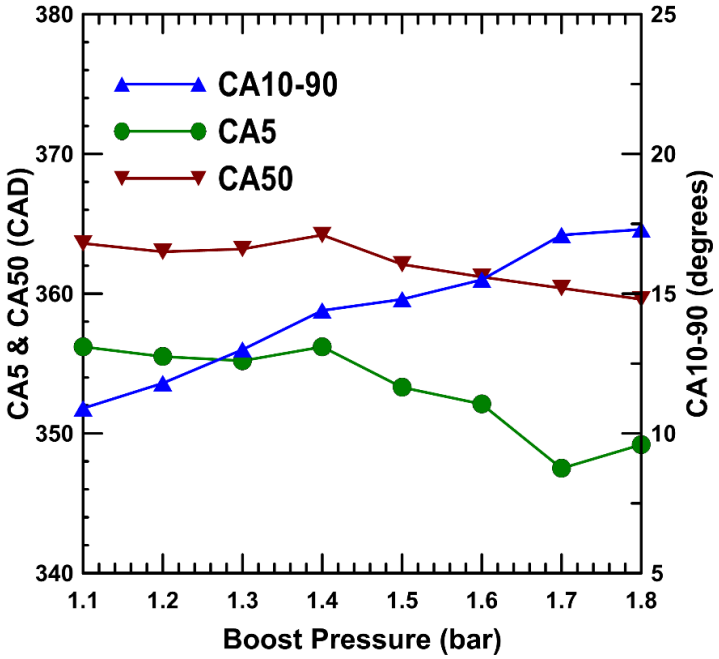

Figure 4.34 CA5, CA50, CA10-90 versus boost pressures for diesel-methane

4.4.3 Fuel Conversion Efficiency and Combustion Efficiency

The effect of intake boost pressure on IFCE, BFCE and combustion efficiency are shown in Figure 4.35. With increasing intake boost pressure, the IFCE decreases from 46.4 percent at 1.1 bar to 43.4 percent at 1.8 bar while the combustion efficiency decreases from 86 percent to 72 percent. This is due to the fact that both CA5 and CA50 shift from after TDC to before TDC with increasing boost pressures as shown in Figure 4.31 and 4.32. For example, at the lowest boost pressure of 1.1 bar, the CA50 occurs at about 363 CAD but is phased around 359 CAD at 1.8 bar boost pressure. Since CA50 is phased after TDC for lower boost pressures along with decreased CA10-90, IFCE increases. In addition, due to the higher overall equivalence ratios at the lower boost pressures, the combustion efficiency is also higher.

www.manaraa.com

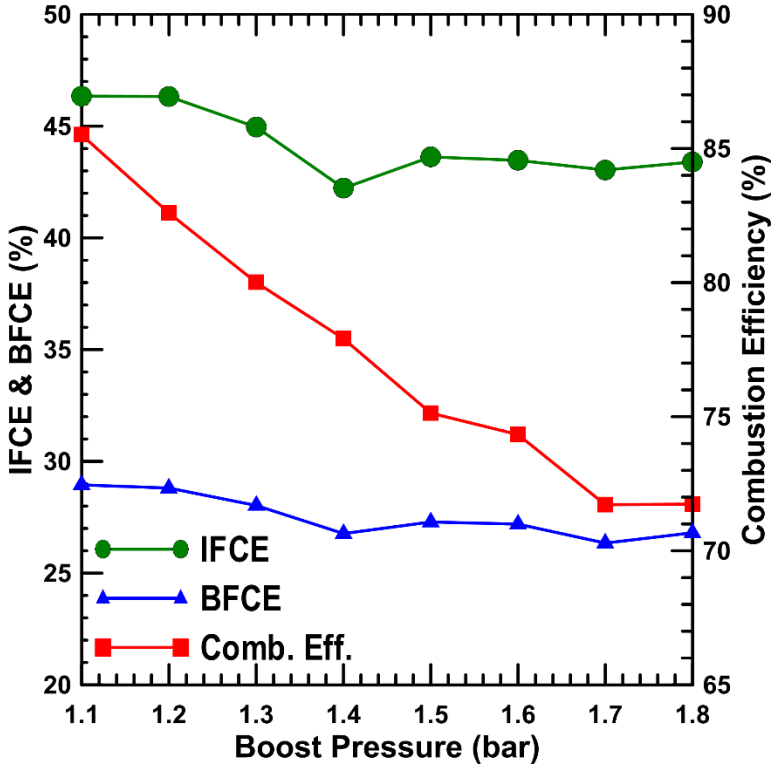

Figure 4.35 IFCE, BFCE and Combustion Efficiency versus boost pressures for diesel-methane

4.4.4 Emissions, Particle Concentrations and Size Distributions

Figure 4.36 shows that faster AHRR and higher local temperatures lead to an increase in ISNO$_x$ emissions for boost pressures lower than 1.3 bar. However, the smoke emissions remain very low (i.e., <0.1 FSN) and fairly invariant with intake boost pressure. Also, from Figure 4.37, it is evident that as intake boost pressure is increased, both ISHC and ISCO increase. These trends can be explained with the AHRR profiles shown in Figure 4.31 and 4.32. From the AHRR profiles, peak AHRR is the highest for the lowest intake boost pressure of 1.1 bar and the peak bulk temperature is also significantly higher for this condition, thereby assisting in better oxidation of CO to CO_2. In addition, the higher

www.manaraa.com

equivalence ratios at lower boost pressures will also aid in CO oxidation. The ISHC trends are also similar since they also increase when bulk gas temperatures are reduced. Also, as unburned fuel trapped in the crevices are one of the main sources of HC emissions, it is possible that higher intake boost pressures (leading to higher in-cylinder pressures) will result in trapping more unburned methane in the crevices. A significant fraction of the unburned methane trapped in crevices may not burn before exhaust valve opens due to incomplete mixing with hot post-combustion gases and unfavorable temperature-time histories.

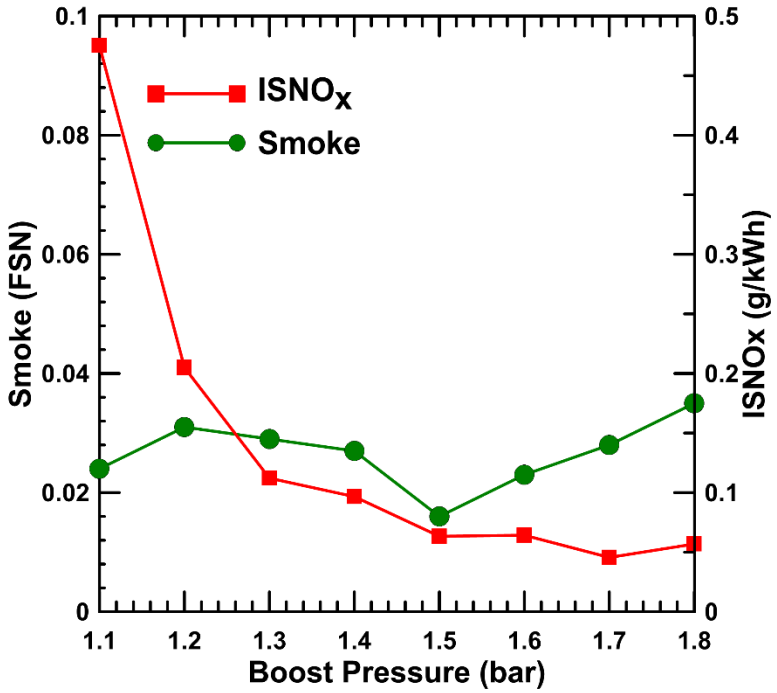

Figure 4.36 Smoke and $ISNO_x$ versus boost pressures for diesel-methane

www.manaraa.com

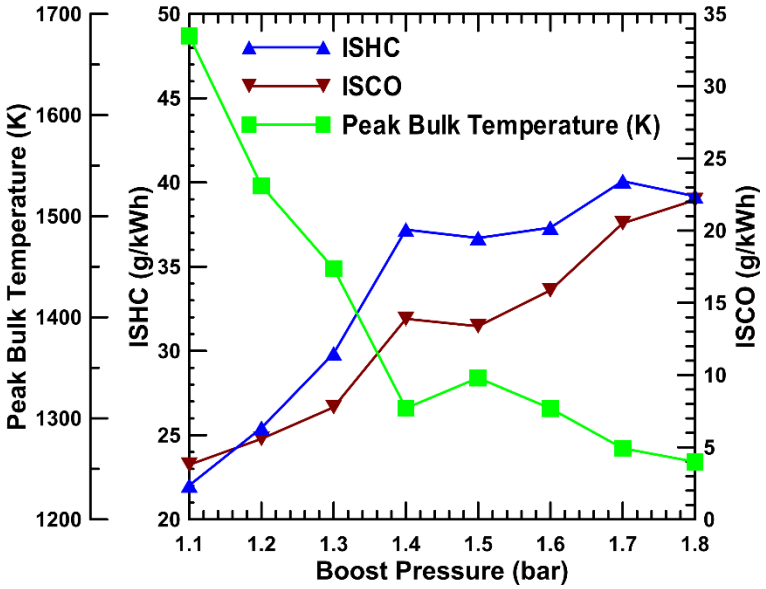

Figure 4.37 ISHC ,ISCO and peak bulk temperature versus boost pressures for diesel-methane

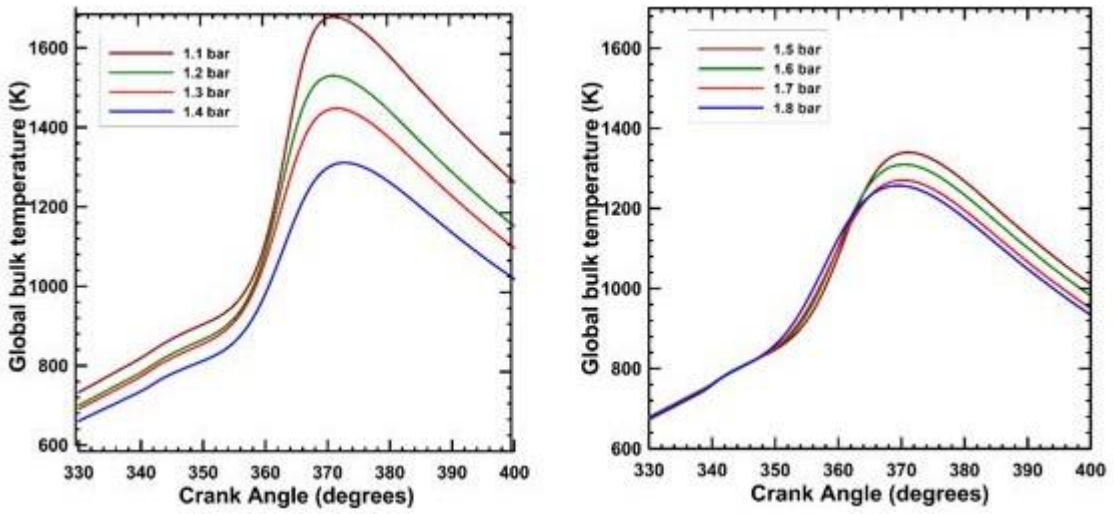

Figure 4.38 Global temperature profiles for various boost pressures for diesel-methane

www.manaraa.com

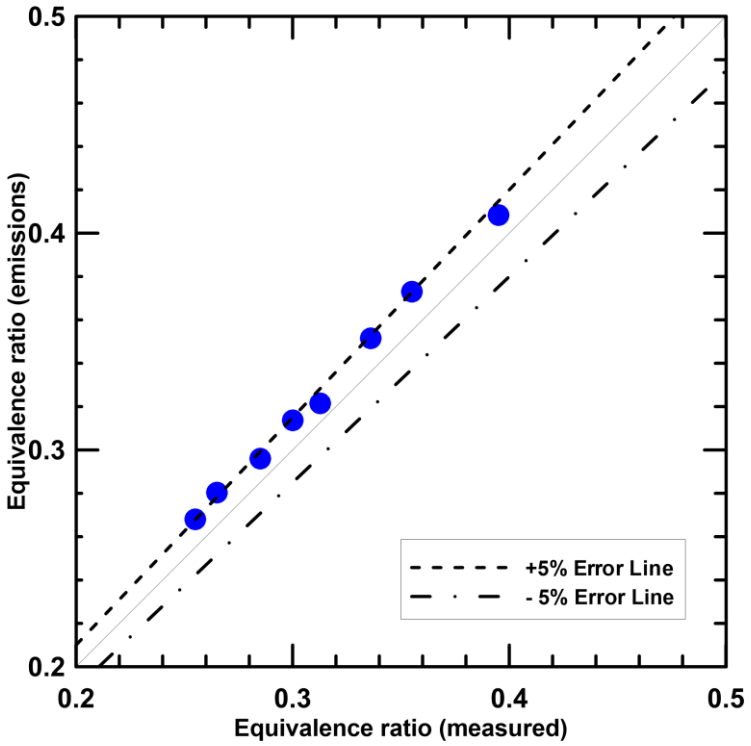

Figure 4.39 Equivalence ratio (emissions) versus equivalence ratio (measured) at various rail pressures for diesel-methane.

Figure 4.40 shows the boost pressure effects on particle number concentrations and size distribution. Again, it is very hard to find any discernible trend as the soot emissions in these conditions are very low and differences in particle concentrations in different boost conditions are not that significant.

www.manaraa.com

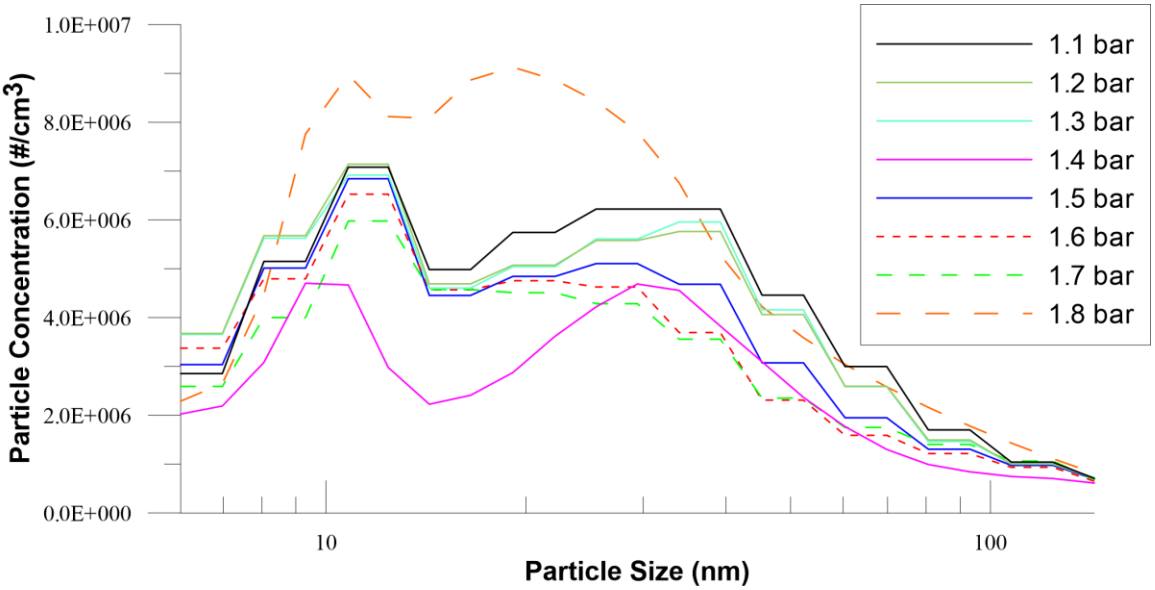

Figure 4.40 Normalized particle number ($dN/dlogD_p$) concentrations and size (D_p) distribution at various boost pressures for diesel-methane

www.manaraa.com

CHAPTER V

CONCLUSIONS AND RECOMMENDATIONS FOR FUTURE WORK

Diesel-ignited propane and methane dual fuel combustion experiments were performed in a single-cylinder research engine at a constant speed of 1500 RPM and a constant load of 5.1 bar net IMEP was maintained. Percentage of energy substitution of propane and methane (PES: 0 to 90 percent), diesel injection timing (SOI: 280-355 CAD), diesel injection pressure (200-1300 bar), and intake boost pressure (1.1-1.8 bar) were varied to isolate and analyze their impacts on combustion heat release (AHRR), indicated fuel conversion efficiency (IFCE) and combustion efficiency, and engine-out $ISNO_x$, ISHC, ISCO, and smoke emissions. The following conclusions can be drawn from the results obtained in these experiments:

5.1 Diesel-Propane Dual Fuel Low Temperature Combustion (LTC)

The optimal propane substitution at 355 CAD SOI, 500 bar rail pressure and 1.5 bar intake boost pressure was determined to be 80 percent. The coefficient of variation (COV) of indicated mean effective pressure (IMEP) increased sharply with a further increase in PES. With increasing PES, the magnitude of the peak AHRR for first stage burn increased, while the second stage AHRR. Two-stage AHRR profiles indicate that the time available for diesel mixing with the surrounding propane-air mixture is not sufficient, and consequently, significant mixture stratification created by the diesel jet is

www.manaraa.com

still present during the combustion process. Moreover, combustion occurred later in the expansion stroke and combustion duration progressively increased, indicating that the combustion becomes slower with increasing PES. The IFCE and combustion efficiency decreased sharply from around 45 percent and 100 percent for straight diesel operation (0 PES) to around 34 percent and 63 percent, respectively, at 80 PES reflecting that the dual fuel combustion process at high PES is less efficient and leads to higher HC and CO emissions. Both $ISNO_x$ and smoke emissions decreased with increasing PES; however, the lowest value of $ISNO_x$ emissions at the highest possible PES was still much higher than US EPA 2010 regulations (0.27 g/kWh) suggesting that the SOI of 355 CAD is not optimum to achieve diesel-propane LTC.

i. The SOI sweep exhibited the most significant effect on both the performance emissions for diesel-propane dual fuel combustion. As SOI was advanced, the combustion process transitioned from two-stage, heterogeneous, diesel-like combustion to single-stage, homogeneous, HCCI-like combustion. For advanced SOIs of 320 CAD and beyond, only single-stage heat release was observed. Combustion phasing shifted from before TDC at retarded SOIs to after TDC at intermediate SOIs and swung back again with further advancement. Ignition delay also increased steadily, while the maximum pressure rise rate (MPRR) decreased for advanced SOIs. Optimal engine performance was obtained at advanced SOIs of 330 CAD and beyond, as the efficiencies are almost invariant for these SOIs. However, high COV of IMEP at advanced SOIs indicates that there may be a level of "optimal homogeneity" for dual fuel combustion beyond which combustion becomes unstable. Moreover, $ISNO_x$ and soot emissions declined sharply between

www.manaraa.com

355 and 320 CAD and decreased slightly with further advancement. At an SOI of 310 CAD, $ISNO_x$ emissions satisfied the US EPA emissions regulations while maintaining ultra-low soot emissions (< 0.1 FSN). Also, ISCO and ISHC emissions increased slightly as SOI was advanced from 330 CAD, thus affecting the efficiencies. So, the SOI of 310 CAD was considered as the optimal SOI for simultaneously reducing NO_x and soot emissions, maintaining stable combustion, achieving high efficiencies, and lower ISCO and ISHC emissions compared to more advanced or more retarded SOIs.

ii. A rail pressure sweep was performed at 310 CAD SOI to isolate the effects of rail pressure on performance and emissions showing that $ISNO_x$ emissions are very high at lower rail pressures due to increased heterogeneity. Increased jet momentum with increasing rail pressures tend to improve mixture entrainment into the diesel jets leading to more homogeneous mixtures, which alter the nature of combustion. This trend toward increasingly homogeneous mixtures at higher rail pressures forces the combustion to start later and to release energy at a much faster rate, resulting in a sharp decrease in combustion duration. However, soot emissions remained invariant for any variation in rail pressure.

iii. An intake pressure sweep between 1.1 bar and 1.8 bar revealed that the combustion phasing shifted toward TDC with increasing boost pressure, demonstrating a gradual decrease in ignition delay and a significant increase in peak pressure. The $ISNO_x$ and smoke emissions exhibited a slightly decreasing trend; however, the $ISNO_x$ remained lower than 0.27 g/kWh for all boost pressures. A slight increasing trend in IFCE with increasing boost pressure indicates the potential benefits of

www.manaraa.com

employing the highest boost pressure. However, considering the very high peak pressures and MPRRs associated with higher boost pressures, as well as increased ISCO emissions, a moderate boost pressure of 1.5 bar was selected as the best compromise.

5.2 Diesel-Methane Dual Fuel Low Temperature Combustion

Diesel-ignited methane dual fuel combustion experiments were performed in the same engine maintaining the same engine operating conditions as done in diesel–propane dual fueling to get a comparative idea of performance and emissions of these two fueling combinations. The experimental results obtained for diesel-methane dual fueling lead to the following conclusions.

i. Advancing SOI from 340 CAD to 310 CAD reduced ISNO$_x$ from 11.6 g/kWh to less than 0.12 g/kWh; further advancement of SOI did not yield significant ISNO$_x$ reduction. Smoke emissions were less than 0.1 FSN at all SOIs. ISHC and ISCO emissions were very high for very late and at very early SOIs. The IFCE increased from 29.1 percent to 42.2 percent as SOI was advanced from 355 CAD to 310 CAD due to better combustion efficiencies, favorable combustion phasing, and shorter combustion durations. Combustion efficiency deteriorated at very late SOIs (355 - 340 CAD) due to substantially higher ISHC and ISCO emissions as the bulk of the combustion process was completed in the expansion stroke. Within the 280-355 CAD SOI range, the maximum pressure rise rate (MPRR) peaked at 6.8 bar/CAD for 340 CAD SOI but was reduced significantly (around 2 bar/CAD) for SOIs earlier than 300 CAD. On the other hand, ignition delay increased steadily with SOI advancement.

www.manaraa.com

ii. An injection pressure sweep from 200 to 1300 bar at 310 CAD SOI, and 80 PES showed that very low injection pressures apparently led to more heterogeneous combustion and higher $ISNO_x$, ISCO, and ISHC emissions, while smoke remained unaffected. The intermediate injection pressure of 500 bar appeared to be optimal vis-à-vis performance and emissions under these conditions. Combustion efficiency and IFCE were unaffected but ignition delay increased and MPRR was reduced with increased injection pressure.

iii. An intake boost pressure sweep from 1.1 to 1.8 bar at 500 bar injection pressure, 310 CAD SOI, and 80 PES showed that $ISNO_x$ and smoke remained fairly low at 1.2 bar or higher boost pressures ($ISNO_x$ < 0.2 g/kWh; smoke < 0.1 FSN) and unaffected by boost pressure. However, increasing intake boost pressure increased both ISHC and ISCO emissions. Consequently, while IFCE was only slightly reduced, combustion efficiency decreased from 85 percent at 1.1 bar intake boost pressure to about 71 percent at 1.8 bar.

5.3 Recommendations for Future Work

- The capability of the current SCRE hardware to perform more detailed dual fuel experiments is constrained by the lack of an EGR system. Emissions and engine performance are expected to improve and substantially higher loads may be realized with minimal adverse effects on MPRR if EGR is employed.
- High ISHC and ISCO emissions are significantly high for dual fuel LTC and cause great concern vis-à-vis the practical feasibility of dual fuel LTC, especially at low loads. However, the sources of ISHC and ISCO emissions are not yet fully

www.manaraa.com

understood. Installing an optically accessible piston to investigate ISCO and ISHC emissions more thoroughly would definitely help in this regard.

- Multiple diesel injection pulses are used in modern diesel engines to reduce engine-out soot emissions. Similarly, a multiple pilot (diesel) injection strategy may be helpful in optimizing the tradeoffs between $ISNO_x$, ISHC, and ISCO emissions for both diesel-methane and diesel-propane dual fuel LTC and should be pursued with carefully designed experiments at low to moderate load conditions.
- Effects of other engine parameters like compression ratio, nozzle geometry, and piston bowl configurations on dual fuel LTC can be systematically studied.
- Experiments should be performed to optimize PES and SOI at all load conditions.

www.manaraa.com

REFERENCES

Abd Alla, G. H., Soliman, H. A., Badr, O. A., & Abd Rabbo, M. F. (2000). Effect of pilot fuel quantity on the performance of a dual fuel engine. Energy Conversion and Management, 41(6), 559-572.

Abd Alla, G. H., Soliman, H. A., Badr, O. A., & Abd Rabbo, M. F. (2002). Effect of injection timing on the performance of a dual fuel engine. Energy conversion and Management, 43(2), 269-277.

Agarwal, A. K. (2007). Biofuels (alcohols and biodiesel) applications as fuels for internal combustion engines. Progress in energy and combustion science, 33(3), 233-271.

Akihama K, Takatori Y, Inagaki K, Sasaki S, Dean AM.(2001) Mechanism of the smokeless rich diesel combustion by reducing temperature. SAE Technical Paper 2001- 01-0655

Badr, O., Karim, G. A., & Liu, B. (1999). An examination of the flame spread limits in a dual fuel engine. Applied Thermal Engineering, 19(10), 1071-1080.

Beck, N. J., Barkhimer, R. L., Johnson, W. P., Wong, H. C., & Gebert, K. (1997). Evolution of heavy duty natural gas engines-stoichiometric, carbureted and spark ignited to lean burn, fuel injected and micro-pilot (No. 972665). SAE Technical Paper.

Bedoya, I. D., Arrieta, A. A., & Cadavid, F. J. (2009). Effects of mixing system and pilot fuel quality on diesel–biogas dual fuel engine performance. Bioresource technology, 100(24), 6624-6629.

Brunt, M., Rai, H., and Emtage, A. (1998). The Calculation of Heat Release Energy from Engine Cylinder Pressure Data , SAE Technical Paper 981052.

Carlucci, A. P., De Risi, A., Laforgia, D., & Naccarato, F. (2008). Experimental investigation and combustion analysis of a direct injection dual-fuel diesel–natural gas engine. Energy, 33(2), 256-263.

Chen, Z., Yao, M., Zheng, Z., & Zhang, Q. (2009). Experimental and numerical study of methanol/dimethyl ether dual-fuel compound combustion. Energy & Fuels, 23(5), 2719-2730.

www.manaraa.com

Contino, F., Dagaut, P., Dayma, G., Halter, F., Foucher, F., and Mounaïm-Rousselle, C. (2014). "Combustion and Emissions Characteristics of Valeric Biofuels in a Compression Ignition Engine." J. Energy Eng. 140, SPECIAL ISSUE: Innovative Technologies on Combustion of Biofuels in Engines: Issues and Challenges, A4014013.

Daisho, Y., Yaeo, T., Koseki, T., Saito, T. et al. (1995). Combustion and Exhaust Emissions in a Direct-injection Diesel Engine Dual-Fueled with Natural Gas. SAE Technical Paper 950465, doi:10.4271/950465

de Ojeda, W., Zoldak, P., Espinosa, R., & Kumar, R. (2008). Development of a Fuel Injection Strategy for Diesel LTC. SAE Technical Paper 2008-01-0057, doi:10.4271/2008-01-0057

Dec, J. E. (1997). A Conceptual Model of DI Diesel Combustion Based on Laser-Sheet Imaging. SAE Transactions, 106(3), 1319-1348.

Dec, J. E. (2009). Advanced compression-ignition engines—understanding the in-cylinder processes. Proceedings of the Combustion Institute, 32(2), 2727-2742.

Debnath, B., Bora, B., Sahoo, N., and Saha, U. (2014). "Influence of Emulsified Palm Biodiesel as Pilot Fuel in a Biogas Run Dual Fuel Diesel Engine." J. Energy Eng. 140, SPECIAL ISSUE: Innovative Technologies on Combustion of Biofuels in Engines: Issues and Challenges, A4014005.

DieselNet (2014), US EPA Heavy-Duty Engine Emissions standards, <http://www.dieselnet.com/standards/us/hd.php> (April 10, 2014)

Dobbins, R. A. (2002). Soot inception temperature and the carbonization rate of precursor particles. Combustion and flame, 130(3), 204-214.

Gibson, C. M., Polk, A. C., Shoemaker, N. T., Srinivasan, K. K., & Krishnan, S. R. (2011). Comparison of propane and methane performance and emissions in a turbocharged direct injection dual fuel engine. Journal of Engineering for Gas Turbines and Power, 133(9), 092806.

Glassman I & Yetter RA. (2008). Combustion. 4th ed., Academic Press.

Giakoumis, E., Rakopoulos, C., and Rakopoulos, D. (2014). "Assessment of NO_x Emissions during Transient Diesel Engine Operation with Biodiesel Blends." J. Energy Eng. 140, SPECIAL ISSUE: Innovative Technologies on Combustion of Biofuels in Engines: Issues and Challenges, A4014004.

Goldsworthy, L. (2012). Combustion behavior of a heavy duty common rail marine diesel engine fumigated with propane. Experimental Thermal and Fluid Science, 42: 93-106.

www.manaraa.com

Hanson, R. M., Kokjohn, S. L., Splitter, D. A., & Reitz, R. D. (2010). An experimental investigation of fuel reactivity controlled PCCI combustion in a heavy-duty engine. SAE Int. J. Engines, 3(1), 700-716.

Hardy, W., & Reitz, R. (2006). A Study of the Effects of High EGR, High Equivalence Ratio, and Mixing Time on Emissions Levels in a Heavy-Duty Diesel Engine for PCCI Combustion. SAE Technical Paper 2006-01-0026

Heywood, J. B. (1988). Internal combustion engine fundamentals. New York: Mcgraw-hill.

Hsu, B. (2002). Practical diesel-engine combustion analysis (1st ed.). Warrendale, Pa.: Society of Automotive Engineers.

Huestis, E., Erickson, P. A., & Musculus, M. P. (2007). In-cylinder and exhaust soot in low-temperature combustion using a wide-range of EGR in a heavy-duty diesel engine. SAE Technical Paper 2007-01-4017, doi: 10.4271/2007-01-4017

Jindal, S., Nandwana, B. P., Rathore, N. S., & Vashistha, V. (2010). Experimental investigation of the effect of compression ratio and injection pressure in a direct injection diesel engine running on Jatropha methyl ester. Applied Thermal Engineering, 30(5), 442-448.

Karim GA. (1991). An examination of some measures for improving the performance of gas fuelled diesel engines at light load. SAE paper 912366

Karim, G. A. (2003). Combustion in gas fueled compression: ignition engines of the dual fuel type. ASME Journal of Engineering for Gas Turbines and Power, 125(3), 827-836.

Kokjohn, S. L., Hanson, R. M., Splitter, D. A., & Reitz, R. D. (2011). Fuel reactivity controlled compression ignition (RCCI): a pathway to controlled high-efficiency clean combustion. International Journal of Engine Research, 12(3), 209-226.

Kook, S., Bae, C., Miles, P., Choi, D., & Pickett, L. (2005). The Influence of Charge Dilution and Injection Timing on Low-Temperature Diesel Combustion and Emissions. SAE Technical Paper 2005-01-3837,doi:10.4271/2005-01-3837

Krishnan, S. R., Biruduganti, M., Mo, Y., Bell, S. R., & Midkiff, K. C. (2002). Performance and heat release analysis of a pilot-ignited natural gas engine. International Journal of Engine Research, 3(3), 171-184.

Krishnan, S. R., Gong, W., Fiveland, S. B., Srinivasan, K. K., Singh, S., Willi, M., ... & Midkiff, K. C. (2004). Strategies for reduced NO_x emissions in pilot-ignited natural gas engines. Journal of engineering for gas turbines and power, 126(3), 665-671.

www.manaraa.com

Kusaka, J., Okamoto, T., Daisho, Y., Kihara, R., & Saito, T. (2000). Combustion and exhaust gas emission characteristics of a diesel engine dual-fueled with natural gas. JSAE review, 21(4), 489-496.

Lee, D., Jho, Y., and Lee, C. (2014). "Effects of Soybean and Canola Oil–Based Biodiesel Blends on Spray, Combustion, and Emission Characteristics in a Diesel Engine." J. Energy Eng. 140, SPECIAL ISSUE: Innovative Technologies on Combustion of Biofuels in Engines: Issues and Challenges, A4014012.

Liu, Z., & Karim, G. A. (1995). The ignition delay period in dual fuel engines. SAE Technical Paper 950466, doi:10.4271/950466.

McTaggart-Cowan, G., Bushe, W. K., Hill, P. G., & Munshi, S. R. (2004). NO_x. reduction from a heavy-duty diesel engine with direct injection of natural gas and cooled exhaust gas recirculation. International Journal of Engine Research,5(2), 175-191.

McTaggart-Cowan, G. P., Reynolds, C. C. O., & Bushe, W. K. (2006). Natural gas fuelling for heavy-duty on-road use: current trends and future direction. International journal of environmental studies, 63(4), 421-440.

Musculus, M. P., Miles, P. C., & Pickett, L. M. (2013). Conceptual models for partially premixed low-temperature diesel combustion. Progress in Energy and Combustion Science, 39(2), 246-283.

Northrop, W., Bohac, S., and Assanis, D. (2009), "Premixed Low Temperature Combustion of Biodiesel and Blends in a High Speed Compression Ignition Engine," SAE Int. J. Fuels Lubr. 2(1):28-40, doi:10.4271/2009-01-0133.

Papagiannakis, R. G., & Hountalas, D. T. (2003). Experimental investigation concerning the effect of natural gas percentage on performance and emissions of a DI dual fuel diesel engine. Applied Thermal Engineering, 23(3), 353-365.

Papagiannakis, R. G., & Hountalas, D. T. (2004). Combustion and exhaust emission characteristics of a dual fuel compression ignition engine operated with pilot diesel fuel and natural gas. Energy conversion and management, 45(18), 2971-2987.

Papagiannakis, R. G., Hountalas, D. T., & Rakopoulos, C. D. (2007). Theoretical study of the effects of pilot fuel quantity and its injection timing on the performance and emissions of a dual fuel diesel engine. Energy Conversion and Management, 48(11), 2951-2961.

Papagiannakis, R. G., Rakopoulos, C. D., Hountalas, D. T., & Rakopoulos, D. C. (2010). Emission characteristics of high speed, dual fuel, compression ignition engine operating in a wide range of natural gas/diesel fuel proportions. Fuel, 89(7), 1397-1406.

www.manaraa.com

Park, C., & Appleton, J. P. (1973). Shock-tube measurements of soot oxidation rates. Combustion and Flame, 20(3), 369-379.

Plee, S., Ahmad, T., and Myers, J. (1981), "Flame Temperature Correlation for the Effects of Exhaust Gas Recirculation on Diesel Particulate and NO_x Emissions," SAE Technical Paper 811195, doi:10.4271/811195.

Plee, S. L., Ahmad, T., Myers, J. P., & Faeth, G. M. (1982, December). Diesel NOx emissions - A simple correlation technique for intake air effects. In Symposium (International) on Combustion (Vol. 19, No. 1, pp. 1495-1502).

Polk, A. C., Gibson, C. M., Shoemaker, N. T., Srinivasan, K. K., & Krishnan, S. R. (2013a). Analysis of Ignition Behavior in a Turbocharged Direct Injection Dual Fuel Engine Using Propane and Methane as Primary Fuels. Journal of Energy Resources Technology, 135(3), 032202.

Polk, A. C., Gibson, C. M., Shoemaker, N. T., Srinivasan, K. K., & Krishnan, S. R. (2013b). Detailed characterization of diesel-ignited propane and methane dual-fuel combustion in a turbocharged direct-injection diesel engine. Proceedings of the Institution of Mechanical Engineers, Part D: Journal of Automobile Engineering, 0954407013487292.

Polk, A.C., Carpenter, C.D., Guerry, E.S., Dwivedi, U., Srinivasan, K.K., Krishnan, S.R., and Rowland, Z.L. (2014a). Diesel-ignited propane dual fuel low temperature combustion in a heavy-duty diesel engine. Trans. ASME: Journal of Engineering for Gas Turbines and Power, 136(9), 091509 (Apr 18, 2014), Paper No: GTP-14-1085; doi: 10.1115/1.4027189.

Polk, A. C., Carpenter, C. D., Srinivasan, K. K., & Krishnan, S. R. (2014b). An investigation of diesel–ignited propane dual fuel combustion in a heavy-duty diesel engine. Fuel, 132, 135-148.

Poonia, M. P., Ramesh, A., & Gaur, R. R. (1999). Experimental investigation of the factors affecting the performance of a LPG-diesel dual fuel engine. SAE Technical Paper 1999-01-1123

Qi, Y., Srinivasan, K. K., Krishnan, S. R., Yang, H., & Midkiff, K. C. (2007). Effect of hot exhaust gas recirculation on the performance and emissions of an advanced injection low pilot-ignited natural gas engine. International Journal of Engine Research, 8(3), 289-303.

Raihan, M., Guerry, E., Dwivedi, U., Srinivasan, K., and Krishnan, S. (2014). "Experimental Analysis of Diesel-Ignited Methane Dual-Fuel Low-Temperature Combustion in a Single-Cylinder Diesel Engine." J. Energy Eng., 10.1061/(ASCE)EY.1943-7897.0000235 , C4014007

www.manaraa.com

Rakopoulos, C. D., Rakopoulos, D. C., Giakoumis, E. G., and Dimaratos, A. M. (2010). Investigation of the combustion of neat cottonseed oil or its neat bio-diesel in a HSDI diesel engine by experimental heat release and statistical analyses. Fuel, 89(12), 3814-3826.

Rakopoulos, D. C., Rakopoulos, C. D., Giakoumis, E. G., & Dimaratos, A. M. (2013). Studying combustion and cyclic irregularity of diethyl ether as supplement fuel in diesel engine. Fuel, 109, 325-335.

Ryan, T., & Callahan, T. (1996). Homogenous Charge Compression Ignition of Diesel Fuel. SAE Paper 96110, doi:10.4271/961160

Ryu, K. (2013a). Effects of pilot injection timing on the combustion and emissions characteristics in a diesel engine using biodiesel–CNG dual fuel. Applied Energy, 111, 721-730.

Ryu, K. (2013b). Effects of pilot injection pressure on the combustion and emissions characteristics in a diesel engine using biodiesel–CNG dual fuel.Energy Conversion and Management, 76, 506-516.

Saidi, M., Far, K., & Pirouzpanah, V. (2005). Analysis of Combustion Process in Dual Fuel Diesel Engines: Knock Phenomenon Approach. SAE Technical Paper 2005-01-1132,doi:10.4271/2005-01-1132

Saxena, S., and Bedoya, I. D. (2013). "Fundamental phenomena affecting low temperature combustion and HCCI engines, high load limits and strategies for extending these limits," Progress in Energy and Combustion Science, 39, 457-488

Sayin, C., Uslu, K., & Canakci, M. (2008). Influence of injection timing on the exhaust emissions of a dual-fuel CI engine. Renewable Energy, 33(6), 1314-1323.

Sayin, C., & Canakci, M. (2009). Effects of injection timing on the engine performance and exhaust emissions of a dual-fuel diesel engine. Energy Conversion and Management, 50(1), 203-213.

Sayin, C. (2010). Engine performance and exhaust gas emissions of methanol and ethanol–diesel blends. Fuel, 89(11), 3410-3415.

Selim, M. Y. (2004). Sensitivity of dual fuel engine combustion and knocking limits to gaseous fuel composition. Energy Conversion and Management, 45(3), 411-425.

Selim, M. Y. (2005). Effect of engine parameters and gaseous fuel type on the cyclic variability of dual fuel engines. Fuel, 84(7), 961-971.

www.manaraa.com

Shoemaker N. T., Gibson, C. M., Polk, A. C., Krishnan, S. R., and Srinivasan, K. K. (2012). Performance and emissions characteristics of bio-diesel (B100)-ignited methane and propane combustion in a four cylinder turbocharged compression ignition engine. Trans. ASME: Journal of Engineering for Gas Turbines and Power, 134 (8): 082803 (10 pages). (http://dx.doi.org/10.1115/1.4005993)

Siebers, D. L. (1999). Scaling liquid-phase fuel penetration in diesel sprays based on mixing-limited vaporization (No. 1999-01-0528). SAE technical paper.

Singh, S., Krishnan, S. R., Srinivasan, K. K., Midkiff, K. C., & Bell, S. R. (2004). Effect of pilot injection timing, pilot quantity and intake charge conditions on performance and emissions for an advanced low-pilot-ignited natural gas engine. International journal of Engine research, 5(4), 329-348.

Sjöberg, M., & Dec, J. E. (2005). An investigation into lowest acceptable combustion temperatures for hydrocarbon fuels in HCCI engines. Proceedings of the Combustion Institute, 30(2), 2719-2726.

Splitter, D., Hanson, R., Kokjohn, S., & Reitz, R. (2011). Reactivity controlled compression ignition (RCCI) heavy-duty engine operation at mid-and high-loads with conventional and alternative fuels. SAE Technical Paper 2011-01-0363, doi:10.4271/2011-01-0363.

Srinivasan, K. K., Bell, S. R., Gong, W., Fiveland, S. B., Krishnan, S. R., Singh, S. & Midkiff, K. C. (2006a). The advanced injection low pilot ignited natural gas engine: A combustion analysis. Journal of engineering for gas turbines and power, 128(1), 213-218.

Srinivasan, K. K., Krishnan, S. R., & Midkiff, K. C. (2006b). Improving low load combustion, stability, and emissions in pilot-ignited natural gas engines. Proceedings of the Institution of Mechanical Engineers, Part D: Journal of Automobile Engineering, 220(2), 229-239.

Srinivasan, K. K., Krishnan, S. R., Qi, Y., Midkiff, K. C., & Yang, H. (2007). Analysis of diesel pilot-ignited natural gas low-temperature combustion with hot exhaust gas recirculation. Combustion Science and Technology, 179(9), 1737-1776.

Jacobs, T. J., & Assanis, D. N. (2007). The attainment of premixed compression ignition low-temperature combustion in a compression ignition direct injection engine. Proceedings of the Combustion Institute, 31(2), 2913-2920.

Tira, H., Tsolakis, A., Turner, D., Herreros, J., Dearn, K., Theinnoi, K., and Wyszynski, M. (2014). ”Influence of Fuel Properties, Hydrogen, and Reformate Additions on Diesel-Biogas Dual-Fueled Engine.” J. Energy Eng. 140, SPECIAL ISSUE: Innovative Technologies on Combustion of Biofuels in Engines: Issues and Challenges, A4014003.

www.manaraa.com

Wong, H. C., Beck, N. J., & Chen, S. K. (2000). The evolution of compression ignition natural gas engines for low emission vehicles. ASME paper, (2000-ICE), 318.

Yao, M., Chen, Z., Zheng, Z., Zhang, B., & Xing, Y. (2006). Study on the controlling strategies of homogeneous charge compression ignition combustion with fuel of dimethyl ether and methanol. Fuel, 85(14), 2046-2056.

Zheng, M., Reader, G. T., & Hawley, J. G. (2004). Diesel engine exhaust gas recirculation––a review on advanced and novel concepts. Energy conversion and management, 45(6), 883-900.

www.manaraa.com